2008

SYNTHESIS AND DEVICE CHARACTERIZATION OF FUNCTIONALIZED PENTACENES AND ANTHRADITHIOPHENES

Sankar Subramanian
University of Kentucky, SankarSubram@gmail.com

ABSTRACT OF DISSERTATION

Sankar Subramanian

The Graduate School

University of Kentucky

2008

SYNTHESIS AND DEVICE CHARACTERIZATION OF FUNCTIONALIZED PENTACENES AND ANTHRADITHIOPHENES

ABSTRACT OF DISSERTATION

A dissertation submitted in partial fulfillment of the
requirements for the degree of Doctor of Philosophy in the
College of Art and Sciences
at the University of Kentucky

By
Sankar Subramanian

Lexington, Kentucky

Director: Dr. John Anthony, Professor of Chemistry

Lexington, Kentucky

2008

ABSTRACT OF DISSERTATION

SYNTHESIS AND DEVICE CHARACTERIZATION OF FUNCTIONALIZED PENTACENES AND ANTHRADITHIOPHENES

Research on pi-conjugated organic materials in the recent past has produced enormous developments in the field of organic electronics and it is mainly due to their applications in electronic devices such as organic field effect transistors (OFETs), organic light emitting diodes (OLEDs) and organic photovoltaic cells (OPVs). The primary goal of this research work is to design and synthesize high performing charge transport organic semiconductors.

One of the criteria for better performance of the organic thin film transistor (OTFT) is to have high uniform thin film morphology of the organic semiconductor layer on the substrate. The first project in this dissertation has been directed towards improving the thin film morphology of the functionalized pentacenes through liquid crystalline behaviour. The results have suggested the possibility of thermotropic liquid crystalline phases in 6,13-bis(diisopropylhexylsilylethynyl) pentacene which has no *pi*-stacking in its solid state and the presence of silyl group at the *peri*-position is crucial for the stability of the functionalized pentacenes. In the second project, i have investigated the effect of alkyl groups with varying chain length on the anthradithiophene chromophore on the performance of the charge transporting devices. Organic blend cell based on solution processable 2,8-diethyl-5,12-bis(triethylsilylethynyl) anthradithiophene has showed 1% power conversion efficiency and the performance is mainly attributed to the large crystalline phase segregation of the functionalized anthradithiophene from the amorphous soluble fullerene derivative matrix. OTFT study on alkyl substituted functionalized anthradithiophenes suggested the need of delegate balance between thin film morphology and the crystal packing. Third project has been directed towards synthesizing halogen

substituted functionalized anthradithiophenes and their influence in the performance of OFETs. OTFT made of 2,8-difluoro-5,12-bis(triethylsilylethynyl) anthradithiophene produced devices with thin film hole mobilities greater than 1 cm^2/Vs. The result suggested that the device is not contact limited rather this high performance OTFTs are due to the contact induced crystallinity of the organic semiconductor.

KEY WORDS: organic thin film transistors, organic solar cells, thin film morphology, crystal packing, pentacenes, anthradithiophenes

Sankar Subramanian

_____

03/03/2008

_____

SYNTHESIS AND DEVICE CHARACTERIZATION OF FUNCTIONALIZED PENTACENES AND ANTHRADITHIOPHENES

By

Sankar Subramanian

Dr. John Anthony
Director of Dissertation

Dr. Robert Grossman
Director of Graduate Studies

03/03/2008

_____

Date

RULES FOR USE OF DISSERTATIONS

Unpublished dissertations submitted for the Doctor's degree and deposited in the University of Kentucky Library are as a rule open for inspection, but are to be used only with due regard to the rights of the authors. Bibliographical references may be noted, but quotations or summaries of parts may be published only with the permission of the author, and with the usual scholarly acknowledgements.

Extensive copying or publication of the dissertation in whole or in part also requires the consent of the Dean of Graduate School of the University of Kentucky.

The library that borrows this dissertation for use by its patrons is expected to secure the signature of each user.

Name Date

_____

_____

_____

_____

_____

_____

_____

_____

_____

_____

_____

_____

DISSERTATION

Sankar Subramanian

The Graduate School
University of Kentucky
2008

SYNTHESIS AND DEVICE CHARACTERIZATION OF FUNCTIONALIZED PENTACENES AND ANTHRADITHIOPHENES

DISSERTATION

A dissertation submitted in partial fulfillment of the
requirements for the degree of Doctor of Philosophy in the
College of Art and Sciences
at the University of Kentucky

By
Sankar Subramanian

Lexington, Kentucky

Director: Dr. John Anthony, Professor of Chemistry

Lexington, Kentucky

2008

Acknowledgements

Last four and a half years have passed in no time but with lots of exciting moments as well as with frustration. Before I take the newer opportunity I have lots of people to thank to make this place a very memorable one in my life. First, the most important person I would like to thank is my research advisor and the director of dissertation, Dr. John Anthony for his guidance. When I joined the Anthony Aromatic Research Group, I had no idea about the electronic theories except little synthetic knowledge. His brilliant and novel ideas in the field of organic electronics have helped me understanding the concepts and stimuated my scientific thinking. His exceptionally adroit trouble shooting character has left an indelible impression in me. I thank my PhD dissertation committee members, Dr. Mark Meier, Dr. Folami Ladipo, and Dr. Bruce Hinds very much for their excellent scientific advices.

I would like to thank all the collaborators, Dr. Tom Jackson and co-workers of Pennsylvania State University, Dr. George Malliaras and co-workers of Cornell University, Dr. David Martin and co-workers of University of Michigan, Ann Arbor, and Dr. Lynn Loo and co-workers of University of Texas, Austin for their excellent efforts in device characterization of our functionalized acenes. I would like to express my gratitude to all the departmental staffs for their help and support throughout my PhD career at University of Kentucky when I needed them the most. Thanks to all the faculties who have shared their wisdom during my stay here.

I would like to thank all my colleagues (in the Anthony lab) the most for their support and co-operation in maintaining great working environment. I would also like to thank all of my friends for making my life at Lexington a very notable one.

Most importantly, I would like to mention my wife, Uma, my parents, Subramanian and Rukmani, my elder brother, Ramkumar and all other family members for their unconditional love and support.

Finally, I would like to thank the Office of Naval Research (ONR), Advanced Carbon Nanotechnology Program (ACNP) and Gill Fellowship for their financial support.

Table of Contents

ACKNOWLEDGEMENTS iii
Table of Contents iv
List of Figures. vi
List of Synthetic Schemes x
List of Tables xii
List of Files xii

Chapter 1 Introduction

1.1 Organic electronic materials 1
1.2 Fundamental concepts of charge transport in organic electronic materials 2
1.3 Organic field effect transistors (OFETs) 3
1.3.1 Functionalized acenes and derivatives 11
1.4 Organic solar cells (OSCs) 14
1.4.1 Important Parameters 15
1.4.2 Organic photovoltaic processes 17
1.4.3 Different architectures of OSCs 19
a. Single layer OSCs 19
b. Bilayer heterojunction OSCs 20
c. Bulk heterojunction OSCs 22
1.5 Objectives of functionalized pentacene and anthradithiophene researchs 25

Chapter 2 Thermotropic Functionalized Pentacenes

2.1 Liquid crystalline materials 26
2.2 Liquid crystalline materials for organic electronics 26
2.3 Alkynyl pentacenes 29
2.4 Diisopropylalkylsilyl pentacenes 37
2.5 Experimental details 44

Chapter 3 Alkyl Substituted Functionalized Anthradithiophenes

3.1 Thienyl electronic materials 52
3.2 Alkyl substituted functionalized anthradithiophenes 54
3.3 Organic thin film transistor (OTFT) studies 61
3.4 Organic solar cell (OSC) studies 63
3.5 Experimental details 73

Chapter 4 Halogen Substituted Functionalized Anthradithiophenes

4.1 Halogen effects in conjugated materials 79
4.2 Halogen substituted functionalized anthradithiophenes 81
4.3 Organic single crystal transistor study 90
4.4 Organic thin film transistor (OTFT) study 91
4.5 Experimental details 98

Chapter 5 Attempted Functionalization on Anthradithiophene Chromophore

5.1 Methoxy substituted functionalized anthradithiophene 105
5.2 Trimethoxyphenyl substituted functionalized anthradithiophene 107
5.3 Cyano substituted functionalized anthradithiophene 110
5.4 Trimethylsilylethynyl substituted functionalized anthradithiophene 114
5.5 Experimental details 117

Chapter 6 Conclusion

6.1 Summary of functionalized pentacenes and anthradithiophenes 124
6.2 Future targets 126

References 129
Vita 138

List of Figures

Figure 1.1 Polyacetylene 1

Figure 1.2 (a) Phthalocyanine (b) Polythiophene 4

Figure 1.3 Two types of organic thin film transistor (OTFT) device configuration (a) Bottom-contact configuration (b) Top-contact configuration 5

Figure 1.4 Output characteristics of a typical organic field effect transistor (OFET) ... 6

Figure 1.5 Examples of p-type organic semiconductors 8

Figure 1.6 Examples of n-type organic semiconductors 9

Figure 1.7 Poly (3-hexylthiophene) 10

Figure 1.8 α, α’ -Diethylsexithiophene. 10

Figure 1.9 Pentacene 11

Figure 1.10 6,13-Bis(triisopropylsilylethynyl) pentacene 12

Figure 1.11 2,8-Dihexylanthradithiophene 13

Figure 1.12 5,12-Bis(triethylsilylethnyl) anthradithiophene 13

Figure 1.13 Current-voltage plot of a photovoltaic (PV) cell 16

Figure 1.14 Light conversion steps in a organic PV cell. 17

Figure 1.15 Different architectures of an organic solar cell (OSC) (a) single layer OSC (b) Bilayer heterojunction OSC (c) Bulk heterojunction OSC 19

Figure 1.16 Examples of organic photovoltaic materials 24

Figure 1.17 Structure of PCPDTBT 24

Figure 2.1 2,3,6,7,10,11-Hexahexylthiotriphenylene 27

Figure 2.2 (a) α,ω-Dihexylquarterthiophene (b) 5,5’-Bis(5-hexyl-2-thienylethynyl)-2,2’.5’,2’-terthiophene 28

Figure 2.3 As-spun thin film image of TIPS pentacene 29

Figure 2.4 Thermal cracking of the thin film made of TIPS pentacene 30

Figure 2.5 Pictorial representation of calamatic liquid crystals 31

Figure 2.6 Thermal ellipsoid plots of 34,35, and 36 33

Figure 2.7 *pi*-stacking of alkynyl pentacenes 34

Figure 2.8 UV-vis absorption spectra of 34 and 53 35

Figure 2.9 Electrochemistry of 34 35

Figure 2.10 Alternative route to induce liquid crystallinity to pentacene 36

Figure 2.11 Thermal ellipsoid plots of 50, 51, 53 and 54 38

Figure 2.12 *pi*-stacking of diisopropylalkylsilyl pentacenes 39

Figure 2.13 Electrochemistry of 53 40

Figure 2.14 DSCs of 6,13-di(alkynyl) pentacenes (34-38) 41

Figure 2.15 DSCs of 6,13-bis(diisopropylalkylsilylethnynyl) pentacenes 41

Figure 2.16 Proposed pathway of decomposition of functionalized pentacenes 42

Figure 2.17 Optical micrographs of the functionalized pentacene thin films made of 35 and 53 43

Figure 3.1 Unsubstituted anthradithiophene 53

Figure 3.2 Thermal ellipsoid plots of 66-67. 56

Figure 3.3 Solid state pi-stacking arrangement for 66, 67, 68 57

Figure 3.4 Thermal ellipsoid plots of 71 and 72 59

Figure 3.5 UV-vis spectra of alkyl substituted anthradithiophenes 60

Figure 3.6 Thin film morphological images of functionalized anthradithiophenes 61

Figure 3.7 Thin film transistor characteristics of functionalized anthradithiophenes . 62

Figure 3.8 Current-voltage characteristics of 68- based PV device 65

Figure 3.9 UV-vis spectra of 19 and 68 66

Figure 3.10 Structure of PαMS 67

Figure 3.11 Cross polarized micrographs of thin films made of 66 and 72 with and without PαMS.....67

Figure 3.12 Diels-Alder reaction study of TIPS pentacene (19) and PCBM (23).....68

Figure 3.13 Photostability study of thin film made of 21.....68

Figure 3.14 X-shaped oligothiophene (74).....69

Figure 3.15 Optical microscopic images of spherulite growth.....70

Figure 3.16 General structure of 67 based organic PV device.....71

Figure3.17 Current-voltage characteristics of a device with high spherulite coverage.....72

Figure 4.1 Structures of tetracene and dichlorotetracene..... 80

Figure 4.2 Structure and crystal packing of pentacene and perfluoropentacene 80

Figure 4.3 Thermal ellipsoid plots of 87 and 88.....83

Figure 4.4 pi-stacking solid state arrangements of 85-88.....84

Figure 4.5 Thermal ellipsoid plots of 89 and 94.....86

Figure 4.6 pi-stacking interactions in 89 and 94.....87

Figure 4.7 UV-vis absorption spectra of functionalized anthradithiophenes.....88

Figure 4.8 DSC experiment on 89.....89

Figure 4.9 Photostability of thin films made of 85.....89

Figure 4.10 Crystals of 89 from (a) toluene (b) dichloroethane.....90

Figure 4.11 Organic single crystal transistor characteristics of 89.....91

Figure 4.12 Structure of parylene.....91

Figure 4.13 Optical micrographs of 85 based OTFT devices with channel length (a) 5 µm, (b) 10 µm, (c) 20 µm, (d) 50 µm.....92

Figure 4.14 (a) The transfer characteristics of a 85-based transistor with channel length L = 5 µm and channel width W = 1000 µm, (b) The output characteristics of the same device (c) Structure of 85 and pentafluorobenzene thiol, (d) General structure of OTFT device.....93

Figure 4.15 Output and transfer characteristics of a spin-coated 85-based OTFT device.....94

Figure 4.16 Output characteristics of a drop-cast 85 based OTFT device.....95

Figure 4.17 Thermal ellipsoid plot of 85a.....96

Figure 4.18 Optical micrographs of thin films made of 87 and 89.....97
Figure 5.1 pi-stacking interactions in 100.....106
Figure 5.2 Thermal ellipsoid plot of 107.....109
Figure 5.3 pi-stacking interactions in 107.....110
Figure 5.4 Thermal ellipsoid plot of 109..... 112
Figure 5.5 pi-stacking interactions in109.....113
Figure 5.6 Thermal ellipsoid plot of 110.....115
Figure 5.7 pi-stacking interactions in 110.....116
Figure 6.1 Future targets.....127

List of Synthetic Schemes

Scheme 2.1 Synthesis of alkynyl pentacenes.....32

Scheme 2.2 Synthesis of diisopropylsilyl pentacenes.....37

Scheme3.1 Synthesis of alkyl substituted TES (triethylsilyl) anthradithiophenes.....55

Scheme 3.2 Synthesis of alkyl substituted TIPS (triisopropylsilyl) anthradithiophenes.....58

Scheme 4.1 Synthesis of halogen substituted TES anthradithiophenes.....82

Scheme 4.2 Synthesis of halogen substituted TIPS anthradithiophenes.....85

Scheme 5.1 Synthesis of methoxy substituted TES anthradithiophene.....105

Scheme 5.2 Synthesis of 3,4,5-trimethoxyphenyl substituted TIPS anthradithiophene.....108

Scheme 5.3 Synthesis of cyano substituted functionalized anthradithiophene.....111

Scheme 5.4 Synthesis of trimethylsilylethynyl substituted functionalized anthradithiophene.....114

List of Tables

Table 6.1 UV-vis and electrochemical measurements on functionalized anthradithiophenes 128

List of Files

Sankar Dissertation.pdf ……....4 MB

Chapter 1: Introduction

1.1 Organic Electronic Materials

The microelectronics industry of the 20th century has been completely dominated by inorganic field-effect transistors (FETs) ever since the invention of the first transistor in 1947 at Bell Laboratories. However, the high cost of production for these traditional silicon based FETs has stimulated extensive scientific research on π-conjugated organic small molecule, oligomer, dendrimer and polymer based semiconductors.[1-4] Interest in organic materials is mainly due to the electronic and optical properties that come from the delocalization of charges in a system of atoms covalently bonded with alternating single and multiple bonds. Unlike their inorganic counterparts, organic electronic materials can be processed using low-cost solution-based techniques such as spin-coating and ink-jet printing at low temperature, and have the potential to eliminate the use of high vacuum deposition and photolithography. Mechanical flexibility,[5] and the possibility of large area deposition onto substrates[6] are other advantages of these carbon-based semiconductors.

The breakthrough in the research of organic electronics was the discovery of electrically conducting organic polymers by Shirakawa[7] and co-workers in 1977. By means of suitable halogen doping, polyacetylene (**1**, Fig. 1.1) showed high conductivity at room temperature. For this discovery, Shirakawa, MacDiarmid and Heeger were awarded with Nobel Prize for Chemistry in 2000.

Figure 1.1 Polyacetylene

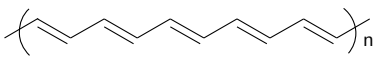

1

Over the past three decades, extensive research has been dedicated to understanding charge transport mechanisms in organic semiconductors in order to employ them in devices such as organic field effect transistors (OFETs), organic light emitting diodes (OLEDs) and organic photovoltaics (OPVs).[8-11] The efficiency of conduction of charge carriers (electrons and holes) in semiconductors is referred to as their mobility, which will be discussed in the following sections.

1.2 Fundamental Concepts of Charge Transport in Organic Electronic Materials

There are several ways to introduce charge carriers into the lowest unoccupied molecular orbital (LUMO) energy level or the highest occupied molecular orbital (HOMO) energy level in organic semiconductors, by means of photo-generation, chemical doping, excess thermal energy, and most importantly through injection from metal electrodes.

Charge transport in semiconductors is mainly determined by the type of atomic or molecular interactions present in the solid. Organic molecular solids possess weak van der Waals interactions between neighboring molecules. On the other hand, atoms are held together with very strong covalent bond interactions in traditional inorganic semiconductors. Due to strong overlap of atomic orbitals observed in these conventional silicon based semiconductors, charge transport occurs in delocalized bands which are limited by the phonon (thermally induced lattice vibrations) scattering within the solid and show a very high single crystal charge carrier mobility (electron mobility, μ_e = 1430 cm^2/Vs, and hole mobility, μ_h = 466 cm^2/Vs).[12] Therefore, the mobility is lowered as the temperature increases. In contrast, even after tremendous advances in the field of organic

semiconductors over several decades, the exact charge transport mechanism in organic electronic materials is a frequently contested subject. Part of the confusion arises because there are various methods to determine the electrical characteristics of organic electronic materials, including time-of-light (TOF), space charge limited current (SCLC), and field-effect transistor (FET) measurements.[13-17] In chapter 3 and 4, I will describe the electrical properties of functionalized anthradithiophenes that have been measured by organic FET studies. A detailed structure of a field effect transistor, followed by its study in the developments of organic semiconductors, will be discussed in the following sections.

1.3 Organic Field Effect Transistors (OFETs)

In principle, a FET acts as a capacitor, as first proposed by Lilienfeld in 1930.[18] However, it was only after the introduction of the silicon-based metal-oxide-semiconductor FET (MOSFET) concept in 1960, that FETs became an important element in modern microelectronic chips.[19] Even though they are not expected to compete with high performing crystalline silicon-based FETs, organic semiconductor based devices have the potential to overcome amorphous silicon (a-Si:H) based transistors (hole mobility in the range of 0.1 - 1 cm^2/Vs) where low on-off switching speed is required. In 1970, the first organic FET was described when FET measurements were carried out on the surface of metal-free phthalocyanine (**2**, Fig. 1.2a).[20] The first organic semiconductor based thin-film transistor was demonstrated in 1987 by Koezuka et al. when electrochemically polymerized polythiophene (**3**, Fig. 1.2b) showed thin film hole mobility of $2 \times 10^{-5} cm^2/Vs$.[21, 22]

In field effect transistors, the conductivity or flow of charges across the semiconducting material is influenced by the voltage applied at the gate electrode with respect to source (Fig. 1.3). The organic field effect transistor plays a critical role in carbon based electronics, and the success in the development of these organic electronic devices mainly relies on improved charge career mobility of organic semiconductors and reduced operation voltage of the transistors. The architecture of an OFET is generally similar to that of thin film transistor (TFT) based on amorphous hydrogenated silicon.

Figure 1.2 a. Phthalocyanine **b. Polythiophene**

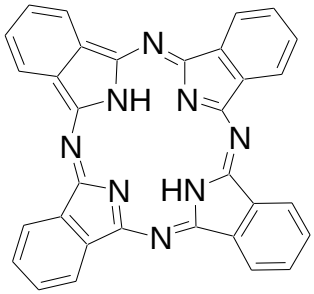

2

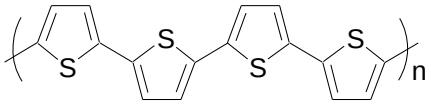

3

An organic thin film transistor (OTFT) consists of three major components; three electrodes (source (S), drain (D), and gate (G)), a dielectric layer (insulator), and an active organic semiconductor layer. It can be constructed either with top-contact or bottom-contact geometry (Fig. 1.3 b and a, respectively). In the top-contact devices, an active organic semiconductor layer (OSL) is first deposited on the dielectric, and then the two electrodes (source and drain) are evaporated through a shadow mask. In the bottom-contact device, the source and drain electrodes are pre-patterned on the dielectric, and then the organic layer is deposited on top of them.

Figure 1.3 Two types of organic thin film transistor device configuration:

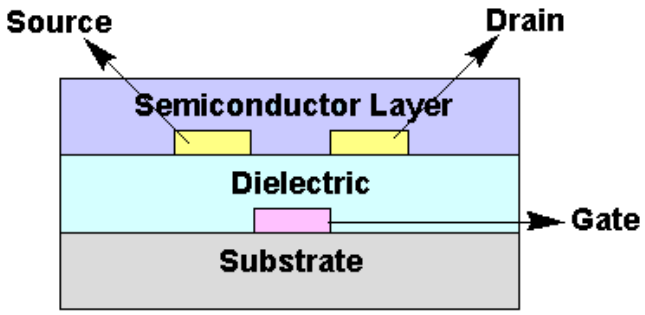

a. Bottom-Contact Configuration

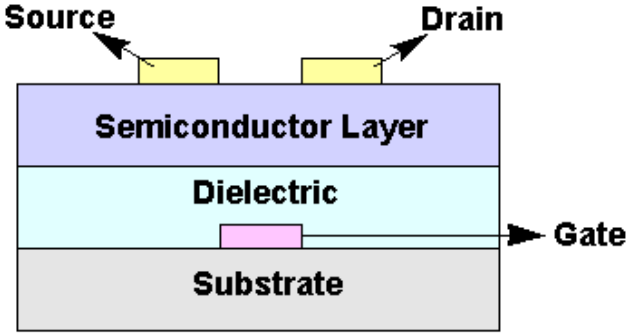

b. Top-Contact Configuration

The current flow between the source and drain electrodes is controlled by the applied gate voltage. When no voltage is applied at the gate electrode, there will be low or no current, and the transistor is said to be *off*. When the gate voltage is applied, charge carriers (holes or electrons depending on the polarity of gate voltage) will be accumulated at the interface between the dielectric and the organic semiconductor layer due to the polarization of dielectric. The charge carriers will allow current flow between the source and drain electrodes under applied voltage, and the transistor is *on*.

The potential usefulness of an OTFT is mainly determined by four important parameters; First, charge carrier mobility (μ), which is the drift velocity of charge carriers in the conducting channel (the region covered between source and drain electrodes) under electric field (measured in cm^2 / Vs). Second, the on / off current ratio ($I_{on\,/\,off}$) is the ratio of current flow between the source and drain electrodes at the *on* state of the transistor to that of *off* state. Third, threshold voltage (V_T) is the voltage required at the gate electrode to induce the current flow in the channel. And, finally, the sub-threshold slope (S), determines how fast the device can switch back to the *on* state in the region of exponential current increase from the *off* state.

Figure 1.4 Output characteristics of a typical OFET

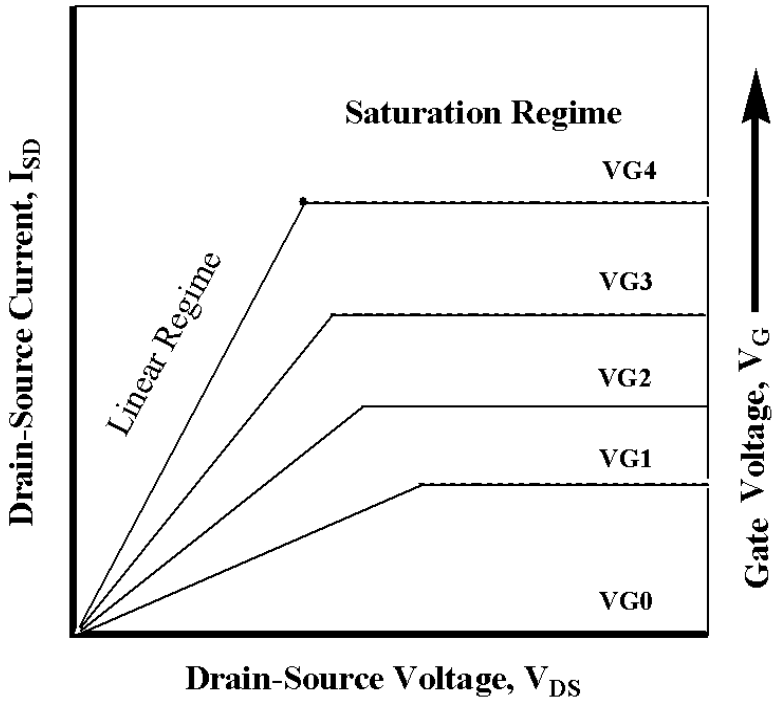

At constant gate voltage (V_G), as the drain-source voltage (V_{SD}) increases, the current flow in the conducting channel increases almost linearly and then gradually saturates at higher V_{SD} (see Fig. 1.4).The source-drain current (I_{SD}) generated in the linear and saturation regions can be calculated by the following equations.

For the linear region,

$$I_{SD,\ Linear} = (C_i W \mu_{FET} / L)\ (V_G - V_T) V_{SD}$$

For the saturation region,

$$I_{SD,\ Saturation} = (C_i W \mu_{FET} / 2L)\ (V_G - V_T)^2$$

Where C_i is the capacitance of the dielectric, W and L are the distance across the conducting channel, *channel width* and distance between the source and drain electrodes, conducting *channel length* respectively**,** V_T is the threshold voltage, and μ_{FET} is the charge carrier mobility.

Figure 1.5 Examples of p-type organic semiconductors

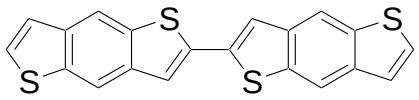

4

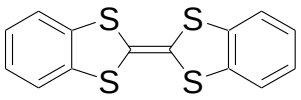

5

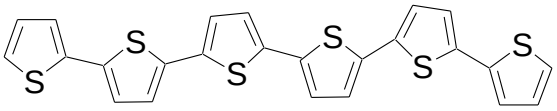

6

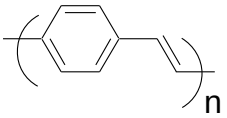

7

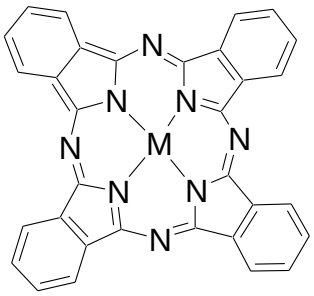

8

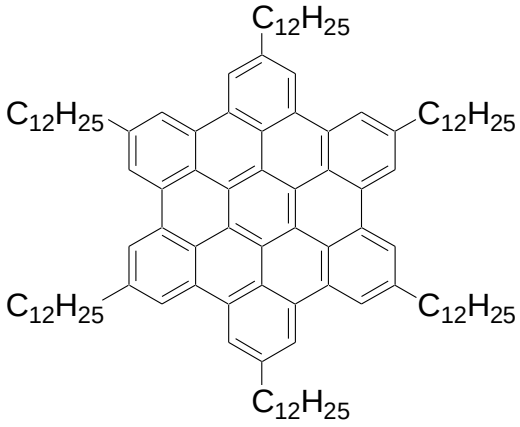

9

In general, organic semiconductors can be classified into two categories; p-type (majority hole carriers) and n-type (majority electron carriers) depending on the density of states in the energy band – a high dispersion in the valence band for p-type materials, and high dispersion in the conduction band for n-types. Energy levels in organic materials can be tuned through functionalization. Electron donating groups such as alkyl,

Figure 1.6 Examples of n-type organic semiconductors

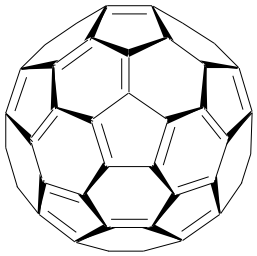

10

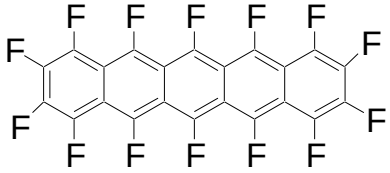

11

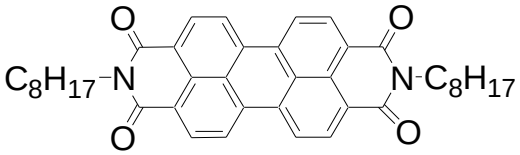

12

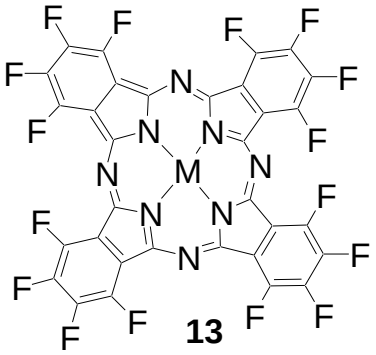

13

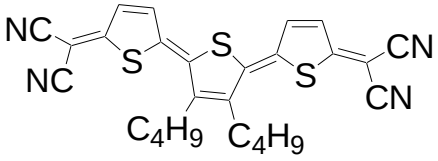

14

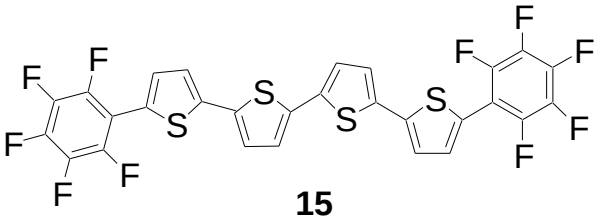

15

alkoxy, amino are used to synthesize p-type organic materials. On the other hand, electron withdrawing groups such as cyano, fluoro, nitro are used to make n-type materials. Figures 1.5 and 1.6 depict some examples of commonly studied p-type and n-type organic semiconductors respectively.[23-34] The active layer is usually deposited through either vacuum-sublimation or from solution.

The first solution processable organic semiconductor based FET was demonstrated in the late 1980s using the alkylated polythiophene poly(3-hexylthiophene),[35] **P3HT** (**16**,

Fig. 1.7). Even though polymer based FETs produced highly uniform thin films over a large area, the performance of the devices was limited by the poor control of conjugation length,

Figure 1.7 Poly (3-hexylthiophene)

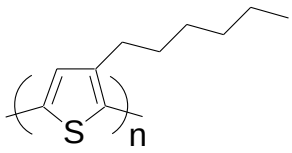

16

and the difficulties in purification of polymers to remove impurities. Improving regioregularity (>91 % of head-tail linkages) of the P3HT thin film improved hole mobility to 0.1 cm^2/Vs.[36] Recently, using a dip coating technique which induced high regioregularity produced mobilities approaching 0.2 cm^2/Vs.[37]

In contrast with polymeric systems, the solid state order of small molecules can be more effectively controlled by chemical modification. The addition of alkyl chains to the

Figure 1.8 α, α'-diethylsexithiophene

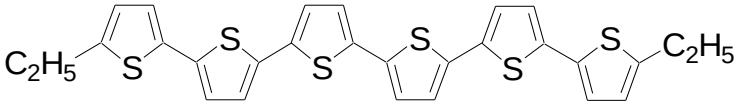

17

end of α-sexithiophene (**6**, Fig. 1.5) rings enhanced the molecular orientation and improved π-π stacking of the oligomer layer, and the extracted thin film hole mobility of α, α'-diethylsexithiophene (**17**, Fig. 1.8) was around 1.1 cm^2/Vs.[38, 39]

1.3.1 Functionalized Acenes and Derivatives

Pentacene (**18**, Fig. 1.9), an acene oligomer, has been extensively studied for OTFT devices because of its unique thin film forming ability.[40] High performance pentacene based OTFTs with spin coated polymer dielectric layers were fabricated by Klauk and co-workers, [41] showing an extracted thin film hole mobility of 3 cm^2/Vs and on/off

Figure 1.9 Pentacene

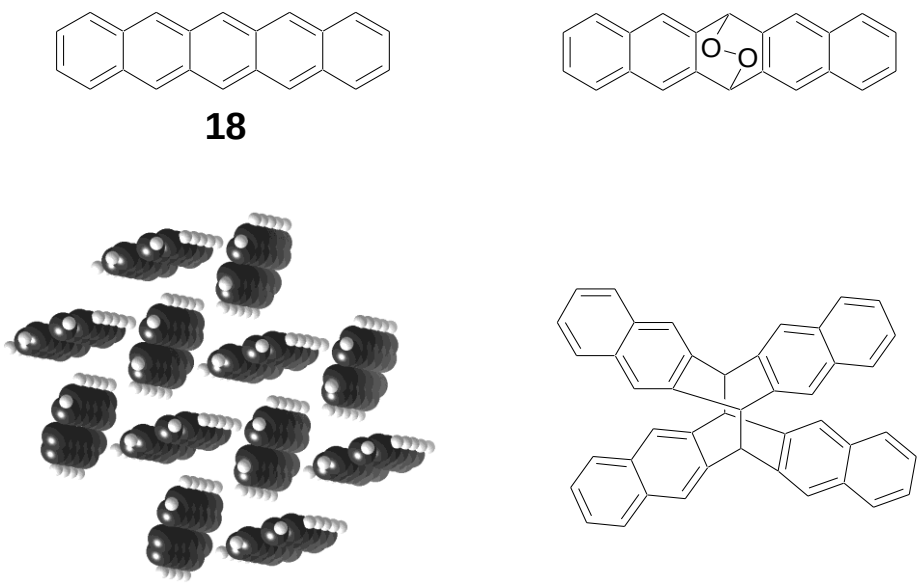

current ratio of 10^5. Further improvements on pentacene based devices are limited by *herringbone* interactions between neighboring molecules, insolubility in commonly used organic solvents, and poor oxidative stability. Typical pathways of pentacene degradation are endo-peroxide formation by interacting with singlet oxygen in air or dimerization at the central ring of the pentacene (Fig. 1.9). Earlier, our group overcame these problems through peri-functionalization of pentacene using trialkylsilyl groups as solubilizers and an ethynyl spacer was employed to avoid complete disruption of π-stacking between the

neighboring molecules due to the bulkiness of silyl substituents. It was found that the size of the silyl substituents determines the crystal π-stacking of the molecules. Improved π-overlap and stability were imparted when the diameter of the silyl group is

Figure 1.10 TIPS Pentacene

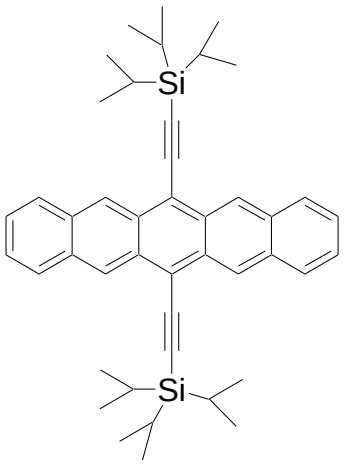

19

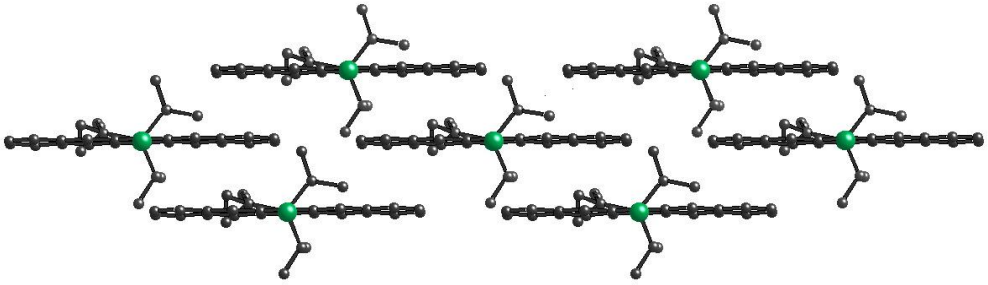

half the length of the length of the acene core. From X-ray crystal diffraction studies, the solid-state arrangement of 6,13-bis (triisopropylsilylethynyl)pentacene (TIPS pentacene, **19**) is found to be a two-dimensional π-stack (brickwork arrangement)[42] with interatomic distances as close as 3.41Å (Fig. 1.10). Recently, researchers at Penn State fabricated solution-processed TIPS pentacene OTFTs with thin film hole mobility of 1.21 cm^2/Vs and On/Off current ratio of 10^7.[43]

Figure 1.11 2, 8- dihexylanthradithiophene

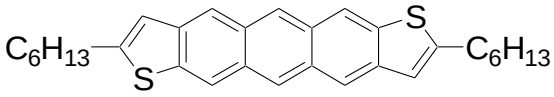

20

Figure 1.12 TES Anthradithiophene

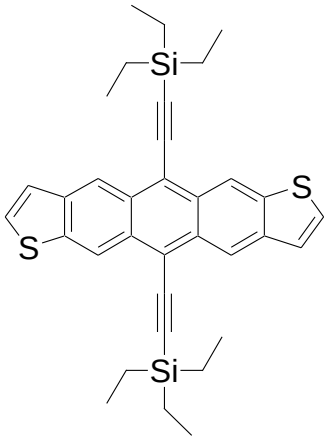

21

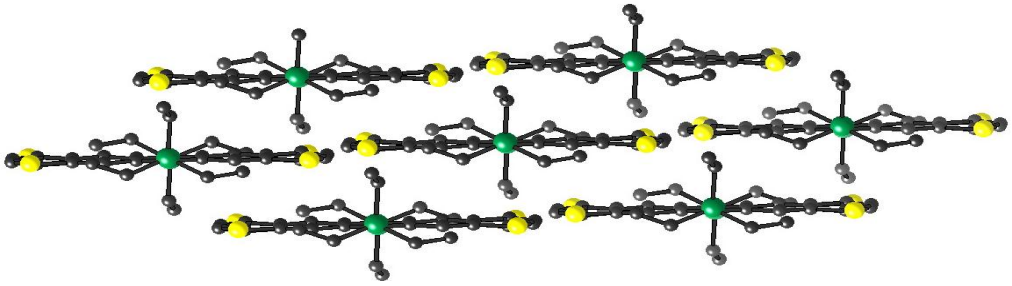

Anthradithiophene, a pentacene analogue where the two terminal benzene rings are replaced by two thiophene units, shows greater stability over pentacene because of high energy barrier to oxidation. Katz et al. demonstrated that vacuum evaporated 2,8-dihexylanthradithiophene **20** (Fig. 1.11) formed high quality thin films with extracted charge carrier mobility of vacuum sublimed thin films as high as 0.15 cm^2/Vs.[44]

Applying our peri-functionalization approach to anthradithiophene also produced materials with excellent electronic properties. Our best performing functionalized anthradithiophene was 5,12-bis (triethylsilylethynyl)anthradithiophene (TES Anthradithiophene, **21**) which adopts two-dimensional π-stacks with carbon-carbon interatomic distances as close as 3.25 Å (Fig. 1.12). Our collaborator fabricated the solution processed TES anthradithiophene based OTFTs with extracted thin film hole mobility of 1.0 cm^2/Vs. However, hole injection from the metal electrode is limited by its high oxidation potential (E_{ox} = 904 mV).[45] **21** can easily be chemically tuned due to the presence of acidic hydrogens in the terminal thiophene rings of the acene core. In chapters 3-5, I will discuss my work on the chemical synthesis of functionalized anthradithiophenes in detail.

1.4 Organic Solar Cells (OSC)

As natural energy sources such as coal, oil, and natural gas are depleted and the price of energy continues to rise, a high demand for renewable energy (such as solar, wind, hydroelectric, bio) production prevails around the world. According to a recent US department of energy report, the United States government spends 500 billion dollars[46] annually on energy production which is not really surprising since energy drives everything from businesses to transportation. The sun being a plentiful energy source on earth, solar energy has been widely recognized as an indispensable element to fulfill global energy needs. Otherwise known as a photovoltaic (PV) cell, a solar cell is a device which converts sunlight energy into electrical energy.

Since the discovery of the photovoltaic effect in 1839,[47] silicon-based photovoltaic cells have been predominantly utilized for the conversion of sunlight into electrical energy. In 1954, the first crystalline silicon PV cell was developed by scientists at Bell Laboratories, and showed a 6% power conversion efficiency.[48] The maximum efficiency predicted for crystalline Si (band gap = 1.1eV) based solar cell is 30%[49] and 25% efficiency has already been achieved from these conventional cells.[50] Other inorganic-based solar cells have produced even higher results.[51] Spectrolab, a well known solar cell company, recently developed a solar cell that can harvest energy at up to 36% efficiency.[52] However, installations of these traditional inorganic semiconductor based power plants are very expensive and an alternative to reduce the cost of energy production is a desperate objective. The process of refining silicon is highly resource and cost-intensive. (the cost of a silicon chip factory is more than $ 1 billion[53]) The thirst for developing inexpensive renewable energy sources encourages effective research on low-cost solar cells.

1.4.1 Important Parameters:

The performance of a PV device is determined by the following four important parameters.

(i) Power conversion efficiency (η) is the number relating the amount of power generated from a PV cell to the energy of incident photons. This value is decided by the absorption efficiency of the thin film (η_{abs}), exciton dissociation efficiency (η_{diss}) into electrons and holes, and charge collection efficiency (η_{coll}) at the electrodes. The overall power conversion efficiency can be determined as

$$\eta_{overall} = \eta_{abs} \times \eta_{diss} \times \eta_{coll}$$

Figure 1.13 Current –Voltage plot of a photovoltaic (PV) cell

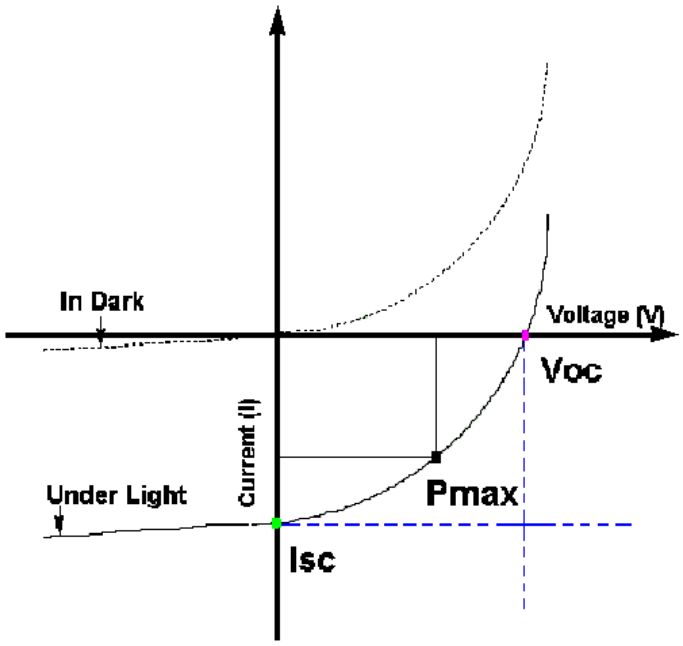

(ii) Short circuit current (I_{sc}) is the maximum current that one can generate through an external circuit that has no load or resistance upon illumination.

(iii) Open circuit voltage (V_{oc}) refers to the maximum possible voltage across a PV cell when no current is flowing. Usually, V_{oc} is determined by the difference between the work functions of the two metal electrodes used. However, in many organic systems a deviation from this definition is also observed.[54]

(iv) Fill Factor (FF) measures the squareness of fourth quadrant in the I-V curve, hence the performance of the PV cell. This can also be defined by the ratio of the maximum power point (Fig. 1.13) output to the maximum possible power that can be generated when the current and voltage are at their maximum (ie, I_{sc} and V_{oc} respectively). Hence, FF can be expressed as

$$FF = I_{mpp}V_{mpp}/I_{SC}V_{OC}$$

and, the power conversion efficiency can be rewritten as

$$\eta = I_{SC}V_{OC}FF/P_{in}$$

In traditional inorganic solar cells, the absorption of photons generates electron-hole pairs evenly distributed in the semiconductor layer and the photocurrent is controlled by the electrostatic field generated across the cell due to the drift of charge carriers (electrons and holes).

1.4.2 Organic Photovoltaic Processes

The process of converting light energy into electrical energy in an organic PV is executed by the following five consecutive steps (Fig. 1.14).

Figure 1.14 light conversion steps in an organic PV cell

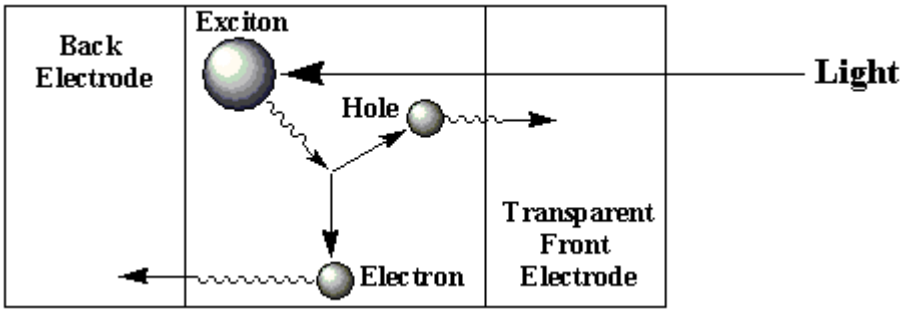

(i) Absorption of photons in the solar spectrum results in the photogeneration of excitons (mobile electron-hole pairs). This is mainly affected by the absorption coefficient of the organic material and the thickness of the organic film.

(ii) Diffusion of photoexcited excitons in the organic thin film to reach the dissociation sites. This is affected by the lifetime of the excitons and the exciton diffusion length.

(iii) Charge separation of electron-hole pairs into individual charge carriers when excitons reach the dissociated sites (usually, the organic donor–acceptor interface or the organic- metal electrode interfaces).

(iv) Charge transport of the electrons and holes in the organic semiconductor layer to the organic-electrode interface.

(v) Charge collection at the conductive electrodes to supply a direct current (DC) for power generation. Holes will be collected at the high work function electrode and electrons will be collected at the low work function electrode.

The first organic photovoltaic was investigated in 1958 by Kallmann and Pope when an anthracene thin single crystal was examined by placing the crystal between two 0.01M NaCl solutions and Ag electrodes were used to make contact with the solutions.[55] The PV cell exhibited a photovoltage of 200 mV with an exceedingly low efficiency of 2×10^{-6}. Since then, various device architectures have been introduced by different research groups in order to improve the power conversion efficiency of an organic PV cell. Here, I describe three of the device structures and their advantages over one another. Fig. 1.15 depicts the three different architectures of organic PV cells. One of the common criteria of all these device structures is one of the the two electrodes used in the solar cell should be at least semi-transparent in order for light to pass through the film, and two major differences between them lie in the exciton dissociation and charge transport processes.

Figure 1.15 Different architectures of an organic solar cell. a. single layer organic solar cell. b. Bilayer heterojunction PV cell and c. Bulk heterojunction PV.

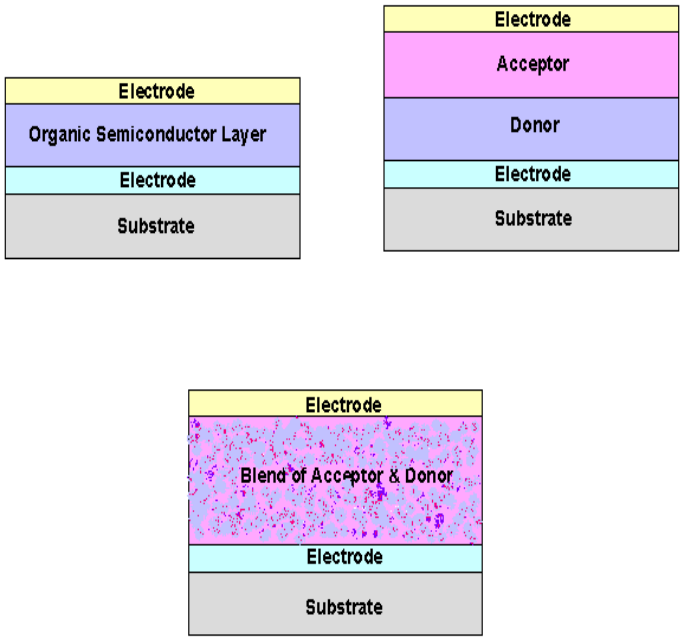

1.4.3 Different architectures of OSCs

(a) Single layer PV cell

The first organic PV cells were investigated on a single thermally evaporated or spin-coated organic semiconductor layer sandwiched between two different metal electrodes. One of the electrode interfaces in this is assumed to be an *Ohmic*-contact, and the other end is considered to be Schottky diode since exciton dissociation occurs at the rectifying metal-semiconductor junction. A recent study on MEH-PPV (**27**) based devices proclaimed that only 10% of excitons were dissociated into free charge carriers and that is attributed to the high exciton binding energy and recombination of free carriers after a

very short time.[56] Although it is the simplest form of all PV cells, the typical single layer PV cell light conversion efficiency still remains below 0.05%.[57]

(b) Bilayer heterojunction PV cell

A major discovery in the field of organic solar cells was the introduction of a novel single-heterojunction approach in 1986 by C. W. Tang of Eastman Kodak Company,[58] where electron acceptor material (A) and electron donor material (D) are deposited separately with a planar interface and the bilayer is sandwiched between two different electrodes. The organic layers can be deposited either through vacuum evaporation or from solution techniques such as spin-coating. Electrodes are chosen according to the work function of the metal electrodes and energy levels of the organic semiconductors for the best charge injection (low work function electrode is near the electron-acceptor layer and high work function electrode for the electron-donor organic material). Since the free charge carriers (electrons and holes) generated after the exciton dissociation at the donor-acceptor interface move in the pure layers (either n-type or p-type) towards their corresponding electrodes, the recombination pathways in this type of PV cell are significantly reduced.

Since the organic semiconductor molecules are bound by weak van der Waals interactions, high charge carrier mobility is required in order to drive the free charge carriers generated at the D-A interface to their respective electrodes. During the photoexcitation process, an electron is promoted from the HOMO energy level to the LUMO of the donor molecule. If the potential difference between the ionization potential of the donor and the electron affinity of the acceptor is larger than the exciton binding energy, then the photoexcited electron in the LUMO of donor will transfer to LUMO of

the electron acceptor material provided the HOMO the donor is higher than HOMO of the acceptor molecule so that the hole will remain in the HOMO of the donor material. This is commonly known as photo-induced charge transfer. On the other hand, if the HOMO of the electron acceptor material is higher than that of the donor, then the photogenerated exciton will be completely transferred through energy loss to the low band gap material. This process is called energy transfer.

The first bilayer organic PV cell consisted of 3, 4, 9, 10 - perylenetetracarboxyl-bis-benzimidazole (**25**, electron acceptor layer) and copper phthalocyanine (electron-donor layer), and produced a power conversion efficiency of about 1%. Since then many different material combinations have been employed in bilayer devices.[59] Solar cells made from sequential spin-coating of p-type poly(p-phenylene vinylene) (PPV, **7**) and n-type conjugated ladder polymer poly (benzimidazobenzophenanthroline ladder) (BBL, **23**) produced a power conversion efficiency of 2%.[60] Forrest et al. demonstrated vacuum-evaporated copper phthalocyanine (CuPc) / 3,4,9,10- perylenetetracarboxylic-bis-benzimidazole (PTCBI, **25**) thin film bilayer heterostructure organic PV cells incorporating an exciton blocking layer (EBL) with an external power conversion efficiency of 2.4%.[61]

By replacing the electron acceptor material PTCBI with C-60 (**10**), the solar cell efficiency increased to 3.6%.[62] The same research group recently achieved power conversion efficiency of 4.2% under simulated Air Mass 1.5G solar spectrum (4 -12 suns intensity) with low series resistance and the FF of >0.6%.[63] One of the drawbacks of these bilayer heterojunction PV devices is that only photogenerated excitons that are 10-20 nm or closer to the D-A interface will dissociate into free carriers. In other words, if

the thickness of the individual layers is larger than the exciton diffusion length, then the free charge carriers (electrons and holes) generated tend to recombine. This leads to the low photon to power conversion efficiency of the solar cells. On the other hand, if the active layers are very thin, then, less amount of light is absorbed which leads to low currents.

(c) Bulk heterojunction PV cell

The significance of the bulk heterojunction is to increase donor-acceptor (D-A) interfacial area in such a way that the distance between each D-A interface is less than the photogenerated exciton diffusion length of each photon absorbing site. This type of PV cell is made from an intimate blend of electron acceptor and electron donor molecules deposited between two different electrodes (see Fig. 1.15). The bulk heterojunction can be achieved by either co-vacuum-evaporation of small molecules or by depositing mixtures of polymers or small molecules from solution. Currently, this device structure becomes cynosure of organic PV scientific research due to low-cost solution processing techniques such as spin-coating, screen printing and ink-jet printing that can be used over large areas on flexible substrates. Since the discovery of two layer heterojunction PV cells in 1986, many material combinations have been extensively studied for improved power efficiency of organic solar cells.[64]

In 1995, Yu et al, demonstrated the first organic bulk heterojunction cell employing mixture of a soluble conjugated polymer (poly(2-methoxy-5-(2'-ethyl-hexyloxy)-1,4-phenylene vinylene, (MEH-PPV, **26**)) as an electron donor and a soluble fullerene derivative (methanofullerene (6,6)-phenyl c61-butyric acid methyl ester, (PCBM, **22**)) as an electron acceptor.[65] A major breakthrough in BHJ solar cells happened when Shaheen

et al. obtained 2.5% power conversion efficiency by mixing a p-type conjugated polymer (poly(2-methoxy-5-(3',7'-dimethyl-octyloxy)-p-phenylene vinylene), (MDMO-PPV, **24**)) and the soluble n-type PCBM in 2001.[66] The performance of the device is affected by nanoscale morphology of the thin film and observed threefold improvement when they changed the solvent from toluene to chlorobenzene. Atomic force microscopic (AFM) studies suggested that the tendency of PCBM molecules to form clusters due to phase segregation is reduced when chlorobenzene is used compared with toluene as the solvent. Recent results show that the pristine PCBM crystals exhibit high degree of intermolecular coupling when they were grown from chlorobenzene instead of toluene.[67]

Research on conjugated block co-polymers has received attention very recently because of their ability to form self-organized nanostructures. Romero et al. found that the molecular morphology and the PV characteristics of the devices are strongly affected by the block copolymer concentration of the blend.[68]

BHJ solar cells based on polythiophene derivatives as photon absorbing materials have shown very promising results with power conversion efficiency of > 4.4%.[69] Previous results confirm that the thin film morphology can be controlled by post-fabrication annealing techniques or controlled solvent evaporation rate.[70] Very recently, Bazan et al. discovered that by incorporating a few volume percent of alkanedithiols in the blend of low band gap polymer (poly(2,6-(4,4-bis-(2-ethylhexyl)-4H-cylcopenta(2,1-b;3,4-b')-dithiophene)-alt-4,7-(2,1,3-benzothiadiazole), (PCPDTBT, **27**)), and PCBM before spin-casting increased the cell efficiency from 2.8 % to 5.5 % without the use of any post-annealing methods.[71] They suggested that addition of dithiols to the solution induces the

physical interaction between the polymer chains and/or between the polymer and fullerene phases.

Figure 1.16 Examples of Organic photovoltaic materials

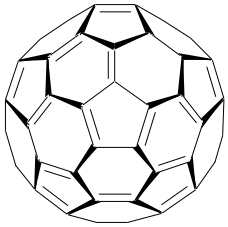

10

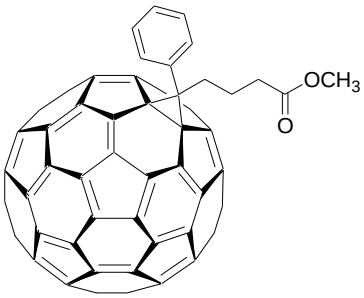

22

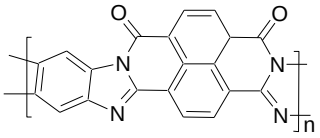

23

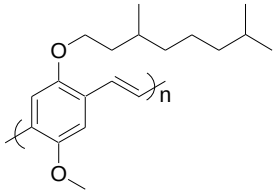

24

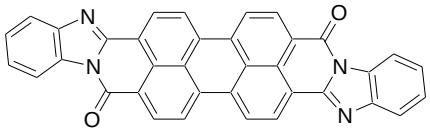

25

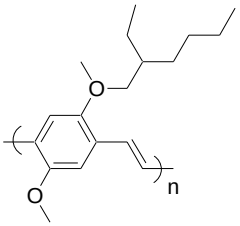

26

Figure 1.17 Structure of PCPDTBT

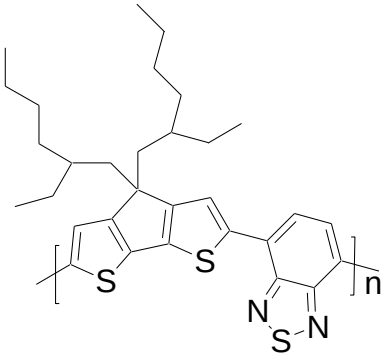

27

One of the challenging problems of the bulk heterojunction devices is to generate phase separated domains in the bulk smaller than the exciton diffusion length in order to avoid recombination losses of free charge carriers. The second demanding problem is inducing a percolating pathway (interpenetrating network) in the bulk volume of the organic semiconductor layer so that the free charge carriers can easily travel towards their respective electrodes. In chapter 3, I will describe the success of our alkylated functionalized anthradithiophenes in the fully solution processed organic solar cell.

1.5 Objectives of functionalized pentacene and anthradithiophene researchs

In the following four chapters, I will describe the synthesis and device characterization of functionalized pentacenes and anthradithiophenes. Chapter 2 will relate my attempts to functionalize pentacene in order to induce liquid crystallinity, and studies of the thermal properties of these compounds. Chapter 3 will describe the blocking of the active C – H bonds in the terminal thiophene rings of the anthradithiophene core using alkyl chains for the improvement of chemical and thermal stability, high solubility and their applications in organic thin film transistors and bulk heterojunction layer organic solar cells. Chapter 4 will detail the synthesis of halogen substituted functionalized anthradithiophenes and the application of fluorinated anthradithiophenes in organic thin film transistors as well as organic single crystal transistors. In chapter 5, I will describe my attempts to increase the conjugation length of the heteroacene core and will outline the outcome of all of my investigation along with prospective ideas to improve the performance of OTFTs and OSCs.

Chapter 2: Thermotropic Functionalized Pentacenes

2.1 Liquid Crystalline Materials

Theoretically, liquid crystalline materials exhibit properties in-between perfect solid phase (with properly aligned positional and directional order) and isotropic liquid phase (disordered) materials, and possess some orientational order and partial positional order. Their physical properties can be easily affected by external influences such as pressure, temperature, applied electric and magnetic fields, and different composition of mixture. Depending on their behavior under external circumstances, liquid crystals (LCs) can be mainly classified into two categories. First, *thermotropic liquid crystals*, which undergo phase transition upon varying the temperature. Second, *lyotropic liquid crystals*, which show phase transition due to change in concentration of the mesogen (a fundamental unit which determines the orientational order in the liquid crystals) in a solvent as well as temperature. When a polarized light is passed through the LCs, they exhibit different textures of characteristic liquid crystalline phases (such as *birefringence*). Each texture is related to the orientation of the molecules in one direction.

2.2 Liquid Crystalline Materials for Organic Electronics

Due to low-cost manufacturing and the possibility to deposit them over large areas, organic π-conjugated materials have been identified as potential fundamental constituents in the development of carbon-based electronics. Very recently, the employment of liquid crystalline materials has become a promising novel approach in improving the performance of organic electronic devices[72-76] since they can self-organize themselves to form uniform thin films. The breakthrough in the liquid crystalline materials approach in

thin film organic electronics came from the success of discotic (disc-like structure) liquid crystals developed by Adam and co-workers in the early 1990s.[77] They found that the highly ordered columnar stacked molecule, 2, 3, 6, 7, 10, 11-hexahexylthiotriphenylene (**28**, Fig. 2.1) exhibits charge carrier mobility of 0.1 cm^2 / Vs, which is in the range of hole mobility shown by amorphous silicon.

Figure 2.1 2, 3, 6, 7, 10, 11 - Hexahexylthiotriphenylene (28)

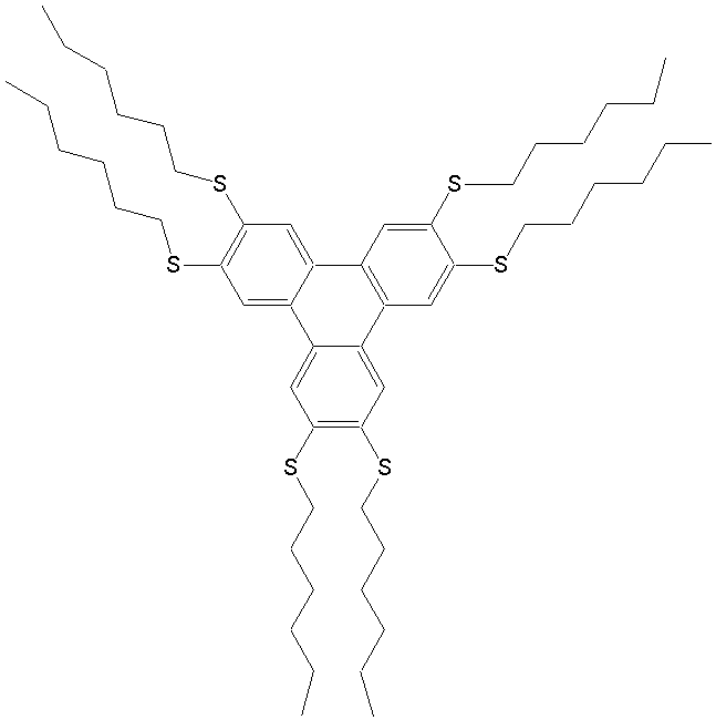

28

Rod-like (calamitic) liquid crystal structures have the advantage of achieving two-dimensional maximum π-stacking solid state arrangements required for high performance of OTFTs, in contrast to the one-dimensional columnar π-stacking of discotic materials. Garnier et al., demonstrated that the end-substitution of quarterthiophene with alkyl

groups improved the morphology of the thin films as compared to unsubstituted quarterthiophene (**4T**). Both spin-coated and vacuum deposited α, ω - dihexylquarterthiophene (**DH4T, 29**) OTFTs produced extracted hole mobilities of 10^{-2} cm^2 / Vs, due to the highly ordered structure within the thin films.[78]

Figure 2.2 (a) α, ω -dihexylquarterthiophene (29), (b) 5,5" -bis(5-hexyl-2-thenylethynyl)-2,2':5',2' -terthiophene (30)

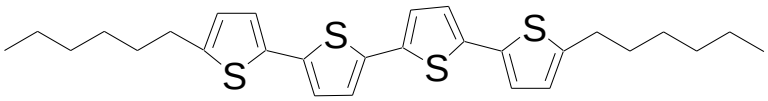

29

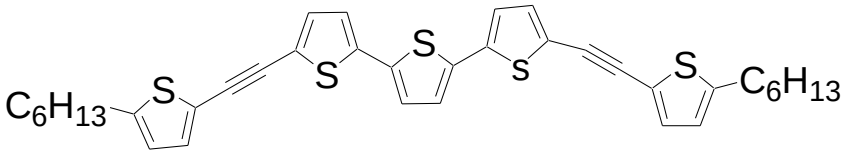

30

Recently, Van Breemen et. al developed calamitic liquid crystalline materials that formed thin films with large area coverage. Thermally annealed spin-coated thin films of **30** resulted in the formation of monodomains up to 150 mm in diameter, showing saturation hole mobility as large as 0.02 cm^2 / Vs. This high thin film hole mobility was attributed to the absence of domain boundaries of the thin film on the substrate.[79] Most recently, Bao el. at at Stanford University used a photoalignment technique in solution deposited liquid crystalline polymer and small molecule semiconductor based OTFTs to improve the morphology of the thin films.[80] This method has been remarkably helpful in avoiding sample contamination, static charge generation and reducing the high degree of

surface roughness at the dielectric interface that were caused by traditional techniques used for alignment of LC molecules.

2.3 Alkynyl Pentacenes:

Though an extensive research on pentacene (**18**) based electronic devices has been done for many years due to its excellent thin film forming ability,[40] its poor solubility, oxidative instability under ambient conditions, and herringbone crystal packing has restricted commercial applications. Earlier, the Anthony group overcame these problems by means of a *peri*-functionalization approach using trialkylsilylethynyl groups. **19** adopts a two dimensional π-stacking with the closest interatomic carbon-carbon distance of 3.41 Å as shown in Fig. 1.11. The extracted mobility of **19** from a solution-cast device is reported as 1.21 cm^2 / Vs.[43] However, the thin film made from the solution processable techniques (such as spin-coating and drop-casting) were not uniform (see Fig. 2. 3).

Figure 2.3 As-Spun Thin Film Image of 19 [81]

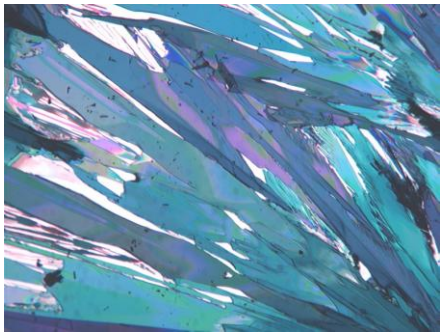

There are many post-fabrication methods, such as solvent vapor annealing and thermal annealing that have been commonly used in the organic electronics field in order to improve the morphology of thin films. Upon thermal annealing of spin-cast thin films,

19 exhibits thermal cracking (see Fig. 2.4) in the long-axis orientation, which was studied by our collaborators at University of Michigan using Hot-Stage Optical Microscopy (HSOM).

Figure 2.4 Thermal cracking of thin films made of 19.

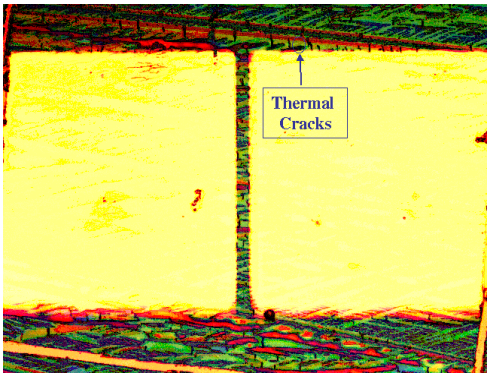

Differential Scanning Calorimetry (DSC) experiments showed a reversible endothermic peak at 124 °C before **19** melts at 268 °C.[82] These data confirm the presence of thermally induced solid-state phase transition in the as-deposited crystalline thin film of **19** that causes the cracking.

For this project, my goal was to design soluble, low-melting functionalized pentacenes with liquid crystalline properties in order to produce high quality thin films on the devices. The hypothesis of this project is: *first*, deposit the organic semiconductor layer on the substrate through a solution-based technique, *second*, thermal annealing the active layer followed by slow cooling will induce the alignment of the molecules in one direction due to liquid crystallinity, to form continuous high quality thin films. From the previous studies, it is well understood that liquid crystals are generally made with rigid π-electronic chromophore as the central part of the molecule, which induces the directional

order in the system, and flexible alkyl chains on the terminal or peripheral positions, which induce the self assembly of the molecules on the substrate. My first approach was to introduce alkyl groups at the peri-positions of

Figure 2.5 Pictorial representation of calamitic LC

R = substituent

the pentacene ring. To avoid difficulties in synthesis, ethynyl groups were utilized as a bridge between alkyl group and acene chromophore. Alkyl groups were chosen not only to induce liquid crystallinity but also to increase the solubility of the molecule.

Synthesis of 6,13-di(alkynyl) pentacenes were done in a straight forward two-step process (see Scheme 2.1). In the first step, quadruple aldol condensation of phthalaldehyde (**31**) and 1,4-cyclohexane dione (**32**) in THF / absolute ethanol (EtOH) solvent mixuture was carried out to generate pentacene-6,13-quinone (**33**) in nearly quantitative yield which immediately came out of the reaction mixture as bright yellow precipitate with the addition of a few drops of 15 % potassium hydroxide (KOH) solution.[83] And, in the second step, the lithium alkyl acetylide in THF was added to **33** at room temperature, and the mixture was allowed to stir overnight. It was followed by the deoxygenation of the resulting diol in-situ with stannous chloride dihydrate / 10 %

aqueous hydrochloric acid to yield the desired alkynyl pentacenes (**34 - 38**) in moderate to good yields. They were easily purified by chromatography

Scheme 2.1 Synthesis of 6,13-di(alkynyl) pentacene derivatives

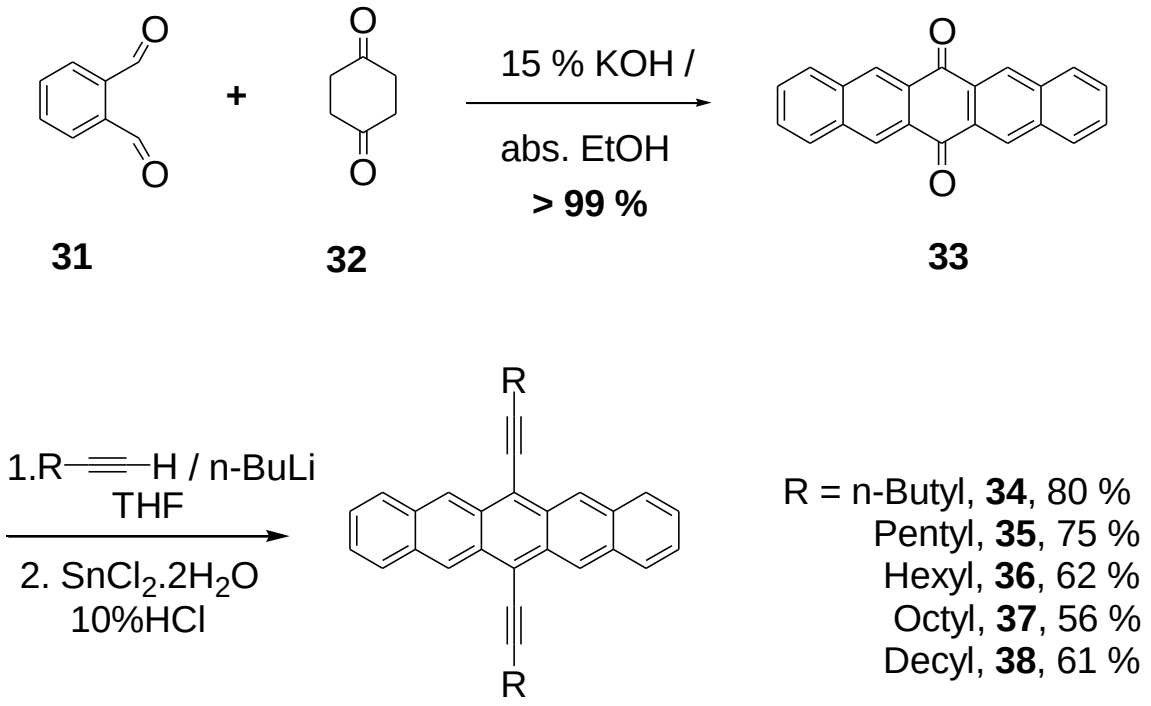

and recrystallization. It should be noted that the higher alkyl chain pentacenes (**37** and **38**) tend to decompose on exposure to air and light for more than 1h.

Functionalized pentacenes **34 - 36** formed dark blue crystals which were stable enough to analyze by single crystal X-ray diffraction. On the other hand, with higher alkyl chain lengths on the acene chromophore, both **37** and **38** tend to decompose yielding orange crystals. The thermal ellipsoid plots of **34 - 36** are shown in Fig. 2.6

Figure 2.6 Thermal ellipsoid plots of 34, 35 and 36.

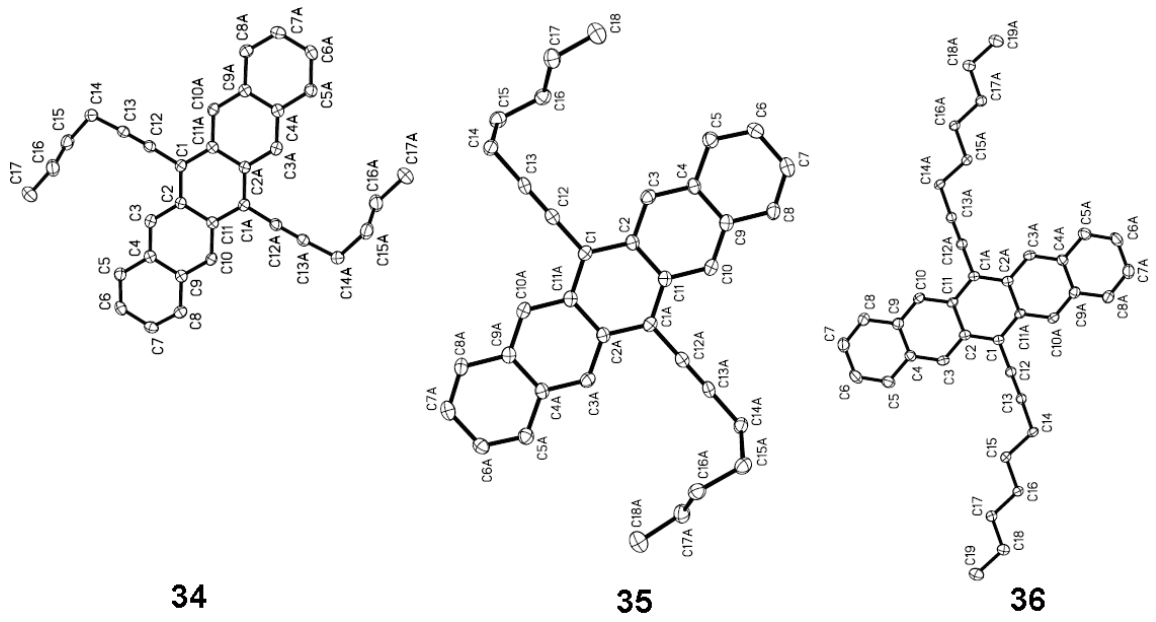

Single-crystal XRD studies reveal that **34** adopts a one-dimensional pi-stacking arrangement with the closest interatomic carbon-carbon distance of 3.41 Å. On the other hand, **35** and **36** didn't show any π-face interactions within the system. It is observed that as the length of the alkyl chain increases, the aryl-aryl π-face interaction becomes an aryl-alkyl interaction with no π-interactions between the neighboring molecules. In other words, longer alkyl groups act as an insulating layer between the π-systems (see Fig. 2.7). 35 is found to be the most unstable derivative in the solid state due to close interaction between the rigid aromatic core and the ethynyl spacer.

Figure 2.7 π-Stacking of Alkynyl Pentacenes: a. Hexynyl Pentacene (34), b. Heptynyl Pentacene (35), c. Octynyl Pentacene (36).

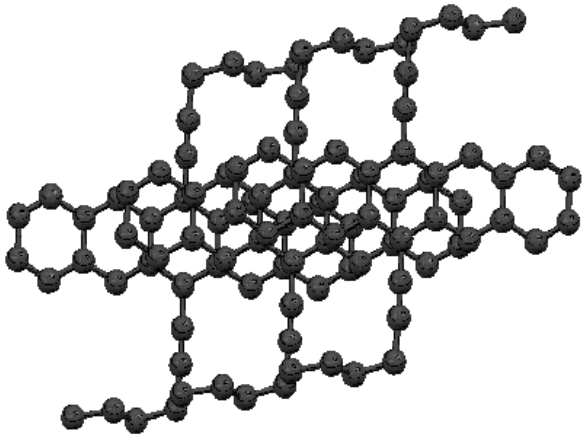

34

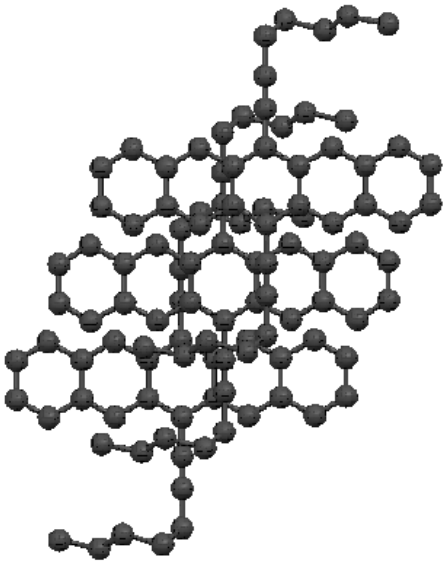

35

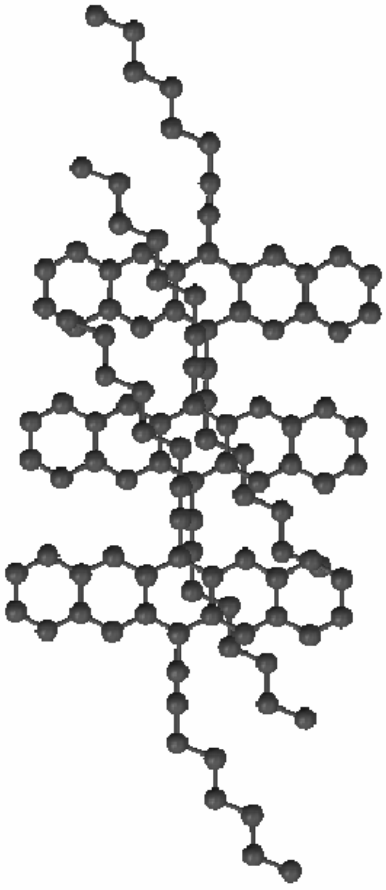

36

Figure 2.8 UV-vis absorption spectra of 34 and 53.

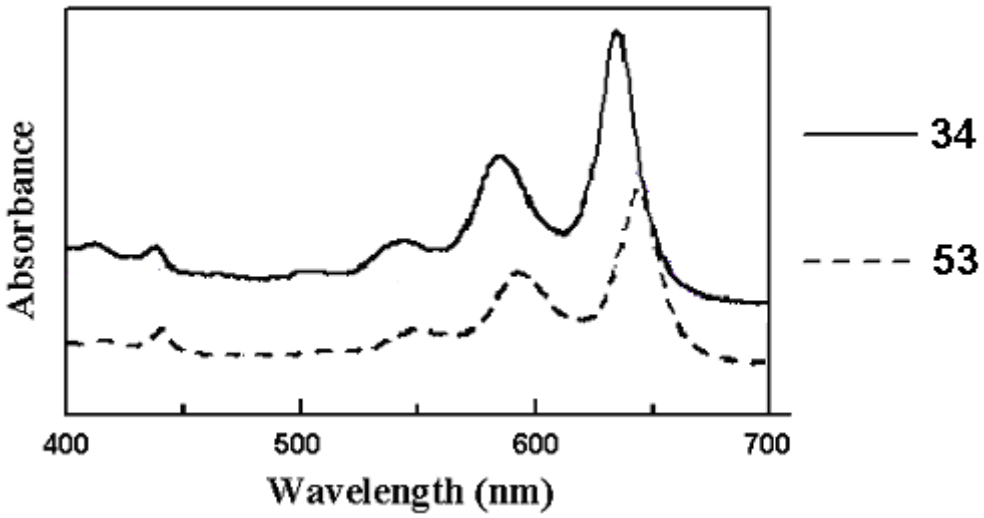

Figure 2.9 Electrochemistry of 34 (Ferrocene was used as an internal standard. Cyclic Voltammetry experiment was carried out using 0.1 M solution of Bu_4NPF_6 in dichloromethane as an electrolyte with the scan rate of 150 mV / s.**)**

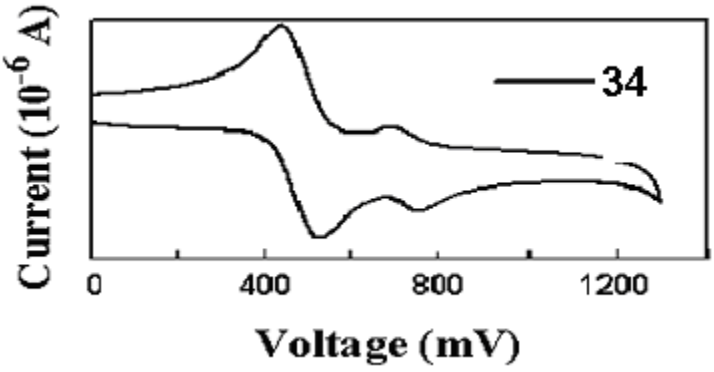

The UV-vis absorption spectra of 6,13-alkynyl pentacenes recorded in dichlormethane show a characteristic maximum long wavelength absorption (λ_{max}) of 635 nm (see Fig. 2.8) and the electrochemical measurements demonstrate that these alkynyl pentacene derivatives exhibit a reversible oxidation centered at 0.72 V vs SCE (see Fig. 2.9).

The possible explanation for the relatively low stability of 6,13-di(alkynyl) pentacene derivatives (**34 - 38**) could be due to either endo-peroxide formation, the dimerization of π-electronic core, or intermolecular reaction between the alkyne and the aromatic core. From our group's earlier empirical model for peri-functionalizing pentacene,[40] it is understood that we need to have bulky groups at the peri-positions of pentacene in order to avoid the possible degradation pathways, hence, improving the stability of the acenes. Keeping this concept in mind, my next strategy

Figure 2.10 Alternative Route to Induce Liquid Crystallinity to Pentacene.

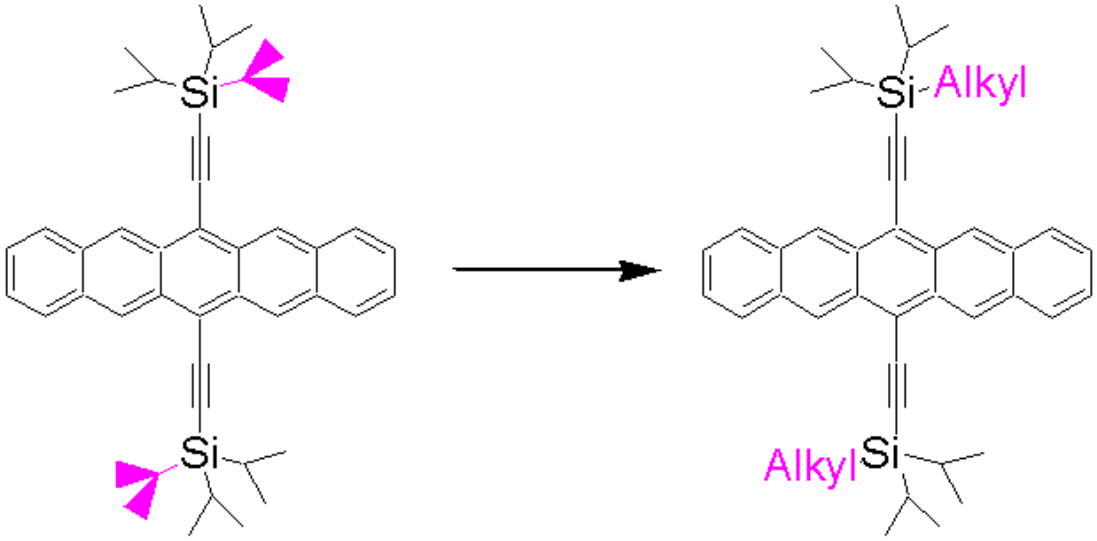

to synthesize stable functionalized pentacenes with liquid crystallinity was to introduce bulky silyl groups at the peri-positions of the acene chromophore. Having shown high stability, solubility in most organic solvents and strong π-stacking between the neighboring molecules, **19** has become an excellent benchmark molecule for the *peri*-functionalization of the acene ring chromophores. In order to induce the liquid

crystallinity into the system, I replaced one of the isopropyl groups of the silyl ball in **19** with a flexible alkyl group, varying the alkyl chain length as shown in Fig. 2.10.

Scheme 2.2 Synthesis of Diisopropylalkyl Silyl Pentacenes.

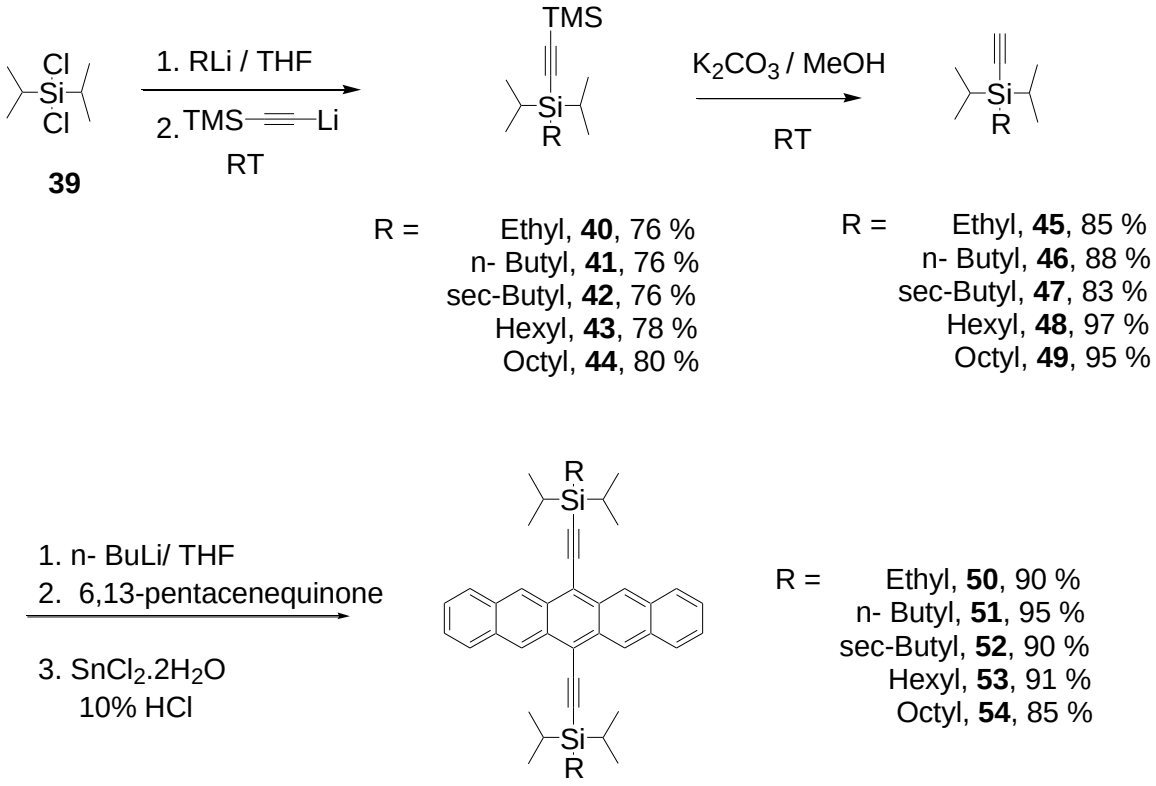

2.4 Diisopropylalkylsilyl Pentacenes

Acene derivatives (**50** - **54**) are made in a four-step process starting from dichlorodiisopropyl silane (**39**) as shown in Scheme 2.2. Addition of equimolar quantities of alkyl lithium and lithium trimethylsilyl acetylide to **39** is the key to generate trimethylsilyl protected diisopropylalkyl silyl acetylenes (**40** - **44**) in good yields. Subsequent deprotection of trimethylsilyl groups from **40** - **44** using potassium carbonate in methanol yields silyl acetylenes **45** - **49** in very good yields. The desired functionalized pentacene derivatives (**50** - **54**) were made using a similar approach to that used for

synthesizing alkynyl pentacenes (**34 - 38**). For purification, elution of the reaction mixture through a silica gel pad was carried out using hexanes / dichloromethane.

Figure 2.11 Thermal ellipsoid plots of 50, 51, 53 and 54.

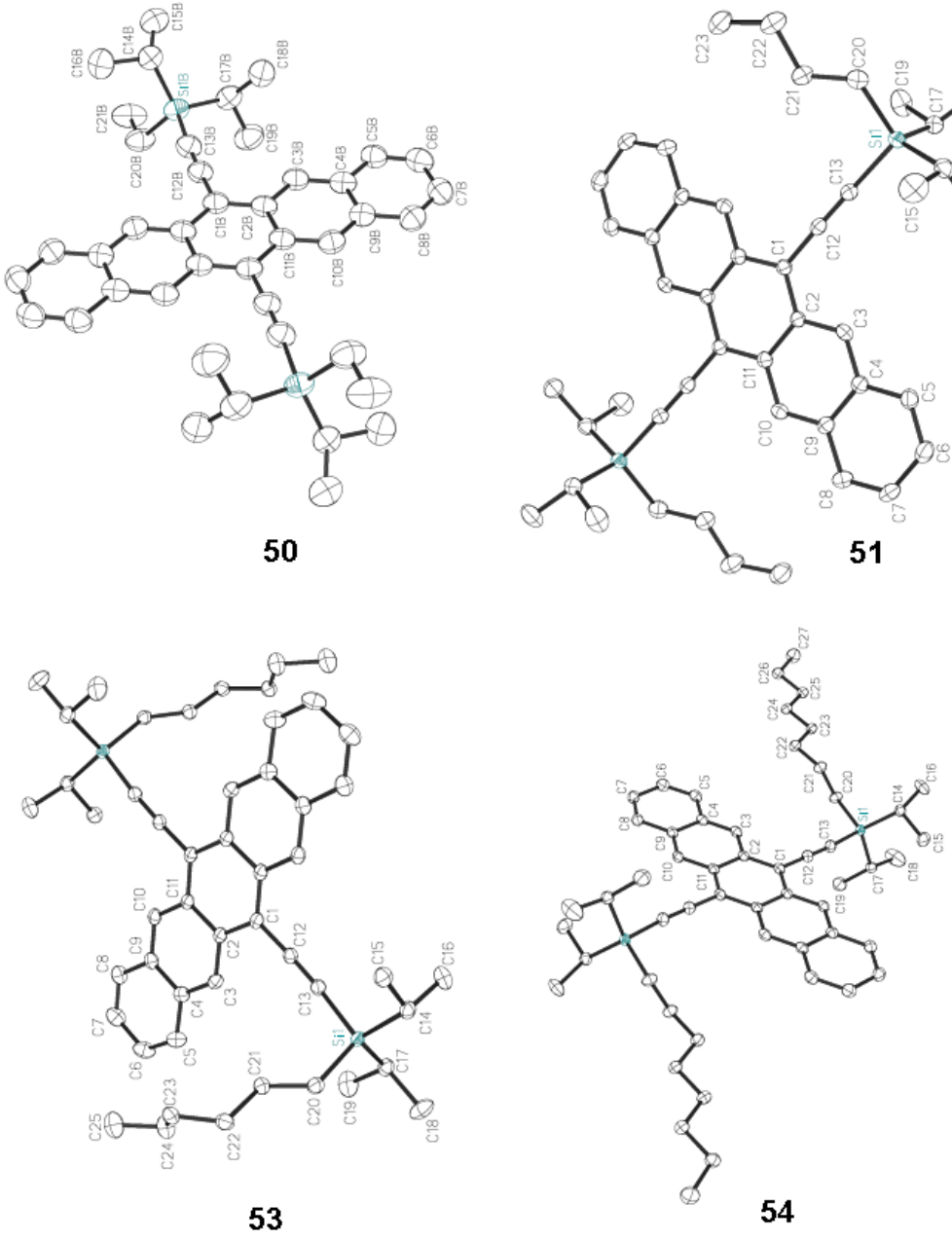

solvent mixture. Evaporation of solvent followed by recrystallization in hexanes produced **50** - **54** as dark blue crystals, which were then analyzed by X-ray

Figure 2.12 π-Stacking of Diisopropylalkyl Silyl Pentacenes.

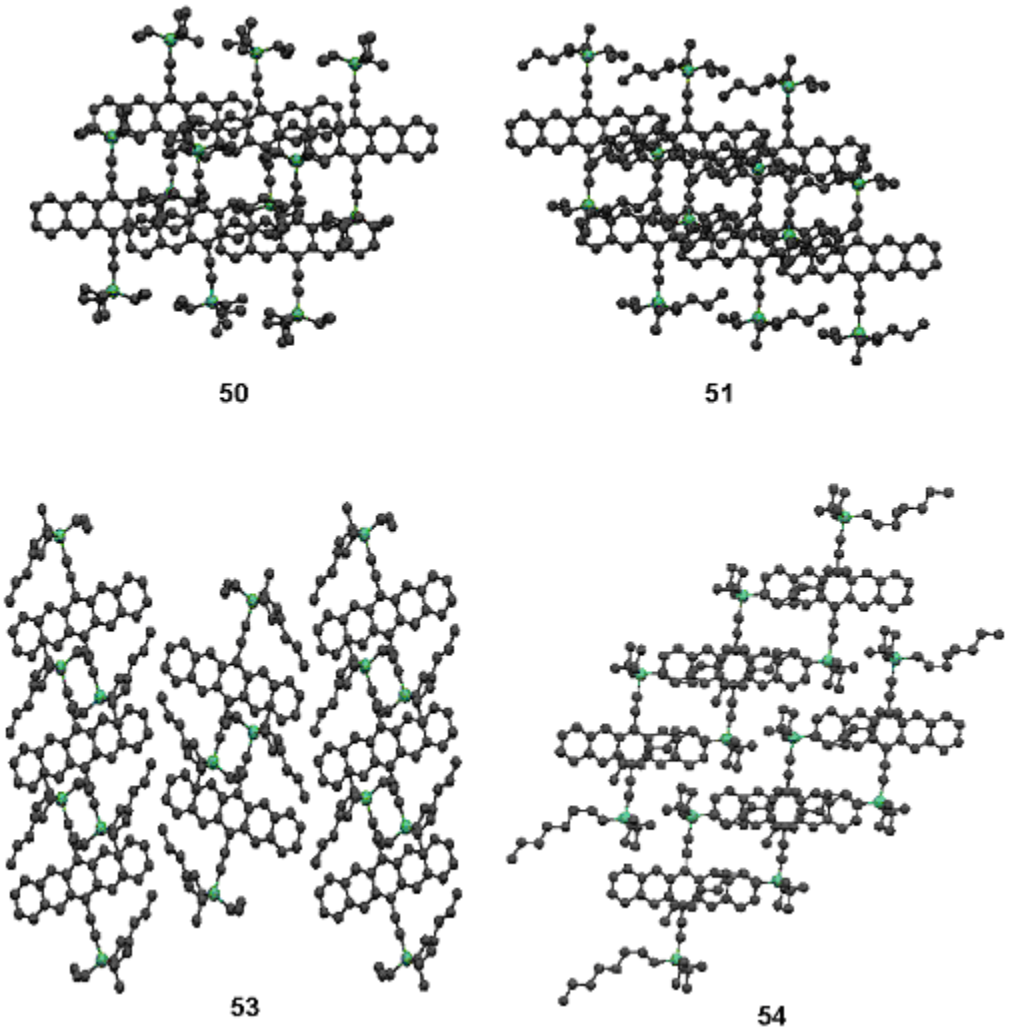

crystallography. They are observed to be highly stable both in solutions and in their crystalline forms.

Single-crystal XRD studies reveal that both **50** and **51** adopt one-dimensional π-stacking arrangements with the closest carbon-carbon contact distance of 3.39 and 3.44 Å respectively. However, as the alkyl chain length on the silyl group increases, alkyl-aryl

interactions again dominate, as seen in the functionalized pentacene derivatives **53** and **54** (see Fig. 2.11 and 2.12). Unfortunately, crystal packing of **52** couldn't be derived since it didn't diffract well during the XRD study. UV-vis spectroscopy and cyclic voltammetry studies report that these 6,13-bis(diisopropylalkylsilylethynyl) pentacenes show a maximum absorption peak (λ_{max}) of 645 nm and an oxidation potential of 0.84 V vs SCE respectively, similar to **19** (see Fig. 2.13).

Figure 2.13 Electrochemistry of 53 (Ferrocene was used as an internal standard. Cyclic Voltammetry experiment was carried out using 0.1 M solution of Bu_4NPF_6 in dichloromethane as an electrolyte with the scan rate of 150 mV / s.**)**

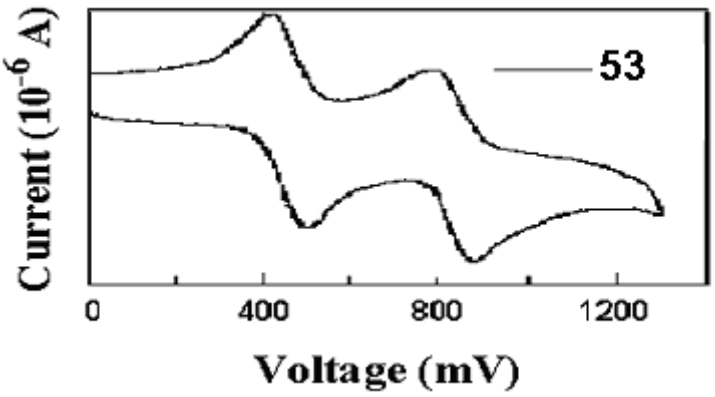

The thermal and morphological studies on the pentacene derivatives I synthesized were done by the Martin group at the University of Michigan, Ann Arbor. Study on thermal stability of these functionalized pentacenes **34 - 38** and **50 - 54** were carried out by Differential Scanning Calorimetry (DSC). It was observed that all the alkynyl pentacenes (**34 - 38**) tend to decompose before melting, at temperatures below 150°C (Fig. 2.14). Also, as the length of the alkyl chain increases the decomposition point decreases. This

Figure 2.14 DSCs of 6,13-di(alkynyl) pentacenes (34 - 38).

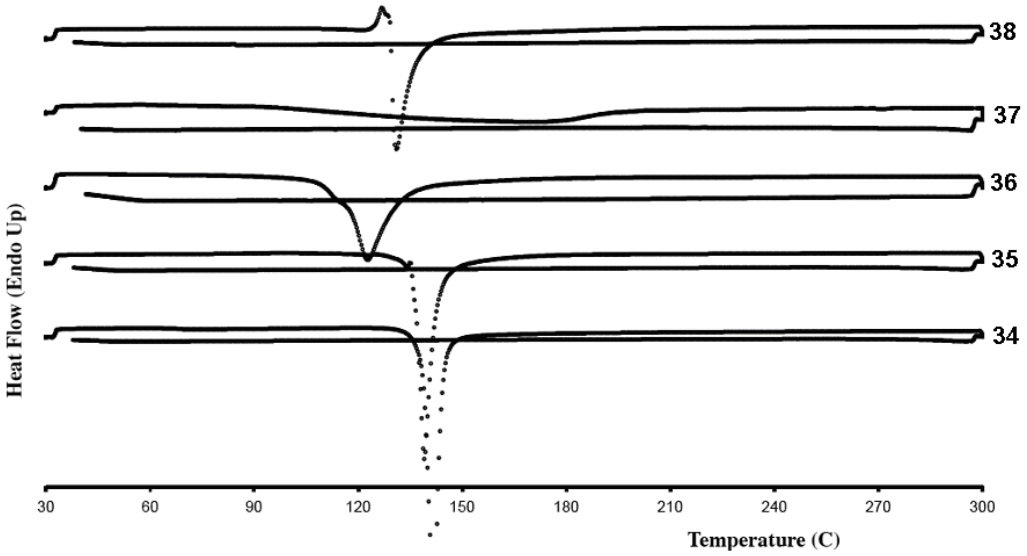

Figure 2.15 DSCs of 6,13-bis(diisopropylalkylsilylethnyl) pentacenes 50 - 54 and 19.

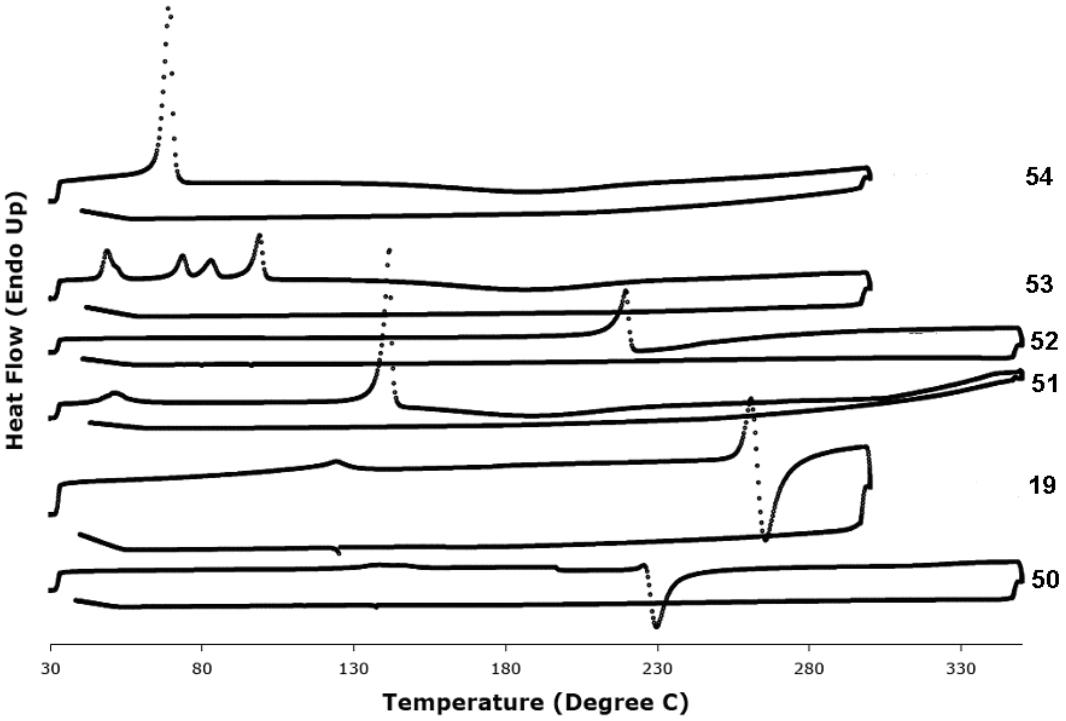

result correlates well with our earlier observation from the single-crystal XRD studies that alkyl-aryl interactions become predominant as the length of the alkyl chain increases.

The presence of silyl groups on the acenes helped to improve their thermal stability which was demonstrated by DSCs of **50**, **19** and **52** with melting points of 226 °C, 263 °C and 220 °C respectively (Fig. 2.15). As the alkyl chain length on the silyl group increases the melting point can decrease dramatically as shown by acenes **51**, **53** and **54,** which melt at 142°C, 99°C and 68°C respectively. The decrease in melting point also correlates with a decrease in the amount of π-stacking observed in the crystals. It is also noticed that **19**, **51** and **53** exhibit one or more sub-melting phase transitions. Especially, **53** shows three sub-melting phase transition before its melting point which suggested the possibilities of thermotropic crystalline phases.

Figure 2.16 Proposed pathway of decomposition.

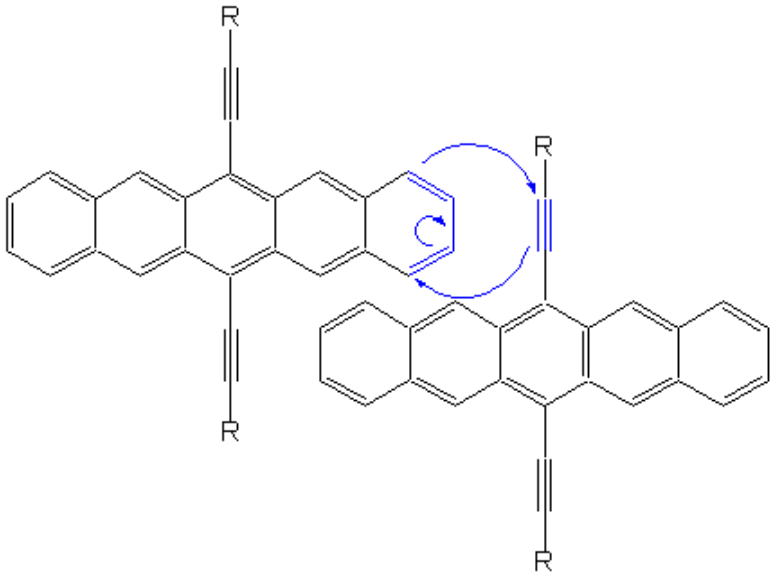

R = silyl group

The DSCs on diisopropylalkylsilyl pentacenes (**50 - 54**) also reveal the fact that those molecules with low melting point, show a broad decomposition point centered at 180 °C. This could possibly be due to a Diels-Alder reaction between the ethynyl portion of one molecule and the pentacene chromophore of the other molecule in the melt as shown in Fig. 2.16. The acenes which have high melting point decompose immediately upon melting, which could be explained by the ability of molecules in the melt to arrange themselves in such a way to undergo Diels-Alder reaction. The reversibility of heating curve of all these pentacene derivatives (**50 - 54**) was noticed if they are heated only up to 150°C. Thin film morphology of alkynyl (**34 - 38**) and diisopropylalkylsilylethynyl pentacenes (**50 - 54**) were studied by solution casting them in THF on a clean glass slide. From the bright-field transmission electron microscopy (TEM) and optical microscopy data, it was observed that **51, 52** and **53** form larger crystalline domains than **50** and **54**, suggesting that the π-stacking solid state arrangement in the crystal is affected by too long (octyl) or too short (ethyl) alkyl groups.

Figure 2.17 Optical micrographs of the functionalized pentacene thin films made of 35 and 53.

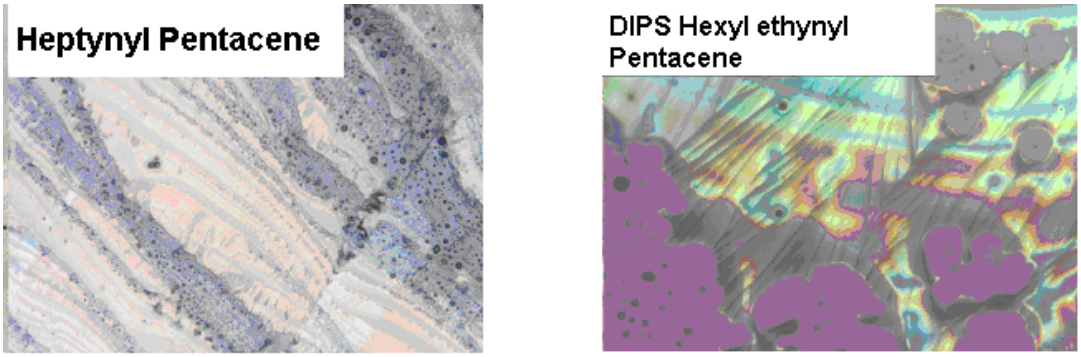

The effect of evaporation rate on the thin film morphology was studied by two different sets of experiments. One is with a cover on the as-deposited film and the other is without the cover on. For both alkynyl and diisopropylalkylsilyl pentacenes, uncovered drying was found to be more advantageous since prolonged existence of molecules in solution (in air) led to decomposition. Hence, higher evaporation rate is required to form crystalline films. Optical micrographs reveal that diisopropylalkylsilyl pentacenes form birefringent crystalline thin films. On the other hand, alkynyl pentacenes form non-birefringent amorphous thin films (see Fig. 2.17).

This project demonstrated that 6,13-di(alkynyl) pentacene derivatives (**34 - 38**) are stable enough to do UV, NMR and electrochemical studies, and a number of derivatives could also be analyzed through single crystal XRD. We observed that their stability decreases as the alkyl chain lengths increase. My approach to use the silyl groups dramatically improved the stability of the molecules. Even though the possibility of thermotropic liquid crystalline phases could be observed from the DSC of **53**, due to the lack of any π-stacking interactions, it is not a suitable organic semiconductor for high performance electronic devices.

2.5 Experimental Details

General Procedure for 6,13-di(Alkynyl) Pentacene.

To an oven dried 100 mL single necked round bottom flask, n-BuLi (2.5 mmol) was added slowly to 1-alkyne (4.6 mmol) in dry THF (25 mL) under N_2 atm and stirred for 40 minutes at RT. Then, **33** (0.25 g, 0.8 mmol) was added very quickly, to avoid quenching of the lithium acetylide by moisture in air, and the mixture was stirred

overnight at RT. The next day, stannous chloride dihydrate (2 mmol) followed by 10% HCl (2mL) was added and the reaction mixture was stirred for 7 hrs. It was then extracted into hexanes, washed with saturated brine solution, dried over anhydrous $MgSO_4$ and concentrated. The crude products were purified by silica plug using hexanes / methylene chloride (9 / 1).

6,13–di(hexynyl) Pentacene (34). Yield = 0.28 g (80 %), M. P. = 83 °C (dec). ^{1}H NMR (200 MHz, $CDCl_3$): δ 1.15 (t, J = 7.2 Hz, 6H), 1.74-1.99 (m, 8H), 2.95 (t, J = 6.8 Hz, 4H), 7.39 (dd, J = 3.0 Hz, J = 6.6 Hz, 4H), 8.01 (dd, J = 3.0 Hz, J = 6.4 Hz, 4H), 9.18 (s, 4H) ppm. ^{13}C NMR (50 MHz, $CDCl_3$): δ 13.93, 20.46, 25.52, 31.43, 79.11, 105.69, 118.52, 125.92, 126.34, 128.94, 130.73, 132.32 ppm. MS (EI 70 eV) *m/z* 438 (100 %, M^+), 395 (35 %, M^+ - Propyl).

6,13–di(heptynyl) Pentacene (35). Yield = 0.28 g (75 %), M. P. = 115 °C. ^{1}H NMR (200 MHz, $CDCl_3$): δ 1.06 (t, J = 7.2 Hz, 6H), 1.50-1.61 (m, 4H), 1.7 (quintet, J = 7.0 Hz, 4H), 1.97 (quintet, J = 7.0 Hz, 4H), 2.94 (t, J = 6.8 Hz, 4H), 7.39 (dd, J = 2.8 Hz, J = 6.8 Hz, 4H), 8.01 (dd, J = 3.2 Hz, J = 6.4 Hz, 4H), 9.20 (s, 4H) ppm. ^{13}C NMR (50 MHz, $CDCl_3$): δ 14.31, 20.76, 22.57, 29.03, 31.66, 79.13, 105.78, 118.54, 125.94, 126.35, 128.93, 130.76, 132.34 ppm. MS (EI 70 eV) *m/z* 466 (100 %, M^+), 409 (20 %, M^+ - Butyl).

6,13–di(octynyl) Pentacene (36). Yield = 0.25 g (62 %), ^{1}H NMR (200 MHz, $CDCl_3$): δ 0.99 (t, J = 6.7 Hz, 6H), 1.4–1.6 (m, 8H), 1.77 (quintet, J = 6.6 Hz, 4H), 1.96 (quintet, J = 7.06 Hz, 4H), 2.95 (t, J = 6.8 Hz, 4H), 7.39 (dd, J = 3.0 Hz, J = 6.7 Hz, 4H), 8.01 (dd, J = 3.1 Hz, J = 6.6 Hz, 4H), 9.21 (s, 4H) ppm. ^{13}C NMR (50 MHz, $CDCl_3$): δ 14.30, 20.81,

22.92, 29.17, 29.33, 31.74, 79.13, 105.81, 115.59, 126, 126.42, 128.99, 130.82, 132.4 ppm. MS (EI 70 eV) *m/z* 494 (95 %, M^+).

6,13–di(decynyl) Pentacene (37). Yield = 0.25 g (56 %). ^{1}H NMR (200 MHz, $CDCl_3$): δ 0.91 (t, J = 6.6 Hz, 6H), 1.25–1.6 (m, 16H), 1.77 (quintet, J = 6.7 Hz, 4H), 1.96 (quintet, J = 7.06 Hz, 4H), 2.94 (t, J = 7.0 Hz, 4H), 7.39 (dd, J = 3.2 Hz, J = 6.8 Hz, 4H), 8.02 (dd, J = 3.4 Hz, J = 6.6 Hz, 4H), 9.20 (s, 4H) ppm. ^{13}C NMR (50 MHz, $CDCl_3$): δ 14.23, 20.81, 22.88, 29.37, 29.52, 29.59, 32.11, 79.15, 105.8, 118.55, 125.91, 126.35, 128.93, 130.76, 132.33 ppm. MS (EI 70 eV) *m/z* 445 (25 %), 429 (45 %), 308 (100 %).

6,13–di(dodecynyl) Pentacene (38). Yield = 0.3 g (61 %). ^{1}H NMR (200 MHz, $CDCl_3$): δ 0.87 (t, J = 6.6 Hz, 6H), 1.20–1.60 (m, 24H), 1.77 (quintet, J = 7.0 Hz, 4H), 1.96 (quintet, J = 7.06 Hz, 4H), 2.94 (t, J = 6.8 Hz, 4H), 7.39 (dd, J = 3.0 Hz, J = 6.6 Hz, 4H), 8.02 (dd, J = 3.0 Hz, J = 6.6 Hz, 4H), 9.20 (s, 4H) ppm. ^{13}C NMR (50 MHz, $CDCl_3$): δ 14.23, 20.81, 22.85, 29.37, 29.55, 29.87, 29.93, 32.09, 79.14, 105.79, 118.54, 125.91, 126.36, 128.94, 130.76, 132.33 ppm. MS (EI 70 eV) *m/z* 606 (20 %, M^+), 479 (20 %, M^+ -Nonyl).

General procedure for TMS protected diisopropylalkyl silyl acetylene.

In a flame dried 250 mL single necked round bottom flask, trimethylsilyl acetylene (32.4 mmol) was dissolved in dry THF under N_2 atm. To that, n-BuLi (27 mmol) was added slowly at room temperature. The mixture was stirred for 5-6 hrs. In another flame dried 250 mL single necked round bottom flask, **39** (27 mmol) was dissolved in dry THF under N_2 atm. To that, alkyl lithium (27 mmol) was added slowly and the mixture stirred at RT. After 5-6 hrs, lithium trimethylsilyl acetylide was added by cannula. After overnight stirring, the reaction mixture was quenched with DI water carefully and

extracted with hexanes, washed with saturated brine solution, dried over anhydrous $MgSO_4$ and concentrated. The crude compounds were purified by silica plug using hexanes (75 mL).

Trimethylsilylethynyl diisopropylethyl silane (40). Yield = 76%. ^{1}H NMR (400 MHz, $CDCl_3$): δ 0.19 (s, 9H), 0.55–0.69 (m, 2H), 0.5–1.00 (m, 17H) ppm. ^{13}C NMR (100 MHz, $CDCl_3$): δ 0.25, 2.07, 8.29, 11.64, 18.21, 18.44, 110.37, 116.23 ppm. MS (EI 70 eV) *m/z* 218, 207 (M^+ - isopropyl).

Trimethylsilylethynyl diisopropyln-butyl silane (41). Yield = 76%. ^{1}H NMR (200 MHz, $CDCl_3$): δ 0.22 (s, 9H), 0.58-0.72 (m, 2H), 0.90–1.02 (m, 3H), 1.02–1.18 (m, 12H), 1.30–1.53 (m, 4H) ppm. ^{13}C NMR (50 MHz, $CDCl_3$): δ 0.22, 9.91, 11.83, 13.93, 17.58, 18.24, 18.45, 26.79, 26.88, 110.94, 116.35 ppm. MS (EI 70 eV) *m/z* 268 (M^+), 225 (M^+ - isopropyl).

Trimethylsilylethynyl diisopropyl *sec*-butyl silane (42). Yield = 76%. ^{1}H NMR (400 MHz, $CDCl_3$): δ 0.19 (s, 9H), 0.78–0.94 (m, 2H), 1.00 (t, J = 7.2 Hz, 3H), 1.03–1.18 (m, 15H), 1.20–1.34 (m, 2H), 1.66–1.78 (m, 1H) ppm. ^{13}C NMR (100 MHz, $CDCl_3$): δ 0.25, 11.36, 11.38, 13.89, 14.40, 14.56, 18.72, 18.83, 19.06, 25.53, 110.66, 116.37 ppm. MS (EI 70 eV) *m/z* 268 (M^+), 225 (M^+ - isopropyl).

Trimethylsilylethynyl diisopropylhexyl silane (43). Yield = 78%. ^{1}H NMR (200 MHz, $CDCl_3$): δ 0.18 (s, 9H), 0.53–0.70 (m, 2H), 0.91 (t, J = 6.6 Hz, 3H), 0.98–1.12 (m, 16H), 1.20–1.50 (m, 6H) ppm. ^{13}C NMR (50 MHz, $CDCl_3$): δ 0.11, 10.12, 11.76, 14.25, 18.04, 18.15, 18.36, 22.79, 24.44, 31.71, 33.56, 110.76, 116.18 ppm. MS (EI 70 eV) *m/z* 296 (M^+), 253 (M^+ - isopropyl).

Trimethylsilylethynyl diisopropyloctyl silane (44).

In a dried single necked 250 mL RBF, n-BuLi (10.14 mmol) was added to trimethylsilyl acetylene (10.14 mmol) in dry THF slowly. After stirring for 30 minutes at RT, chloro diisopropyloctyl silane (11.16 mmol, purchased from Gelest, Inc.) was added and the mixture stirred at RT overnight. The reaction mixture was extracted into hexanes and purified silica chromatography using hexanes. Yield = 80%. ^{1}H NMR (200 MHz, $CDCl_3$): δ 0.18 (s, 9H), 0.61 (t, J = 8.0 Hz, 2H), 0.9 (m, 6H), 1.05 (m, 15H), 1.29 (m, 10H) ppm. ^{13}C NMR (50 MHz, $CDCl_3$): δ 0.16, 10.14, 11.65, 11.77, 11.88, 14.28, 18.09, 18.19, 18.28, 18.40, 22.40, 24.49, 29.49, 32.18, 33.94, 110.83, 116.23 ppm. MS (EI 70 eV) *m/z* 324 (M^+), 281 (M^+ - isopropyl).

General procedure for the deprotection of the trimethylsilyl group.

The TMS-protected alkyne (6.7 mmol) was dissolved in methanol (50 mL) in a 250 mL RBF. To that, potassium carbonate (7.25 mmol) was added and the mixture stirred for 2 hours at RT. The reaction mixture was taken up in excess hexane and washed with DI water and brine solution, dried over anhydrous $MgSO_4$ and concentrated. Finally, the compounds were purified by silica chromatography using hexanes (75 mL).

Diisopropylethylsilyl acetylene (45). Yield = 85%. ^{1}H NMR (200 MHz, $CDCl_3$): δ 0.55–0.75 (m, 2H), 0.90–1.15 (m, 17H), 0.04 (s, 1H) ppm. ^{13}C NMR (50 MHz, $CDCl_3$): δ 1.91, 8.05, 11.43, 17.98, 18.20, 18.55, 86.38, 94.83 ppm. MS (EI 70 eV) *m/z* 168 (M^+), 125 (M^+ - isopropyl).

Diisopropyl n-butylsilyl acetylene (46). Yield = 88%. ^{1}H NMR (200 MHz, $CDCl_3$): δ 0.60–0.80 (m, 2H), 0.90–1.05 (m, 4H), 1.06-1.20 (m, 12H), 1.30 – 1.55 (m, 5H), 2.38 (s,

1H) ppm. ^{13}C NMR (50 MHz, $CDCl_3$): δ 9.80, 11.65, 13.81, 17.77, 18.04, 18.23, 26.67, 26.89, 86.72, 94.80 ppm. MS (EI 70 eV) *m/z* 196 (M^+), 153 (M^+ - isopropyl).

Diisopropyl *sec*-butyl silylacetylene (47). Yield = 83%. ^{1}H NMR (400 MHz, $CDCl_3$): δ 0.80–0.90 (m, 2H), 0.96–1.02 (m, 3H), 1.02–1.14 (m, 15H), 1.18–1.32 (m, 2H), 1.66–1.78 (m, 1H), 2.35 (s, 1H) ppm. ^{13}C NMR (100 MHz, $CDCl_3$): δ 11.25, 13.83, 14.37, 18.68, 18.70, 18.72, 18.94, 25.37 86.62, 95.00 ppm. MS (EI 70 eV) *m/z* 196 (M^+), 153 (M^+ - isopropyl).

Diisopropylhexylsilyl acetylene (48). Yield = 97%. ^{1}H NMR (200 MHz, $CDCl_3$): δ 0.55–0.70 (m, 2H), 0.90 (t, J = 6.0 Hz, 3H), 0.97-1.15 (m, 16H), 1.20–1.50 (m, 6H), 2.34 (s, 1H) ppm. ^{13}C NMR (50 MHz, $CDCl_3$): δ 10.09, 11.63, 14.23, 18.03, 18.23, 22.80, 24.40, 31.69, 33.66, 86.67, 94.78 ppm. MS (EI 70 eV) *m/z* 224 (M^+), 181 (M^+ - isopropyl).

Diisopropyloctylsilyl acetylene (49). Yield = 95%. ^{1}H NMR (200 MHz, $CDCl_3$): δ 0.64 (m, 2H), 0.9 (m, 3H), 1.00-1.12 (m, 14H), 1.24-1.50 (m, 12H), 2.35 (s, 1H) ppm. ^{13}C NMR (50 MHz, $CDCl_3$): δ 10.89, 11.63, 11.86, 14.25, 18.06, 18.18, 18.26, 18.41, 22.87, 24.42, 29.41, 29.47, 32.14, 33.99, 88.81, 94.78 ppm. MS (EI 70 eV) *m/z* 252 (M^+), 209 (M^+ - isopropyl).

Synthesis of Diisopropylalkylsilyl Ethynyl Pentacene.

In a flame dried 500 mL single necked round bottom flask, diisopropylalkyl silyl acetylene (8 mmol) was dissolved in 50 mL of hexanes under N_2 atm. To that, n-BuLi (4.87 mmol) was added slowly at RT and allowed to stir for 30-45 min. Then, pentacenequinone (1.6 mmol) followed by 150 ml of hexane was added to the reaction mixture which was heated to 65 $^{\circ}$C overnight. The next day, 0.5 mL of DI water, 1.5 mL

of 10% HCl and tin(II)chloride dihydrate (4 mmol) was added to the reaction mixture and stirred at 65 °C for 6-7 h. The reaction mixture was cooled and dried with anhydrous $MgSO_4$, purified through silica plug using hexane/ dichloromethane (9/1) solvent system and concentrated.

6,13-Bis(diisopropylethylsilylethynyl) pentacene (50). Yield = 90 %. ^{1}H NMR (200 MHz, $CDCl_3$): δ 0.90-1.10 (m, 4H), 1.26-1.44 (m, 34H), 7.43 (dd, J = 3.2 Hz, J = 6.8 Hz, 4H), 8.00 (dd, J = 3.2 Hz, J = 6.6 Hz, 4H), 9.31 (s, 4H) ppm. ^{13}C NMR (50 MHz, $CDCl_3$): δ 2.55, 8.74, 12.18, 18.57, 18.86, 104.89, 107.51, 118.65, 126.32, 126.61, 128.99, 130.94, 132.64 ppm. MS (EI 70 eV) *m/z* 611 (56 %, M^+).

6,13-Bis(diisopropyl n-butylsilylethynyl) pentacene (51). Yield = 95 %. ^{1}H NMR (200 MHz, $CDCl_3$): δ 0.96-1.04 (m, 8H), 1.29-1.46 (m, 30H), 1.50-1.60 (m, 4H), 1.70-1.80 (m, 4H), 8.00 (m, 4H), 7.43 (m, 4H), 9.31 (s, 4H) ppm. ^{13}C NMR (50 MHz, $CDCl_3$): δ 10.28, 12.29, 14.10, 18.57, 18.84, 27.05, 27.28 104.64, 107.62, 118.46, 126.18, 126.44, 128.80, 130.75, 132.44 ppm. MS (EI 70 eV) *m/z* 667 (65 %, M^+), 610 (20 %, M^+ - Butyl).

6,13-Bis(diisopropyl *sec*-butylsilylethynyl) pentacene (52). Yield = 90 %, ^{1}H NMR (200 MHz, $CDCl_3$): δ 1.2 (m, 8H), 1.4 (m, 32H), 1.58 (m, 4H), 2.03-2.09 (m, 2H), 7.44 (m, 4H), 8.00 (m, 4H), 9.32 (s, 4H) ppm. ^{13}C NMR (50 MHz, $CDCl_3$): δ 11.89, 14.13, 14.95, 19.22, 19.15, 19.30, 19.54, 25.93, 104.94, 107.70, 118.58, 126.23, 126.53, 128.88, 130.85, 132.47 ppm. MS (EI 70 eV) *m/z* 667 (68 %, M^+), 610 (20 %, M^+ - sec-Butyl).

6,13-Bis(diisopropylhexylsilylethynyl) pentacene (53). Yield = 91 %. ^{1}H NMR (200 MHz, $CDCl_3$): δ 0.90 (m, 12H), 1.35 (m, 38H), 1.76 (m, 4H), 7.45 (m, 4H), 8.00 (m, 4H), 9.30 (m, 4H) ppm. ^{13}C NMR (50 MHz, $CDCl_3$): δ 10.68, 12.38, 14.38, 18.65, 18.92,

22.92, 25.11, 31.92, 33.90, 104.74, 107.71, 118.55, 126.22, 126.53, 128.89, 130.82, 132.50 ppm. MS (EI 70 eV) *m/z* 723 (68 %, M^+), 638 (10 %, M^+ - Hexyl).

6,13-Bis(diisopropyloctylsilylethynyl) pentacene (54). Yield = 85 %. ^{1}H NMR (200 MHz, $CDCl_3$): δ 0.92(m, 10H), 1.38 (m, 48H), 1.77(m, 4H), 7.43 (dd, J = 3.0 Hz, J = 6.6 Hz, 4H), 8.00 (dd, J = 3.2 Hz, J= 6.6 Hz, 4H), 9.30 (s, 4H) ppm. ^{13}C NMR (50 MHz, $CDCl_3$): δ 10.71, 12.42, 14.29, 18.67, 18.94, 22.88, 25.19, 29.60, 29.70, 32.22, 34.26, 104.93, 107.85, 118.71, 126.36, 126.68, 129.05, 131.00, 132.69 ppm. MS (EI 70 eV) *m/z* 779 (68 %, M^+), 666 (15 %, M^+ - Octyl).

Chapter 3: Alkyl Substituted Functionalized Anthradithiophenes

3.1 Thienyl Electronic Materials.

Recent advances in organic semiconductor research have been driven by low-cost solution-based fabrication techniques such as spin coating[84], and ink-jet printing[85] and the potential for processing on large area flexible substrates.[86] Pentacene (**18**), considered to be a benchmark molecule among organic electronic materials, has been subjected to extensive investigation due to its excellent thin film forming ability,[40] and high thin film hole mobility.[41] Very recently, extensive investigations have focused on oligothiophenes and polythiophenes, because of their formation of high charge transport TFTs. Attaching alkyl chains to the thiophene units not only improved the solubility, but also improved the thin film morphology. Halik et al. demonstrated that the longer side chains on oligothiophenes with thick alkyl intrinsic barrier (1.3 nm for decyl chain and 0.3 nm for ethyl chain) at the interface resulted in an increase in contact resistance for the top-contact devices. However, oligothiophenes with longer alkyl chains outperformed the shorter ones in a bottom-contact configuration due to reduced gate current caused by the increase in effective thickness of the gate dielectric.[87] Sirringhaus et al. showed that the thin film hole mobility of poly (3-hexylthiophene) (**16**, see Chapter **1**) increases by two orders of magnitude when the substrate is subjected to surface treatment because of improved film morphology.[88] Studies on the electrical properties of fused thienyl π-conjugated materials was pioneered by Katz and co-workers at Bell Laboratories in the late 1990s. Showing high oxidative stability, vacuum-deposited thin film of benzodithiophene dimer **4** exhibited thin film hole mobility of 0.04 cm^2/Vs.[89] However, alkyl substitution at the terminal thiophene rings didn't improve the solubility of the

parent molecule (**4**). On the other hand, alkyl substitution on anthradithiophene (**55**, a pentacene analogue where the terminal benzene rings are replaced by thiophene rings) provided promising results. Vacuum-deposited *syn*- and *anti*- mixture of 2,8-dihexylanthradithiphene (**20**) formed highly ordered poly-crystalline films on the devices, showed hole mobility as high as 0.15 cm^2/Vs.[44] Moreover, alkyl-substituted anthradithiophene was more soluble and exhibited thin film hole mobility of 0.01 - 0.02 cm^2/Vs from solution-cast films.

Figure 3.1 Unsubtituted anthradithiophene (55).

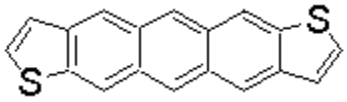

55

Recently, application of the Anthony group's *peri*-functionalization approach to anthradithiophene yielded devices with excellent transistor characteristics. TES anthradithiophene (**21**) which adopts a two-dimensional π-stacking solid state arrangement with interatomic distances as close as 3.25 Å exhibits thin film film hole mobility of 1.0 cm^2/Vs.[45] However, upon illumination, the thin film formed by **21** photobleached completely within 1h. At this point, my goal for this project is to modify **21** through systematically increasing the length of carbon chains at the 2, 8 positions in order to improve the photostability and increase the solubility in common organic solvents, thereby allowing low-cost solution-processing techniques.

3.2 Alkyl Substituted Functionalized Anthradithiophenes.

Alkyl substituted anthradithiophenes **66 - 69** are easily prepared as shown in Scheme **3.1**. Smaller alkyl groups (methyl, ethyl, propyl and butyl) were chosen for the systematic study of the effect of alkyl substitution on crystal packing and electrical properties of the acene derivatives. 5-alkyl thiophene-2,3-carboxaldehydes **58 - 61** were made in two steps starting from thiophene-2,3-dicarboxaldehyde (**56**) using previously reported methods.[44, 45] Condensation of these dialdehydes (**58 - 61**) with cyclohexane-1,4-dione yielded alkyl substituted anthradithiophene quinones (**62 - 65**) as the mixture of *syn*- and *anti*- isomers. Due to insolubility in common organic solvents, all the end-substituted anthradithiophene quinones mentioned in this dissertation were only characterized by mass spectrometry. My initial strategy was to use triethylsilyl (TES) as the *peri*-functionalizing group of anthradithiophene chromophore. Target semiconductors **66 - 69** were synthesized by the addition of lithium triethylsilyl acetylide to the quinone, followed by deoxygenation with stannous chloride / 10% sulfuric acid. All of the derivatives were purified by silica gel chromatography followed by multiple recrystallizations from hexanes.

Scheme 3.1 Synthesis of alkylated TES anthradithiophenes (66 - 69).

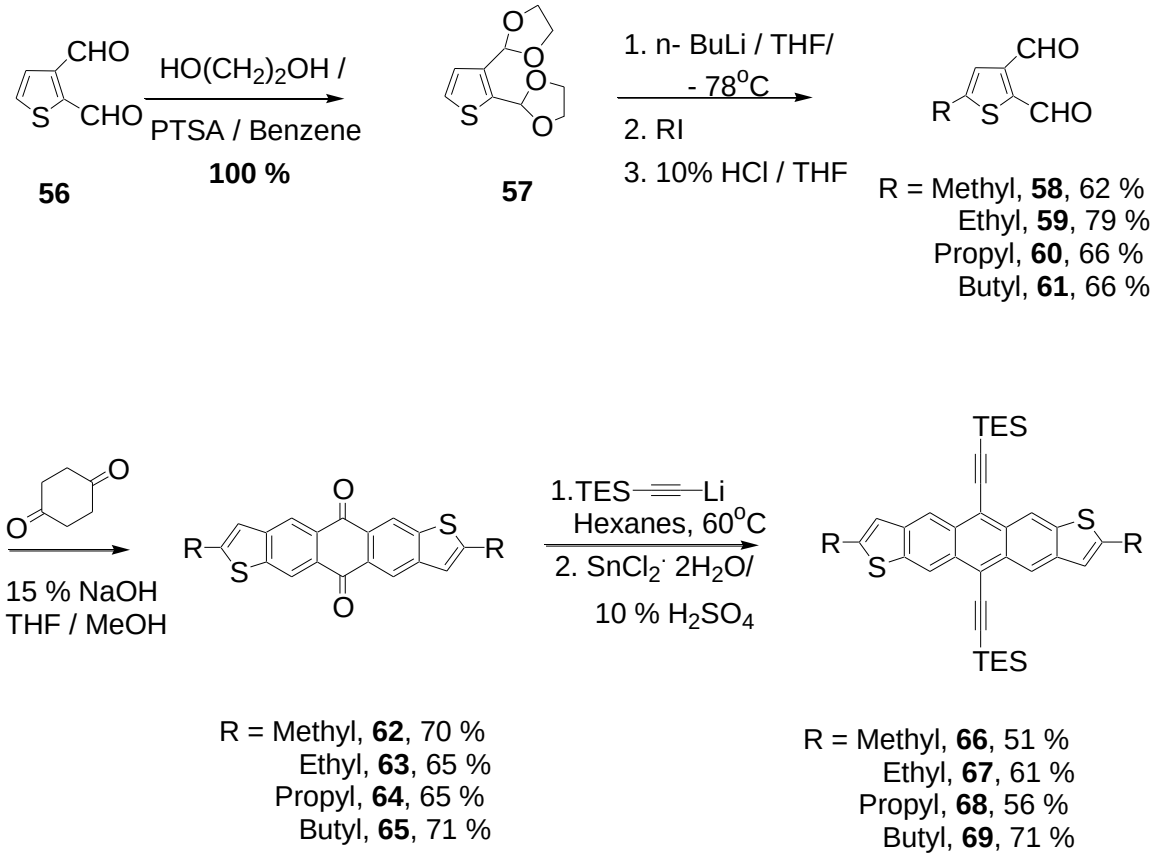

High-quality single crystals of anthradithiophenes **66 - 69** were easily grown from hexanes, and their solid state arrangements were studied by single crystal X-ray diffraction. Thermal ellipsoid plots of **66 - 69** and pi-stacking solid state arrangements of **66 - 68** are shown in Fig. 3.2 and Fig. 3.3, respectively. Ethyl-substituted triethylsilylethynyl anthradithiophene (**67**) exhibits a one-dimensional slipped π-stacked arrangement with an inter-stack carbon-carbon (C-C) distance of 3.84 Å and the closest contact distance of 3.49 Å within the π-stack (intra-stack).

Figure 3.2 Thermal ellipsoid plots of 66 - 69.

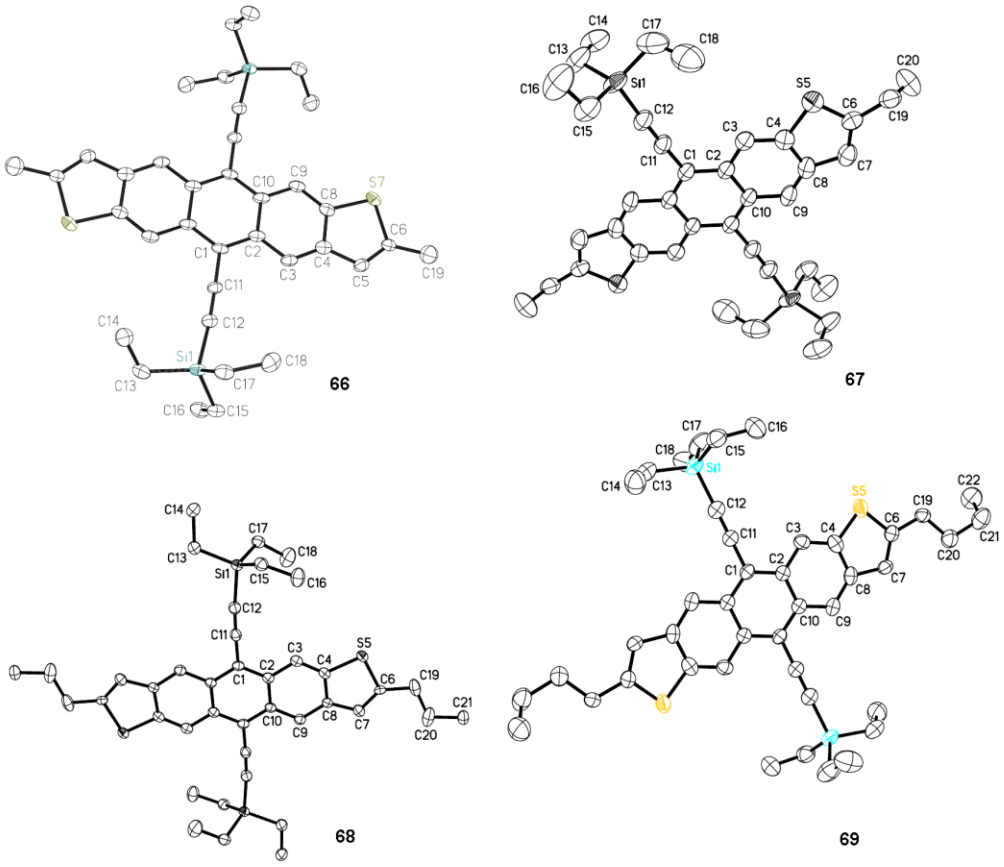

Propyl-substituted anthradithiophene (**68**) adopts a two-dimensional stacking motif, showing very weak π-interactions between the neighboring molecules with 3.62 Å inter-stack contacts and 3.95 Å intra-stack contacts - well outside the van der Waals radius for carbon. Interestingly, methyl-substituted acene derivative (**66**) adopts π-stacking arrangement somewhere between a strict one-dimensional slipped π-stack (**67)** and two-dimensional order (e.g. **21**). Even though both **66** and **67** have similar crystal packing in the solid state, the major difference comes from the distance between the neighboring acene chromophores in the 1-D pi-stacks. The contact distance between two acene cores

Figure 3.3 Solid state pi-stacking arrangement for 66, 67 and 68.

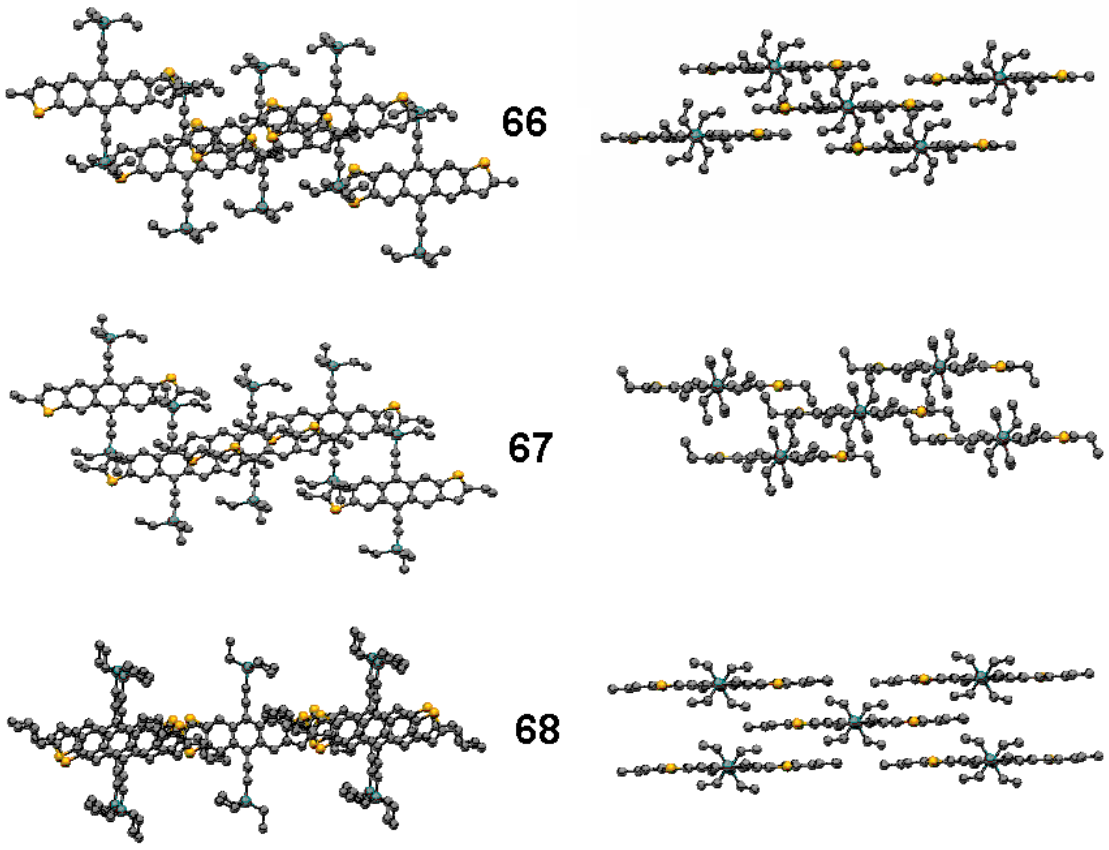

in **66** is as close as 3.50 Å, which is within the range of van der Waals radius of carbon atoms. Hence, stronger π-cloud interactions between the neighboring molecules should lead to improved electronic coupling. Even though the separation is 3.49 Å for intercolumn stacking in **67**, the intra-stack distance is greater than 3.8 Å - well outside the limit for strong electronic coupling. From this rationalization, with strongly interacting adjacent 1-D π-stacks, **66** clearly represents a bridge between purely 1-D π-stacked **67** and strongly 2-D π-stacked **21**.

From the Anthony group's work on the *peri*-functionalization of fused acene ring systems using trialkylsilylethynyl groups,[42] it is understood that the diameter of silyl group should be half the length of the acene chromophore. Also, knowing triethylsilyl (TES) as the best silyl substituent at the *peri*-positions of unsubstituted anthradithiophene for stronger π-interactions,[45] my next strategy was to use bulky triisopropylsilyl (TIPS) at the peri-positions of the larger alkyl substituted anthradithiophene in order to improve π-interactions of

Scheme 3.2 Synthesis of Alkylated TIPS Anthradithiophenes (70 - 72)

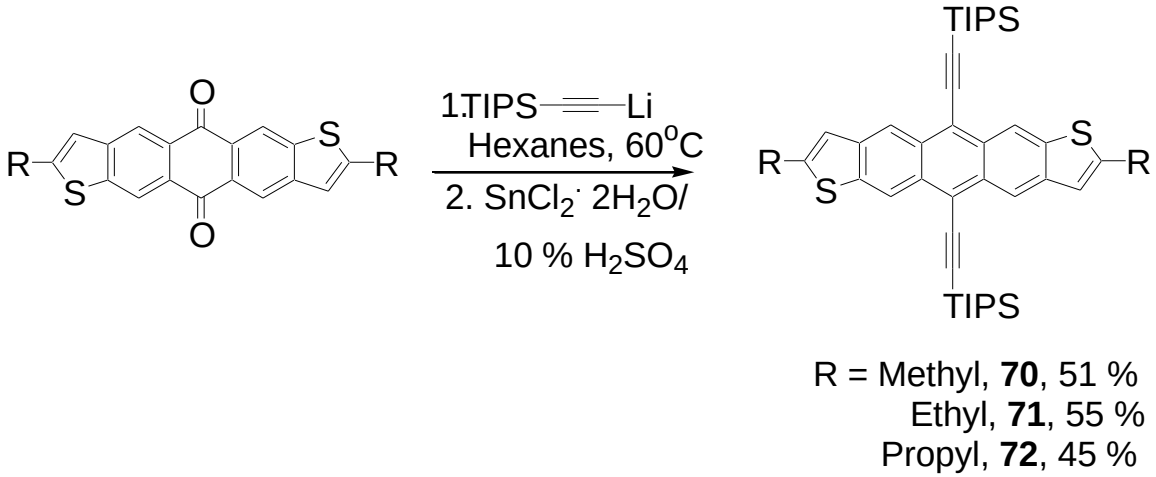

R = Methyl, **70**, 51 %
Ethyl, **71**, 55 %
Propyl, **72**, 45 %

the neighboring acene chromophores. The desired semiconductors **70** - **72** were made by the addition of lithium triisopropylsilyl acetylide to the quinone, followed by deoxygenation with stannous chloride / 10% sulfuric acid as shown in scheme 3.2.

Figure 3.4 Thermal ellipsoid plots of 71 and 72.

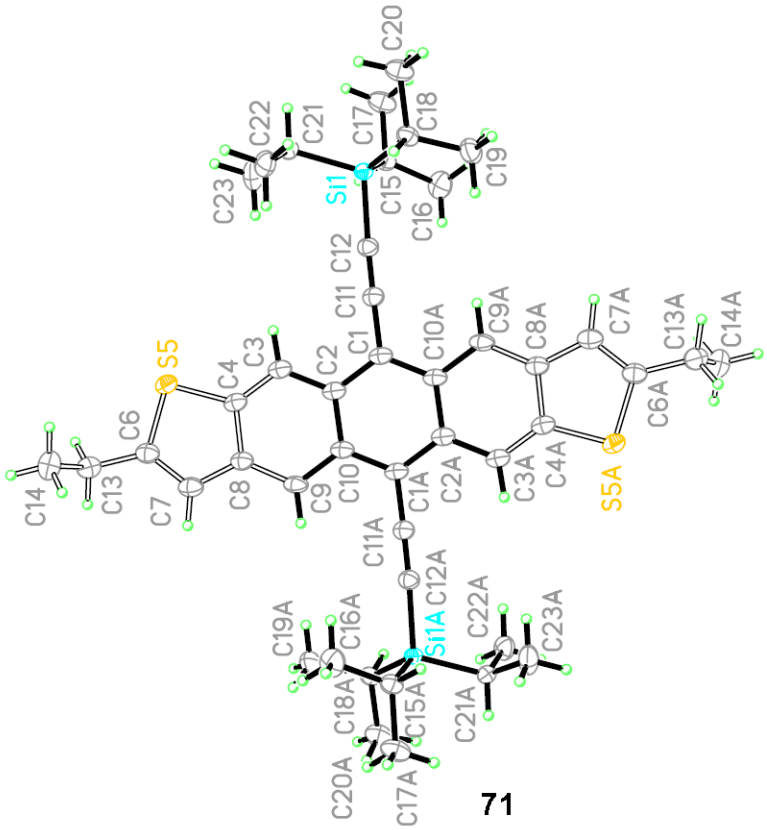

All of the derivatives were purified by silica gel chromatography followed by multiple recrystallizations from hexanes. These alkylated TIPS anthradithiophene derivatives **70** - **72** diffracted poorly during the single crystal XRD study and exhibited 1-D slipped π-stack arrangement with weak intermolecular electronic coupling. Crystals of **70** were difficult to solve by X-ray analysis and the thermal ellipsoid plots of **71** and **72** are shown in Fig. 3.4.

The UV-vis absorption spectra of alkyl substituted functionalized anthradithiophenes **66 - 69** recorded in dichloromethane show the longest-wavelength absorption (λ_{max}) at 550 nm (Fig. 3.5), which matches very closely with that of **21**. These functionalized anthradithiophenes are stable in their crystalline forms as well in

Figure 3.5 UV-vis spectra of alkyl substituted anthradithiophenes (66 - 69).

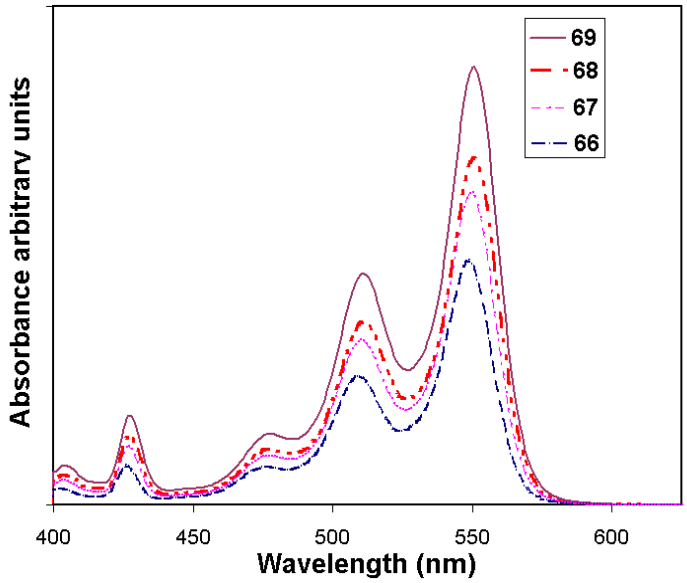

solution. From electrochemical studies, the oxidation potential of all of the derivatives **66 - 72** was found to be 0.84 V vs SCE, a slight decrease from 0.90 V vs SCE reported for

21. Detailed reports of the electrochemical measurements on all the functionalized anthradithiophenes in my dissertation are covered in chapter 6.

3.3 Organic Thin Film Transistor Studies:

OTFT studies on these alkylated anthradithiophenes were done by our collaborators in Prof. Tom Jackson's research group at Penn State. Due to their better crystal packing and easy comparison of the effect of alkyl chain lengths on the functionalized anthradithiophenes in the homologous series, TES derivatives **66 - 68** were chosen for the OTFT study. Bottom contact thin film transistors were constructed on a heavily doped silicon wafer which also acted as gate electrode. The thermally grown oxide layer (2000 Å) was used as dielectric. Gold source and drain electrodes were deposited on the device by evaporation through a shadow mask. A common structure of bottom contact OTFT is depicted in Fig. 1.1.

Solutions (2 wt% in toluene) of functionalized anthradithiophenes **66** – **68** were drop cast on the device surface and the solvent was allowed to evaporate in air. The optical microscopic images of the thin films made of **66 - 68** are depicted in Fig. 3.6.

Figure 3.6 Thin film morphological pictures of functionalized anthradithiophenes (66 - 68) (Optical images were taken by Dr. Tom Jackson's research group).

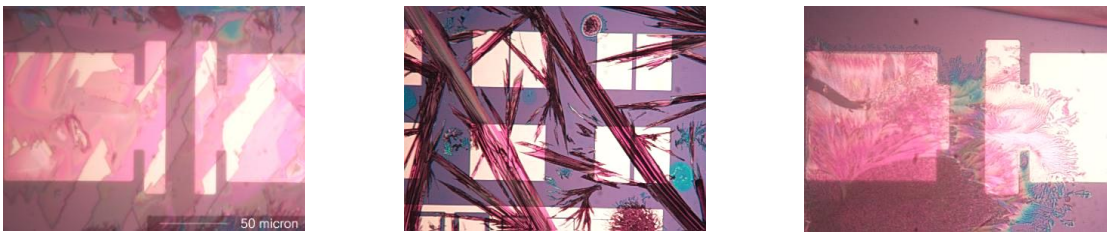

66 **67** **68**

Typical transfer curves for the TFT characteristics of the functionalized anthradithiophenes are shown in Fig. 3.7. From the linear region of the gate voltage vs square root of drain current (V_G-$\sqrt{ID}$) curves, one can extract the thin film hole mobility and the threshold voltage. The bottom-contact OTFTs fabricated using drop-cast **66** rendered devices with extracted hole mobility of 0.3 cm^2/Vs, and on/off current ratio of 10^5. On the other hand, extracted hole mobility for devices made up of **67** and **68** were reduced by more than three orders of magnitude, 2.7 x 10^{-5} cm^2/Vs and 5.2 x 10^{-4} cm^2/Vs respectively. The threshold voltages of devices made up of **66**, **67** & **68** are 21 V, 11 V and 3 V respectively.

Figure 3.7 Thin film transistor characteristics of functionalized anthradithiophenes (66 - 68) (Transistor data were taken by Dr. Tom Jackson's research group).

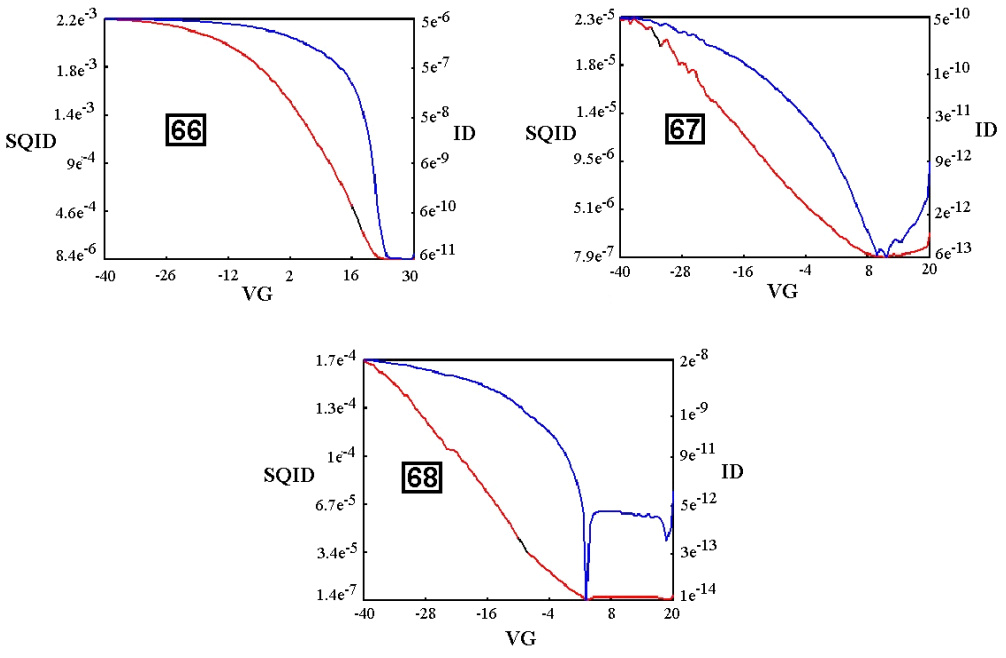

The difference in performance of the devices made up of **66 - 68** can be explained by a combination of film morphology and crystal packing effects. The morphology of the drop-cast films was studied by optical microscopy (Fig. 3.6), which revealed dramatic differences between the materials. Combining figures 3.3 and 3.6, it is understood that **67**, which possesses strong 1-D crystal π-stacking solid state arrangement leading to 3-D thin film growth, formed as discontinuous needle like crystallites, resulting in low extracted hole mobilities. On the other hand, **66** with strong intermolecular electronic coupling in two dimensions, yielded the most uniform 2-D thin films on the devices, leading to high thin film hole mobility. **68**, which adopts 2-D crystal packing motif in the solid state, also yielded 2-D thin film growth with smaller grains and slightly decreased uniformity compared to **66**. However, due to poor intermolecular electronic coupling resulting from the large distance between the neighboring anthradithiophene chromophores, devices made up of **68** led to low hole mobility. From the above discussions, we could say that both thin film morphology and intermolecular electronic couplings are very critical factors in order to develop high-performance OTFT materials.

3. 4 Organic Solar Cell Studies:

OPV studies on these alkyl substituted anthradithiophene derivatives were done by our collaborators in Prof. George Malliaras's research group at Cornell University. Organic solar cells are regarded as a versatile alternative for inexpensive photovoltaics due to the ability of being fabricated on flexible substrates at low temperatures and at low-cost. The small molecule organic semiconductors are considered to be suitable candidates for OPV production because of their facile chemical tunability. Recently, vapor-deposited

pentacene based multilayer photovoltaics have produced high performance devices.[90] Very recently, solution-processed **19** in a thermally evaporated C_{60} (**10**) based bilayer solar cell have demonstrated 0.5% power conversion efficiency.[91]

Researchers at Cornell studied our alkyl substituted functionalized anthradithiophenes along with **19** in a layered device consisting of ITO / PEDOT:PSS / alkyl substituted functionalized anthradithiophenes / C_{60} / BCP / Ag. Poly (3,4-ethylenedioxythiophene):poly(styrene sulfonate) (PEDOT:PSS) was deposited as hole injection layer on a indium-tin oxide (ITO) coated glass substrate. Bathocuprine (BCP) was used as exciton blocking layer. The layered heterojunction was created by thermally evaporating C_{60} on a spin-coated film of functionalized anthradithiophenes. The optical bandgaps for **19**, **66**, **68**, **70** and **72** were found to be 1.59 eV, 1.97 eV, 2.05 eV, 2.09 eV and 2.09 eV respectively. For the photogenerated exciton dissociation via charge transfer to happen at the heterointerface, the difference between the LUMOs of donor and acceptor materials should be larger than the exciton binding energy. For **19**/C_{60} heterojunctions, the LUMO offset was estimated between 1.0 - 1.2 eV, sufficient for exciton dissociation through charge transfer since the exciton binding energy can be as high as 0.5 eV for a five membered acene rings.[92]

For long-range (Forster) resonant energy transfer, the photoexcited donor material and the adjacent acceptor material should be within the Forster resonant energy transfer radius of 2 - 5 nm.[93] Forster radius for **19** and **68** were calculated as 1.6 nm and 2.2 nm respectively, and from the spectral response of these acene based devices, there was no evidence of energy transfer for a donor material E_{gap} below 1.9 eV. However, charge transfer cannot be completely ruled out in these anthradithiophene based devices. Spin-

coated anthradithiophene derivatives produced crystalline thin films. On the other hand, spin-coated amorphous thin films made of **19**, were forced to crystallize by thermal annealing. Charge transfer in these acenes is expected to compete with energy transfer because of the increase in exciton diffusion length derived from crystalline organic semiconductors. From the above PV study, devices consisting of the donor **68** showed 0.7% power conversion efficiency under 100 mW/cm^2 simulated AM1.5 light. The extracted values for V_{oc} and FF are found to be 700 mV and 0.44 respectively. The current-voltage characteristics of a **68** based device are shown in Fig. 3.8. Without the use of thermal annealing or the incorporation of mobile ions, **68** outperformed previously reported **19** based devices, even though they absorb less of the solar spectrum (see Fig. 3.9).[91]

Figure 3.8 Current-Voltage characteristics of 68 based PV device (The I-V plot was taken by Dr. George Malliaras's research group)

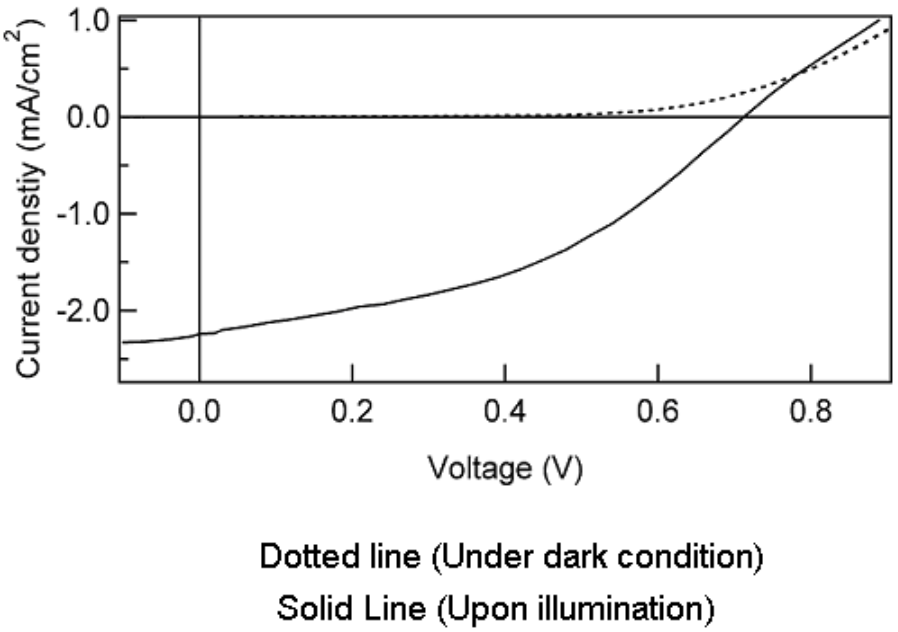

Figure 3.9 UV-vis spectra of 19 and 68.

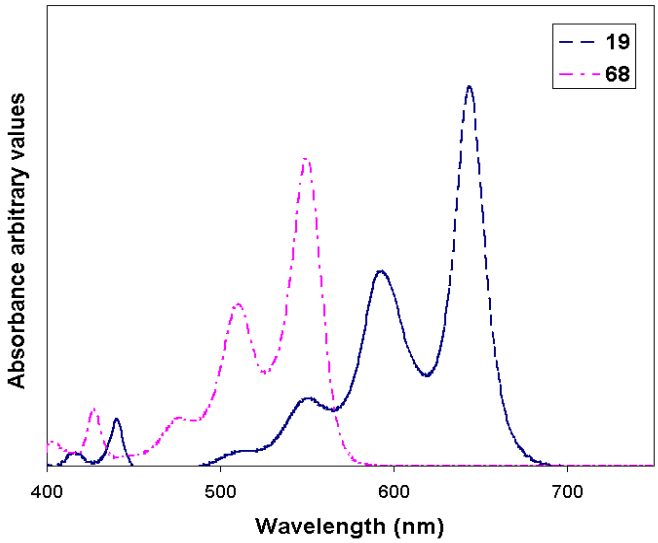

Upon thermal annealing the electron donor film at 70°C, **66**, **70** and **72** based solar cells produced the power conversion efficiencies of 0.5%, < 0.1%, and 0.2% respectively with the same device structure that used for **68**. To study the effect of polymeric binder on the performance of these devices, our collaborators at Cornell University spin-coated the blend of 1:1 ratio of an atactic polystyrene (PαMS, **73** (see Fig. 3.10)) and the functionalized anthradithiophenes before depositing the electron acceptor layer (C_{60}). It was found that the power conversion efficiencies of the bilayer solar cells based on **66** and **70** were increased to 0.7% and 0.4%, respectively, in contrast to dismal performance (< 0.1%) shown by **72** based devices. This was explained using cross-polarized images of the thin film made of functionalized anthradithiophenes as shown in Fig. 3.11. With the use of polymeric binder, the surface roughness of the thin film made of **66** is moderately reduced to 10.4 nm from 45.4 nm that formed without using the polymeric blend. On the other hand, **72** formed very smooth surface (surface roughness of 0.9 nm) thin film upon

blending with PαMS. From the above studies, it is understood that the polymeric blend which restricts the activity of **72** by forming very smooth surface leading to poor performance of the device and optimal surface roughness is required to improve the efficiency of the solar cell.

Figure 3.10 Structure of PαMS, 73.

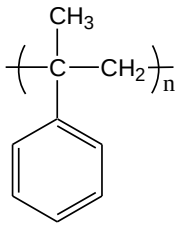

73

Figure 3.11 Cross polarized micrographs of thin films made of 66 and 72 with and without PαMS (Pictures were taken from Dr. George Malliaras's research group).

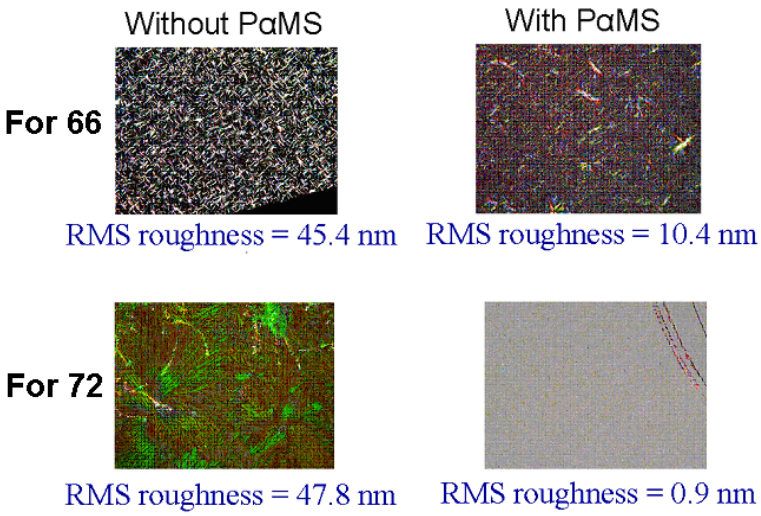

Even though **19**-based layered PV devices performed well, upon blending with soluble fullerene derivative PCBM (**23**), the pentacene underwent degradation. I studied this decomposition by recording UV-vis spectra (see Fig. 3.12) of a mixture of **19** and **23** in

Figure 3.12 Diels-Alder reaction study of TIPS pentacene (19) with PCBM (23).

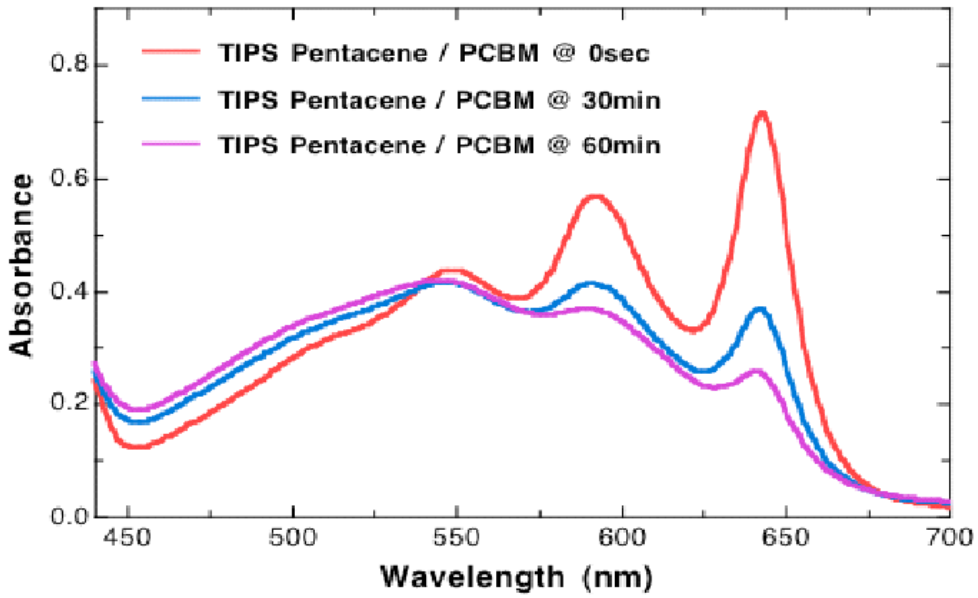

Figure 3.13 Photostability study of thin films made of 21.

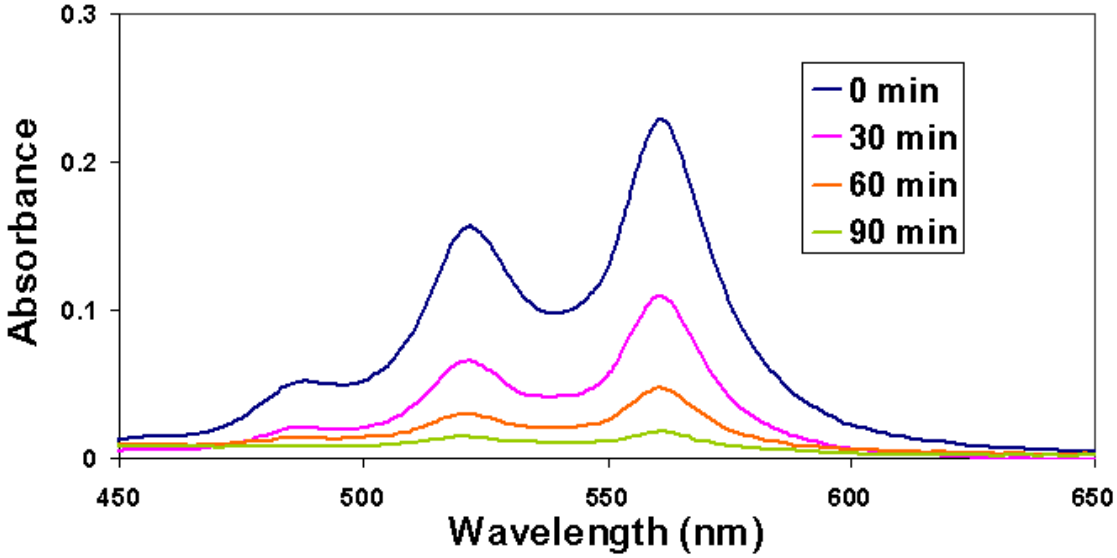

dichloromethane at varying time intervals. It was found that the maximum absorption intensity of **19** completely quenched within 1h, confirming the Diels-Alder reaction between **19** and **23**. We assumed that anthradithiophenes would be less likely to react with fullerenes, but our best performing functionalized anthradithiophene **21**, shows poor thin film photostability. I carried out the photostability study on solution-deposited thin film of **21**, found that it was photobleached completely within 1h under laboratory conditions (Fig. 3.13).

On the other hand, alkyl-functionalized anthradithiophenes possess both photostability and did not undergo Diels-Alder adduct formation with PCBM, making them suitable candidates for PV study where fullerene or fullerene derivatives are used as electron acceptor materials. The use of non-photolithographic solution-processable techniques is critical to reduce the cost of PV devices. While bulk heterojunction (BHJ) solar cells offering solution-processed fabrication, a record high power conversion efficiency > 5% was achieved from the polymer based BHJ solar cells.[68]

Figure 3.14 X-shaped oligothiophene (74).

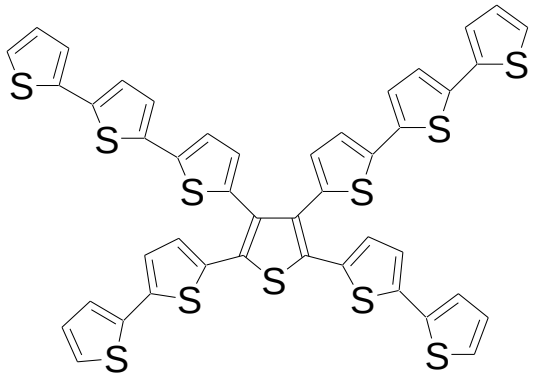

74

For the solution-processed small molecule based BHJ cells, power conversion efficiency of 0.8% have been recently recorded from an X-shaped oligothiophene (**74**, Fig. 3.14).[94] Post-fabrication solvent annealing is one way to form crystalline thin films and **21** has shown increases in thin film charge carrier mobility as much as 2 orders of magnitude upon solvent vapor annealing.[95] Some amount of crystallization is also expected in the case of alkyl substituted functionalized anthradithiophene / **23** blends. Malliaras et al. performed morphological studies on spin-coated films made of **67** in toluene and **23** in ortho-dichlorobenzene at a 70:30 weight ratio. Optical fluorescence microscopy displayed complete photoluminescence quenching of the highly fluorescent **67** in the as-spun blend film. The as-cast blend film was kept in a sealed vessel along with a vapor of solvent mixture, causing fine grain spherulites to nucleate (100-300 nuclei/cm^2) with a high fractional coverage on the substrate at increasing time (see Fig 3.15) leading to phase segregation of **67**.

Figure 3.15 Optical microscopic images of spherulite growth (Pictures were taken by Dr. George Malliaras's research group).

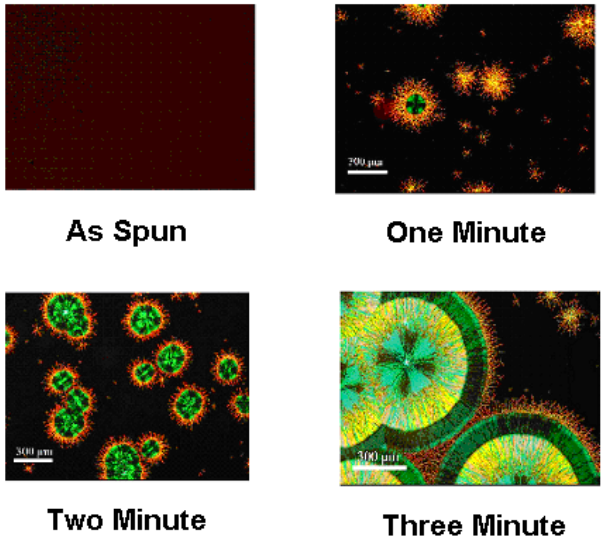

PEDOT: PSS (60 nm) was spin-coated on a pre-patterned ITO coated glass substrate. Blend solutions of **67** and **23** in toluene and *ortho*-dichlorobenzene, respectively at a 70:30 weight ratio were then spin-coated on the device. The films were exposed to solvent mixture vapor at different time interval. Film crystallization of **67** was followed by the deposition of the cathode consisting of a 10 Å layer of CsF and 400 Å of themally evaporated Al as shown in Fig. 3.16. The current-voltage characteristics of the device with high spherulite coverage is shown in Fig. 3.17.

Figure 3.16 General structure of 67 based OPV device.

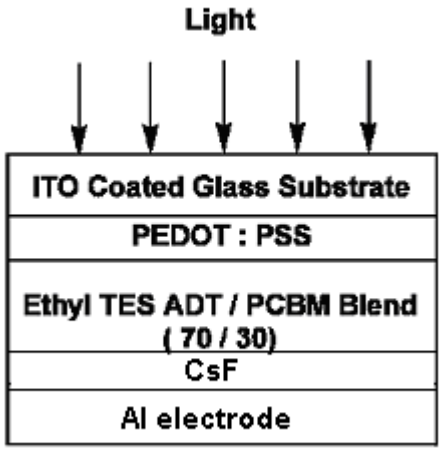

Under reverse bias, a positive slope and direct proportionality between current and voltage were observed in the dark, implying that the device exhibits low shunt resistance or a partial short-circuit. The device produced photocurrent in the low reverse bias and the difference between light and dark current gradually decreases upon illumination. The engineers attribute this behavior to an imperfectly interpenetrating network. However, the I-V curves are well behaved, with I_{sc} of 2.97 mA/cm^2, V_{oc} of 840 mV, FF of 0.40 and the

overall power conversion efficiency is calculated to be 1%. In general, short circuit current (I_{sc}) was proportional to the area of crystalline spherulite coverage on the device.

Figure 3.17 Current-Voltage Characteristics of a device with high sperulite coverage.

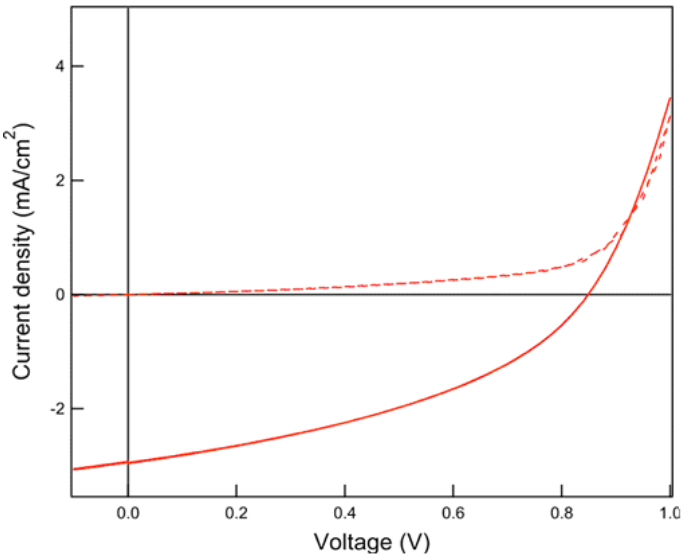

The design and synthesis of alkyl substituted anthradithiophenes has yielded a tremendous amount of information. The optimal alkyl chain length is crucial for strong intermolecular electronic coupling and thin film morphology of anthradithiphene derivatives. **66**, which possess 1-D π-stacks with strong intermolecular coupling and two-dimensional thin film growth, produced OTFT devices with high thin film hole mobility of 0.3 cm^2/Vs. This project shows that a very fine balance of thin film morphology and strong π-stacking is required for high charge transport thin film transistors. These photostable anthradithiophene derivatives also showed excellent performance in PV devices. Without the incorporation of mobile ions and thermal annealing technique, **68** performed well with 0.7% power conversion efficiency from a bilayer heterojunction PV

device. The use of polymeric binder in **66**, **70** and **72** based solar cells explains the importance of the optimal quality thin films for the better performance photovoltaics. Even though thin film morphology of **67** was poor on OTFT devices, it provided excellent performance in OPV studies with 1% power conversion efficiency from a completely solution processed BHJ solar cell.

3.5 Experimental Details

General.

Solvents (acetone, methylene chloride, hexanes) were purchased from Fisher. Dry THF was either purchased in anhydrous form from EMS Science or distilled over sodium / benzophenone under N_2 atmosphere. Trialkylsilyl acetylenes were purchased from GFS Chemicals. Silica gel 230-400 mesh was bought from Sorbent Technologies. NMR spectra were measured on a Varian (Gemini 200 MHz / Unity 400 MHz) spectrometer. Chemical shifts were reported in ppm relative to $CDCl_3$ as internal standard. The UV spectra were measured on a UV-2501PC Shimadzu instrument. Mass spectroscopy was analyzed in EI mode at 70 eV or MALDI with TCNQ matrix on a JEOL (JMS-700T) Mass Spectrometer. Cyclic Voltammetry was carried out on a BAS CV-50W, with ferrocene as an internal standard.

Thiophene-2,3-diacetal (57).

This compound was synthesized using previously reported literature.[44]

General procedure for the synthesis of 5- alkyl thiophene-2,3-dialdehydes.

To a flame dried flask, n-BuLi (27.4 mmol) was added slowly to thiophene-2,3-diacetal **57** (21 mmol) in THF (60 mL) at -78 $^{\circ}C$ under dry N_2 . After stirring 1 h, alkyl iodide (29.5 mmol) was added and the reaction mixture was warmed to room

temperature, and stirred overnight. The next day, the reaction mixture was quenched by adding cold water very carefully, extracted with diethyl ether, and washed with water. The organic layer was dried with anhydrous $MgSO_4$ and concentrated. Without purification, the diacetal was hydrolyzed by 3M HCl / THF (1 / 1) for 1h. The resulting product was purified by column chromatography using hexanes / dichloromethane eluent (2 : 3).

5 - Methyl thiophene-2,3-dialdehyde (58).

Yield = 62%. ^{1}H NMR (200 MHz, $CDCl_3$): δ 2.55 (s, 3H), 7.27 (s, 1H), 10.27 (s, 1H), 10.34 (s, 1H) ppm. ^{13}C NMR (50 MHz, $CDCl_3$): δ 16.16, 128.31, 144.29, 145.55, 150.42, 182.38, 184.91 ppm. MS (EI 70 eV) *m/z* 154 (M^+), 125 (M+ - CHO)

5 – Ethyl thiophene-2,3-dialdehyde (59).

Yield = 79 %. ^{1}H NMR (200 MHz, $CDCl_3$): δ 1.37 (t, J = 7.5 Hz, 3H), 2.92 (q, J = 7.6 Hz, 2H), 7.34 (s, 1H), 10.33 (s, 1H), 10.39 (s, 1H) ppm. ^{13}C NMR (50 MHz, $CDCl_3$): δ 14.99, 23.71, 126.24, 143.98, 144.80, 157.59, 182.20, 184.85 ppm. MS (EI 70 eV) *m/z* 168 (M^+), 140 (M^+ - CHO).

5- Propyl thiophene-2,3-dialdehyde (60).

Yield = 66%. ^{1}H NMR (200 MHz, $CDCl_3$): δ 0.94 (t, J = 7.3 Hz, 3H), 1.68 (m, 2H), 2.80 (t, J = 7.6 Hz, 2H), 7.27 (s, 1H), 10.26 (s, 1H), 10.32 (s, 1H) ppm. ^{13}C NMR (50 MHz, $CDCl_3$): δ 13.51, 24.41, 32.43, 127.07, 143.96, 145.04, 156.03, 182.31, 184.97 ppm. MS (EI 70 eV) *m/z* 182 (M^+), 154 (M^+ - CHO).

5 – Butyl thiophene-2,3-dialdehyde(61).

Yield = 66%. ^{1}H NMR (200 MHz, $CDCl_3$): δ 0.95 (t, J = 7.4 Hz, 3H), 1.41 (m, 2H), 1.71 (m, 2H), 2.88 (t, J = 7.7 Hz, 2H), 7.33 (s, 1H), 10.33 (s, 1H), 10.39 (s, 1H) ppm. ^{13}C

NMR (50 MHz, $CDCl_3$): δ 13.48, 21.91, 30.04, 33.02, 126.93, 144.03, 145.01, 156.24, 182.26, 184.95 ppm. MS (EI 70 eV) *m/z* 196 (M^+), 168 (M^+ - CHO).

General procedure for the preparation of alkyl-substituted anthradithiophene quinones.

A few drops of 15 % aqueous KOH solution was added to a mixture of 1,4-cyclohexanedione (0.6 g , 5.5 mmol) and 5-alkyl thiophene dialdehyde (11.0 mmol) dissolved in tetrahydrofuran / ethanol (5 mL / 15 mL) in a 100 mL round-bottom flask, and the rapidly-precipitating mixture was stirred at room temperature for 3 h. The insoluble yellow precipitate was filtered through a Büchner funnel, washed with ether and dried in air to yield the desired product.

2,8-Dimethyl anthradithiophene-5,11-dione (62). Yield = 70%. MS (MALDI, TCNQ matrix) *m/z* 348 (100%, M^+).

2,8-Diethyl anthradithiophene-5,11-dione (63). Yield = 65%. MS (MALDI, TCNQ matrix) *m/z* 377 (100%, $M^+ + 1$)

2,8-Dipropyl anthradithiophene-5,11-dione (64). Yield = 65%. MS (MALDI, TCNQ matrix) *m/z* 404 (100%, M^+).

2,8-Dibutyl anthradithiophene-5,11-dione (65). Yield = 71%. MS (MALDI, TCNQ matrix) *m/z* 433 (100%, $M^+ + 1$).

General procedure for the synthesis of 5,12-bis(trialkylsilylethynyl) anthradithiophenes.

n-BuLi (1.86 mL, 4.66 mmol) was added to trialkylsilylacetylene (5.32 mmol) in hexanes (50 mL) under dry N_2 at room temperature in a flame dried 500 mL round-bottom flask, and the resulting solution stirred for 30 min. The alkyl substituted

anthradithiophenequinone (1.33 mmol) was then added, followed by dry hexanes (200 mL), and the resulting suspension stirred at 66 °C until the quinone had completely dissolved - typically overnight. Stannous chloride (0.9 g, 3.99 mmol), 0.5 mL of water and 1.5 mL of 10% H_2SO_4 were then added to the reaction mixture, which was maintained at 66 °C for an additional 5 h. The reaction mixture was cooled and dried over anhydrous $MgSO_4$. It was then purified by silica plug, eluted with hexanes. The solvent was evaporated and the product purified further by multiple crystallization from hexanes. The resulting product was filtered and dried in air to obtain the pure product.

2,8-Dimethyl-5,12-bis(triethylsilylethynyl)anthradithiophene (66). Yield = 48%. ^{1}H NMR (200 MHz, $CDCl_3$): δ 0.91 (q, J = 7.6Hz, 12H), 1.25 (t, J = 7.8Hz, 18H), 2.65 (s, 6H), 7.09 (s, 2H), 8.89 (s, 2H), 9.00 (s, 2H) ppm. ^{13}C NMR (50 MHz, $CDCl_3$): δ 4.94, 8.04, 17.15, 103.71, 103.83, 103.95, 106.20, 106.41, 106.63, 116.23, 117.23, 118.23, 119.35, 119.43, 119.61, 119.71, 121.35, 123.95, 129.56, 129.59, 129.84, 130.09, 130.12, 140.44, 140.48, 141.28, 141.30, 144.55, 144.59. MS (EI 70 eV) *m/z* 594 (100%, M^+ - 1), 595 (50%, M^+). Anal. calcd. % C: 72.66, % H: 7.11, Found % C: 72.38, % H: 6.98. MP: 276.5 °C.

2,8-Diethyl-5,12-bis(triethylsilylethynyl)anthradithiophene (67). Yield = 61%. ^{1}H NMR (200 MHz, $CDCl_3$): δ 0.92 (q, J = 7.8Hz, 12H), 1.26 (t, J = 7.7Hz, 18H), 1.46 (t, J = 7.5Hz, 6H), 3.00 (q, J = 7.46Hz, 4H), 7.12 (s, 2H), 8.92 (s, 2H), 9.03 (s, 2H) ppm. ^{13}C NMR (50 MHz, $CDCl_3$): δ 4.91, 7.91, 14.90, 24.94, 103.96, 106.18, 117.26, 119.39, 119.53, 119.62, 119.86, 119.95, 129.70, 130.19, 140.05, 141.22, 151.84, 151.89 ppm. MS (EI 70 eV) *m/z* 622 (25%, M^+ - 1), 623 (15%, M^+). Anal. calcd. % C: 73.25, % H: 7.44, Found % C: 73.21, % H: 7.51. MP: 215 °C.

2,8-Dipropyl-5,12-bis(triethylsilylethynyl)anthradithiophene (68). Yield = 56%. ^{1}H NMR (400 MHz, $CDCl_3$): δ 0.92 (q, J = 8.0Hz, 12H), 1.07 (t, J = 7.4Hz, 6H), 1.25 (m, 18H), 1.86 (m, 4H), 2.94 (t, J = 7.2Hz, 4H), 7.12 (s, 2H), 8.91 (s, 2H), 9.02 (s, 2H) ppm. ^{13}C NMR (100 MHz, $CDCl_3$): δ 4.95, 8.04, 13.97, 23.98, 33.70, 103.86, 103.96, 106.35, 117.18, 119.49, 119.57, 119.76, 119.85, 120.28, 129.59, 130.08, 130.10, 140.04, 140.08, 141.11, 150.15, 150.19. MS (EI 70 eV) *m/z* 650 (100%, M^+ - 1), 651 (50%, M^+). Anal. calcd. % C: 73.78, % H: 7.73, Found % C: 73.55, % H: 7.76. MP: 225.27 °C.

2,8-Dibutyl-5,12-bis(triethylsilylethynyl)anthradithiophene (69). Yield = 71%. ^{1}H NMR (200 MHz, $CDCl_3$): δ 0.95 (q, J = 7.8 Hz, 12H), 1.01 (t, J = 6.8 Hz, 6H), 1.26 (m, 18H), 1.49 (m, 4H), 1.82 (m, 4H), 2.97 (t, J = 7.3 Hz, 4H), 7.11 (s, 2H), 8.91 (s, 2H), 9.03 (s, 2H) ppm. MS (EI 70 eV) *m/z* 678 (15%, M^+-1), 679 (10%, M^+). Anal. calcd. % C: 77.27, % H: 8.01, Found % C: 74.14, % H: 7.98.

2,8-Dimethyl-5,12-bis(triisopropylsilylethynyl)anthradithiophene (70). Yield = 51%. ^{1}H NMR (200 MHz, $CDCl_3$): δ 1.33 (m, 42H), 2.65 (s, 6H), 7.07 (s, 2H), 8.94 (s, 2H), 9.04 (s, 2H) ppm. MS (EI 70 eV) *m/z* 678 (15%, M^+ - 1), 679 (10%, M^+). Anal. calcd. % C: 74.27, % H: 8.01, Found % C: 73.50, % H: 7.62.

2,8-Diethyl-5,12-bis(triisopropylsilylethynyl)anthradithiophene (71). Yield = 55%. ^{1}H NMR (200 MHz, $CDCl_3$): δ 1.34 (m, 42H), 1.46 (t, J = 7.5 Hz), 6H), 3.00 (q, J = 7.6 Hz, 4H), 7.10 (s, 2H), 8.96 (s, 2H), 9.07 (s, 2H) ppm. MS (EI 70 eV) *m/z* 706 (100%, M^+ - 1), 707 (55%, M^+).

2,8-Dipropyl-5,12-bis(triisopropylsilylethynyl)anthradithiophene (72). Yield = 55%. ^{1}H NMR (200 MHz, $CDCl_3$): δ 1.07 (t, J = 7.4 HZ, 8H), 1.33 (m, 40H), 1.86 (m, 4H), 2.94 (t, J = 7.6 HZ, 4H), 7.09 (s, 2H), 8.95 (s, 2H), 9.06 (s, 2H) ppm. ^{13}C NMR (50 MHz,

$CDCl_3$): δ 11.87, 13.98, 19.17, 24.03, 29.94, 33.72, 104.63, 105.13, 105.35, 105.56, 116.30, 117.33, 119.53, 119.63, 119.85, 119.94, 120.29, 129.76, 130.23, 140.04, 141.08, 150.16, 150.26 ppm. MS (EI 70 eV) *m/z* 736 (35%, $M^+ + 1$), 735 (65%, M^+), 734 (100%, $M^+ - 1$). Anal. calcd. % C: 75.14, % H: 8.49, Found % C: 73.76, % H: 8.45.

Chapter 4: Halogen Substituted Functionalized Anthradithiophenes

4.1. Halogen Effects in Conjugated Materials.

Earlier studies demonstrated that both intrinsic properties such as energy level matching,[96] strong π-orbital overlap between neighboring molecules,[97] molecular orientation,[98] and extrinsic properties such as thin film morphology,[99] film thickness,[100] better interfaces with the electrodes[101] and the dielectric[102] are essential for improved charge transport in OTFTs. Substitution on the π-conjugated system is expected to alter not only the electronic properties but also the crystal packing. In 1986, Desiraju et al, demonstrated the influence of non-bonded intermolecular Cl…Cl and C-H…Cl interactions for the β-structures (short axis is below 4 Å) of chlorinated planar aromatics.[103] Recently, Bao et al. demonstrated that 5,11-dichlorinated tetracene (DCT, **76**) exhibited single crystal mobility as high as 1.6 cm^2/Vs which is greater than that showed by unsubstituted tetracene (**75**). This high charge transporting property of **76** was attributed to enhanced π-orbital overlap (Fig. 4.1) because of Cl...Cl spatial interactions (3.86 Å).[104] Due to high electronegativity of the fluorine atom, perfluorination is an efficient way to convert p-type to n-type organic semiconductors. Suzuki and coworkers effectively synthesized perfluoropentacene (**11**), which exhibited herringbone crystal packing similar to that of **18** (see Fig. 4.2), however, with close intermolecular contacts (3.25 Å) and edge-to-face angle of 91.2° (compared to 3.65 Å and 51.9° respectively for **18**).[30] Even though fluorine substitution was not expected to change greatly the molecular packing because of the relatively smaller size of fluorine atom (the atomic radii for H and F are 25 pm and 50 pm, respectively), **11** based OTFTs exhibited electron mobilities as high as 0.22 cm^2/Vs.[105]

Figure 4.1 Structures of tetracene (75), dichlorotetracene (76) and crystal packing of 76.

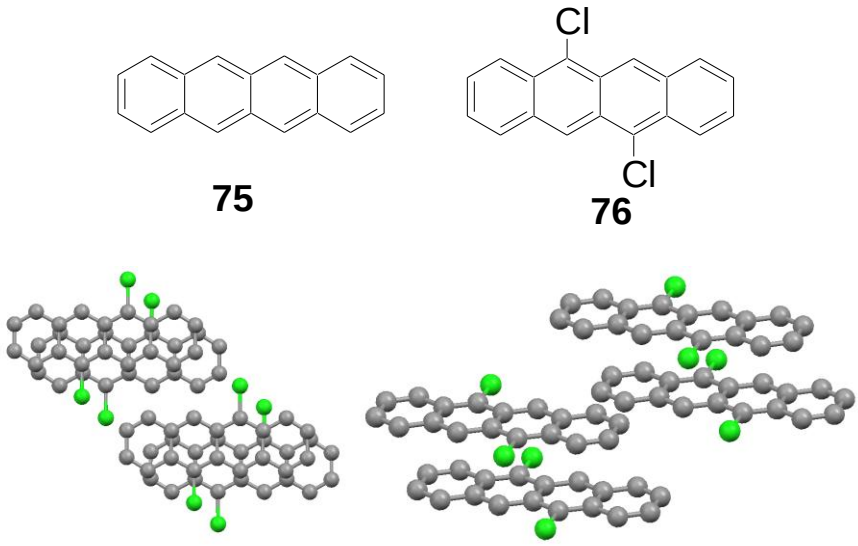

Figure 4.2 Structure and crystal packing of pentacene (18) and perfluoropentacene (11).

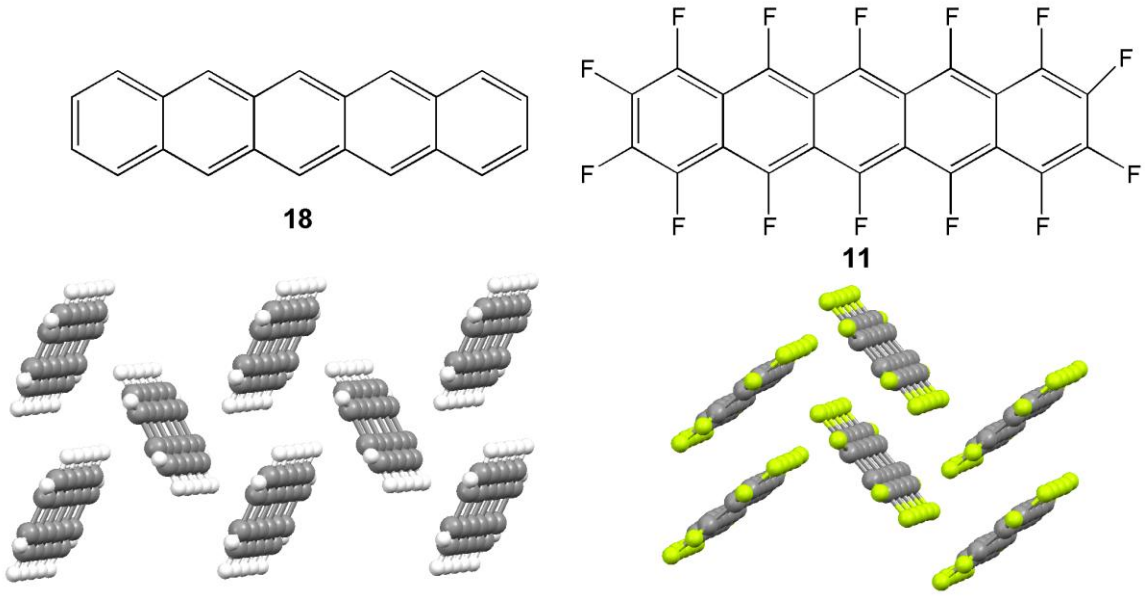

My goals for this project are to increase the π-electron surface interaction through sulfur-halogen and halogen-halogen spatial interactions. We believe that varying the electronegativity and the size of the halogen atoms should not only change the molecule's orbital energy levels, but should also allow us to vary the crystal packing of the functionalized anthradithiophenes.

4.2 Halogen-Substituted Functionalized Anthradithiophenes

Halogen-substituted functionalized anthradithiophenes (**85 - 88**) were synthesized using methods similar to those for the alkyl-substituted functionalized anthradithiophenes mentioned in the previous chapter, and the synthetic routes starting from **57** are shown in Scheme 4.1. 5-fluoro thiophene-2,3-dicarboxaldehyde (**77**) was made in low yields by the addition of electrophilic fluorine (from N-fluoro benzene sulfonimide) to the lithium salt of **57** at - 78°C under N_2 atmosphere, followed by acid hydrolysis. Purification of this material is critical, since even a small amount of thiophene-2,3-dicarboxaldehyde present with **77**, generates mono fluoro-substituted anthradithiophenes (**85a** and **89a**) as the byproduct in the final step. Other 5-halogen substituted thiophene-2,3-dicarboxaldehydes (**78 - 80**) were prepared under same conditions that used for **77** by the addition of N-chlorosuccinimide, N-bromo succinimide, and iodine, respectively, to the lithium salt of **57**.

Scheme 4.1 Synthesis of halogen-substituted functionalized anthradithiophenes (85 - 88).

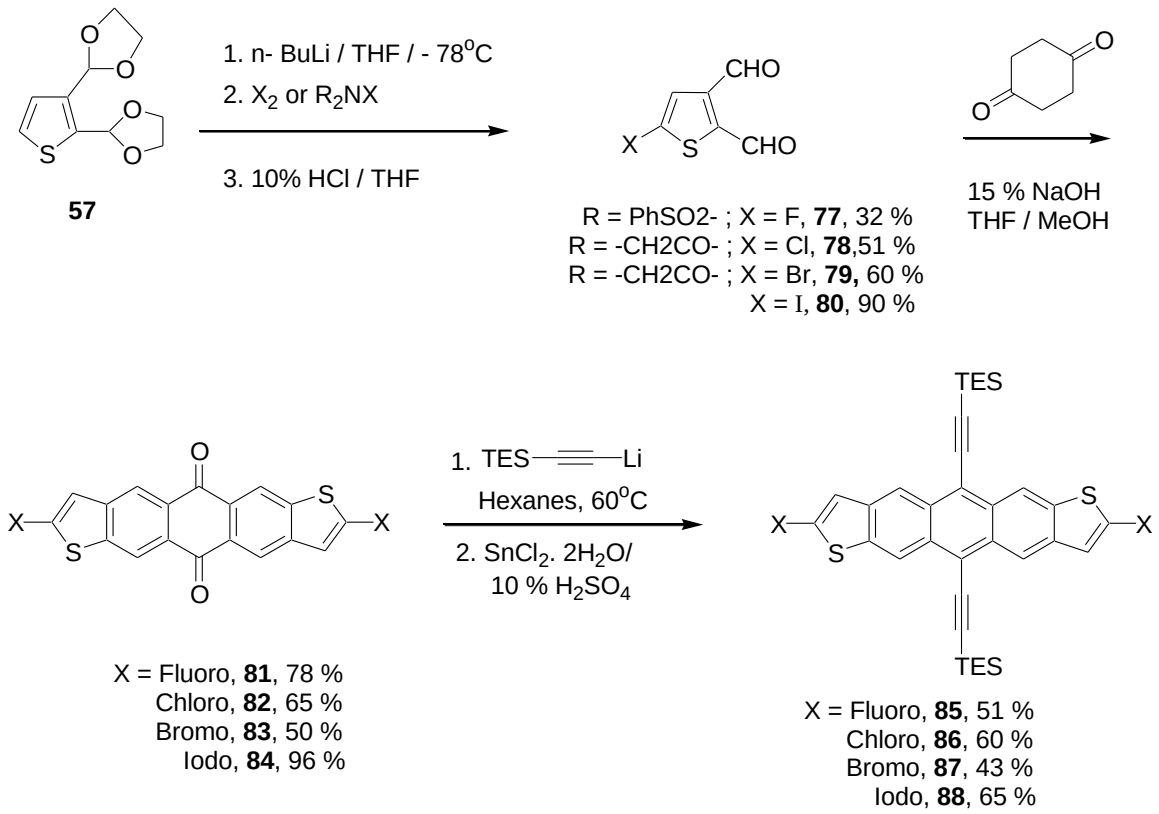

Condensation of these aldehydes (**77** - **80**) with cyclohexane-1,4-dione yielded 2, 8-dihalo anthradithiophene quinones (**81** - **84**) as a mixture of *syn*- and *anti*- isomer.[44, 45] Due to insolubility in common organic solvents, all the end-substituted anthradithiophene quinones mentioned in this dissertation were only characterized by mass spectrometry.

Figure 4.3 Thermal ellipsoid plots of 87, and 88.

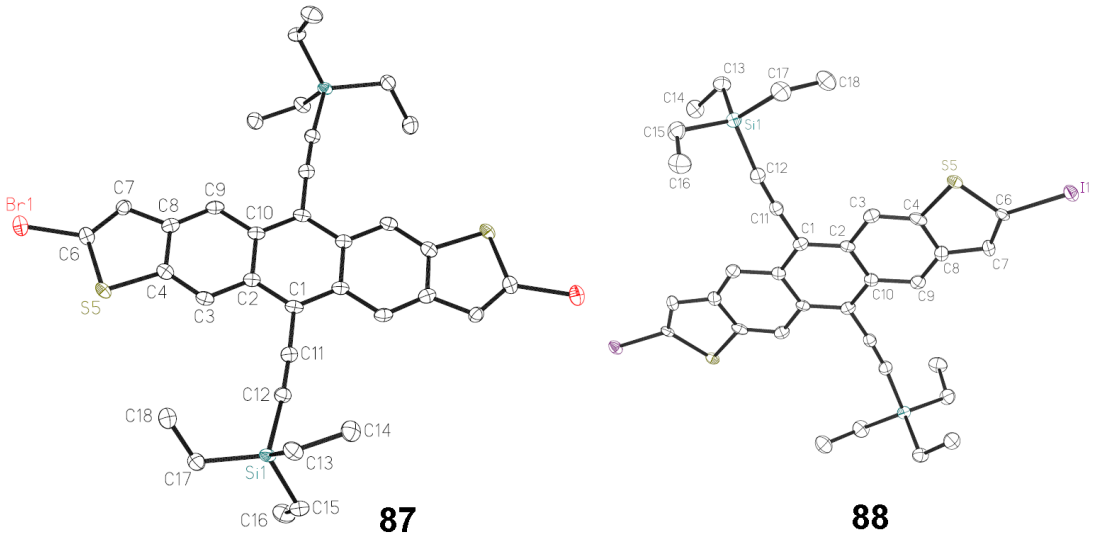

Having found the triethylsilyl ethynyl (TES) group to be the best *peri*-functionalizing group to induce strong π-interactions in **21** and **66**, my first approach was to introduce TES into the *peri*-positions of these end-substituted anthradithiophene chromophores. The desired organic semiconductors (**85 - 88**) were synthesized using similar approach that used for other functionalized anthradithiophenes. All of the derivatives were purified by silica gel chromatography followed by multiple recrystallizations from hexanes.

Single Crystal X-ray Diffraction Studies.

High-quality single crystals of anthradithiophenes **85 - 88** were grown from hexanes, and their solid state arrangements were studied by single crystal X-ray diffraction. Thermal ellipsoid plots of **87** and **88** were shown in Fig. 4.3. From the XRD studies,

Figure 4.4 π-stacking solid state arrangements of 85 - 88.

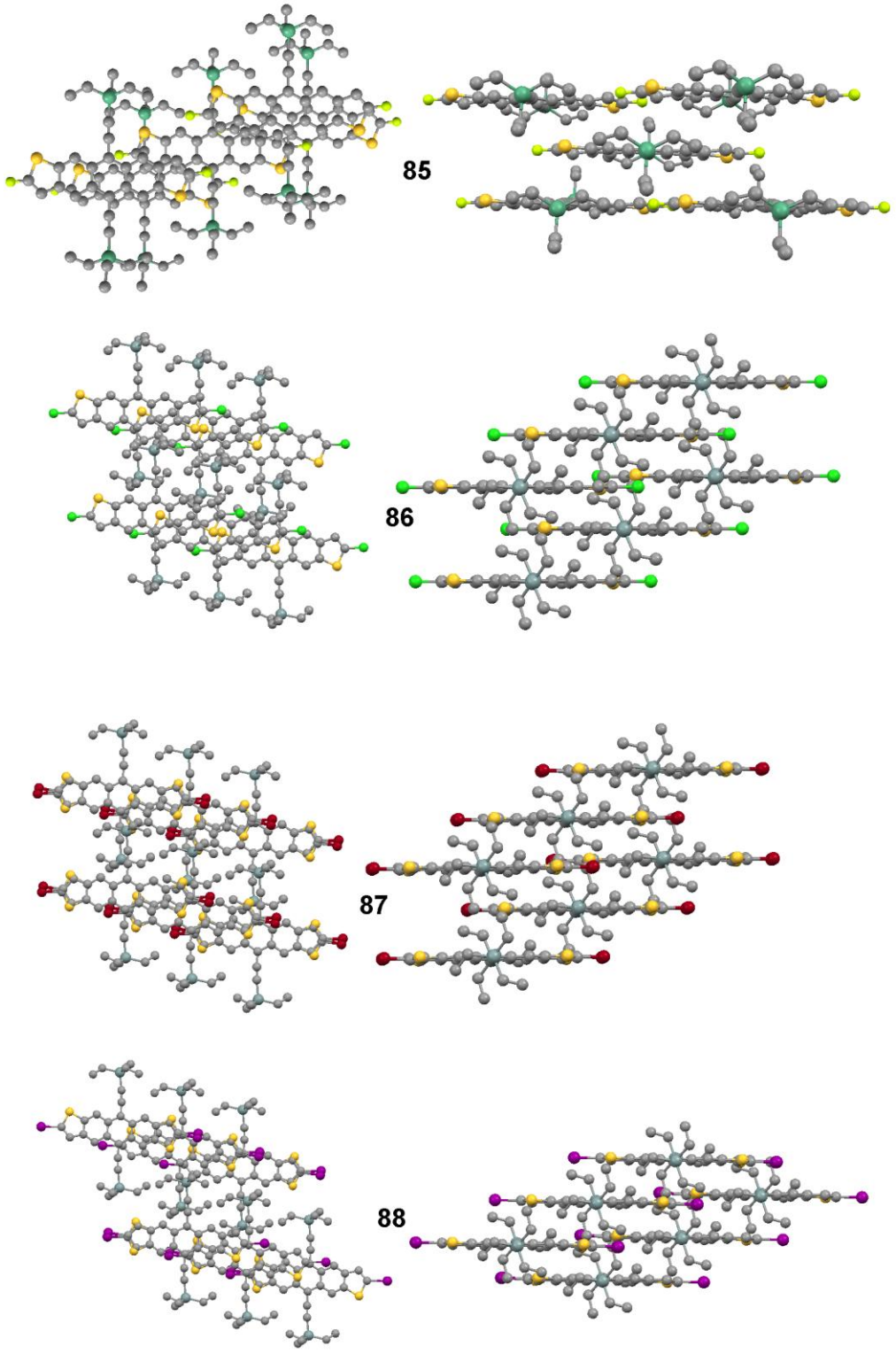

it is observed that molecules in **85** exhibit strong two-dimensional π-stacking interactions with the closest carbon-carbon interatomic distance of 3.36 Å, and S…F contacts as close as 3.16 Å. The other halogenated anthradithiophenes (**86** - **88**) possess one-dimensional slipped π-stacking solid state arrangements as shown in Fig. 4.4.

From our group's empirical model for the *peri*-functionalization of acene chromorphores,[42] it is clearly understood that the size of the silyl group determines the nature of the crystal packing of an acene derivative in the solid state. Having understood this theory, my second approach was to engineer halogen-substituted anthradithiophene chromophores using a bulkier triisopropylsilyl ethynyl (TIPS) group. Organic semiconductors **89** - **91** were prepared by the addition of lithium triisopropylsilyl acetylide to their corresponding quinones, followed by deoxygenation with stannous chloride / 10% sulfuric acid in moderate yields as shown in Scheme. 4.2.

Scheme 4.2 Synthesis of halogen-substituted functionalized anthradithiophenes (89 - 91)

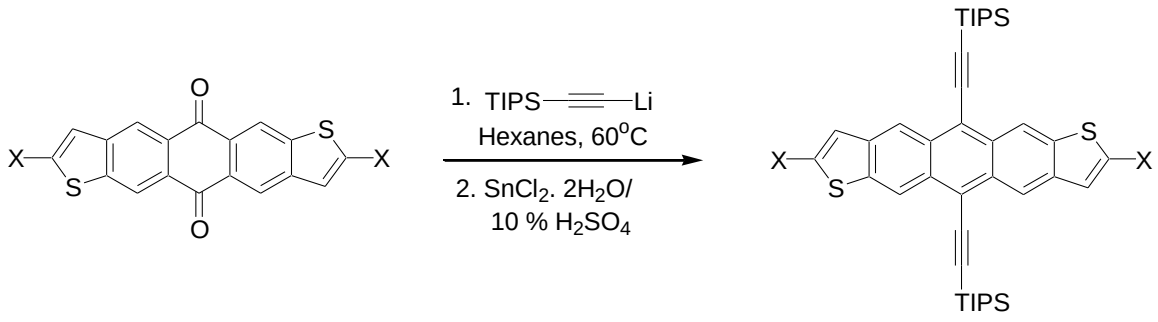

X = Fluoro, **89**, 52 %
Bromo, **90**, 53 %
Iodo, **91**, 70 %

All of these derivatives were recrystallized from various organic solvents such as acetone, hexanes, dichloromethane, toluene. From single crystal X-ray diffraction studies,

89 was found to have very strong two-dimensional π-stacking interactions between the neighboring molecules with the closest carbon-carbon interatomic distance of 3.29 Å and F…F intermolecular

Figure 4.5 Thermal ellipsoid plots of 89 and 94.

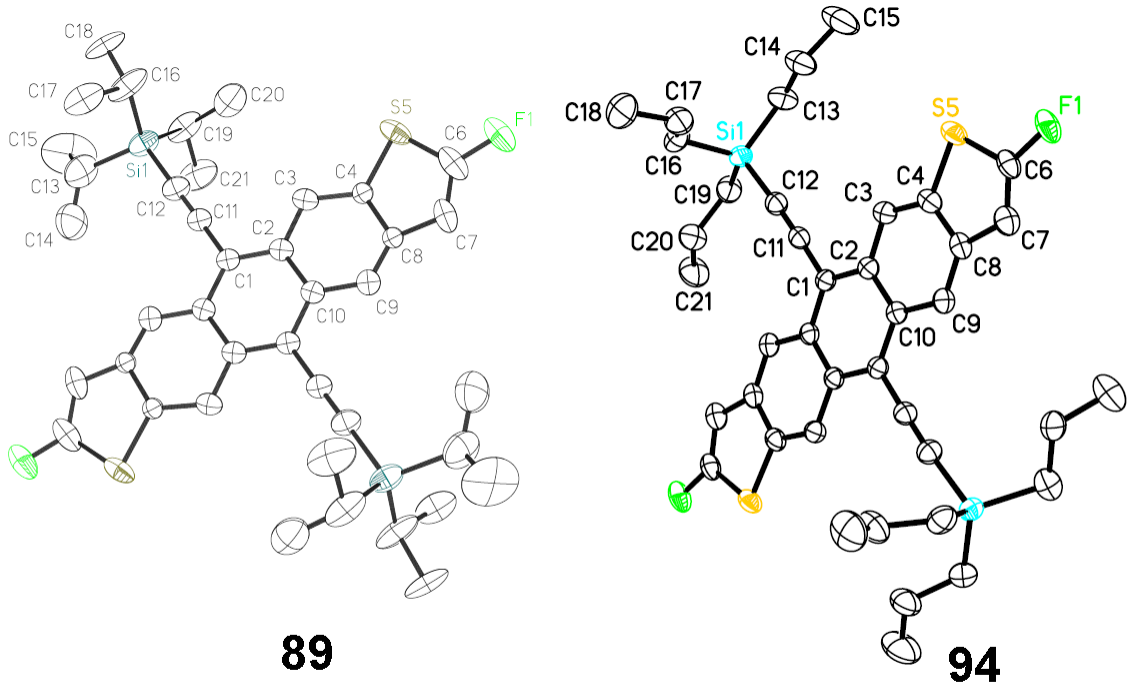

interactions predominate the pi-stacking with the contacts as close as 2.53 Å (see Fig. 4.6). **90** and **91** diffract poorly and possess 1-D slipped π-stacking solid state arrangements. The thermal ellipsoid plot of **89** can be seen in Fig. 4.5. It is noteworthy that among the halogen-substituted derivatives, only the fluoro derivatives **85** and **89** show strong two-dimensional interactions in the crystal packing. To determine how much the silyl group can be varied in this class of materials, my next plan was to use the tri-n-propylsilyl ethynyl group to engineer the packing of the acene chromophore. The synthetic routes for this functionalized heteroacene (**94**) are the same as that used for other functionalized anthradithiophenes.

Figure 4.6 π-stacking interactions in 89 and 94.

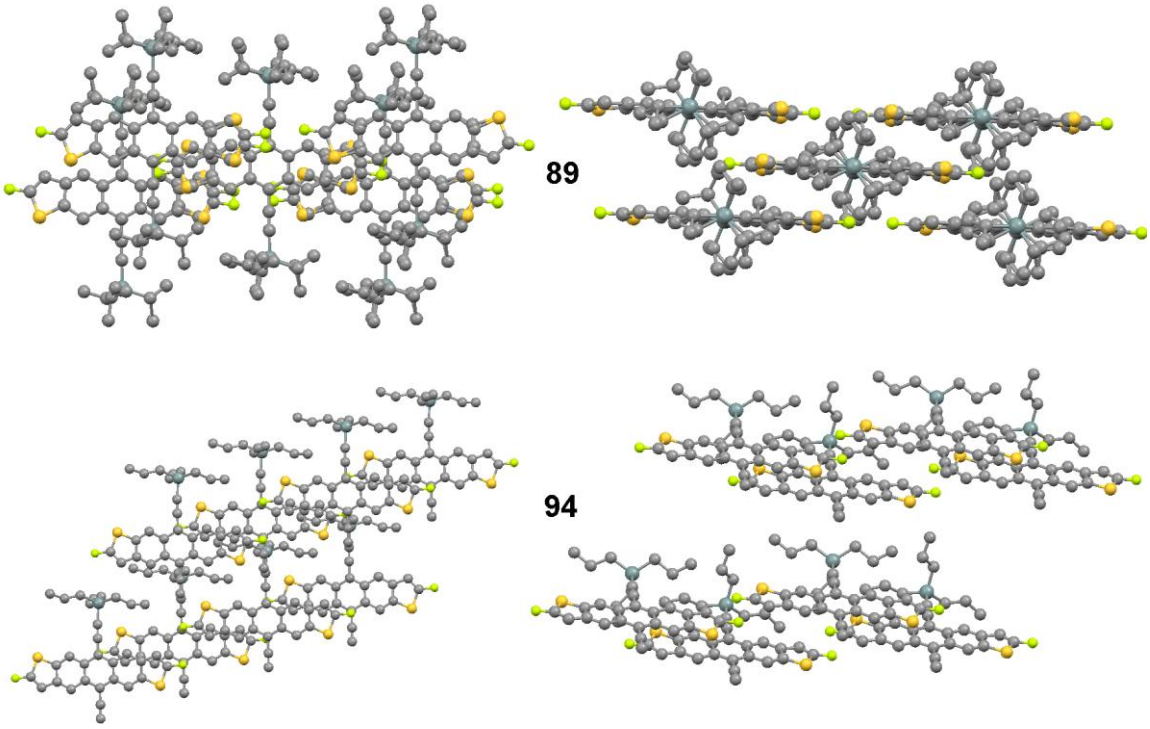

The single crystal X-ray diffraction study confirms that **94** exhibits one-dimensional slipped π-stacking in the solid state with the closest carbon-carbon interatomic distance of 3.38 Å. The thermal ellipsoid plots and π-stacking interactions in **94** are shown in Fig. 4.5 and Fig. 4.6, respectively. The UV-vis absorption spectra of anthradithiophenes **85 - 88** recorded in dichloromethane are shown Fig. 4.7. As the electronegativity of halogen atom increases, λ_{max} decreases, and a particularly significant blue shift can be seen upon fluorination (525 nm), as compared to **21** (555 nm). One of the criteria for developing organic electronic devices is the use of environmentally stable organic semiconductors. All of these halogen-substituted functionalized anthradithiophenes have shown excellent stability when exposed to heat, air and light.

Figure 4.7 UV-vis absorption spectra of functionalized anthradithiophenes (21 and 85 - 88).

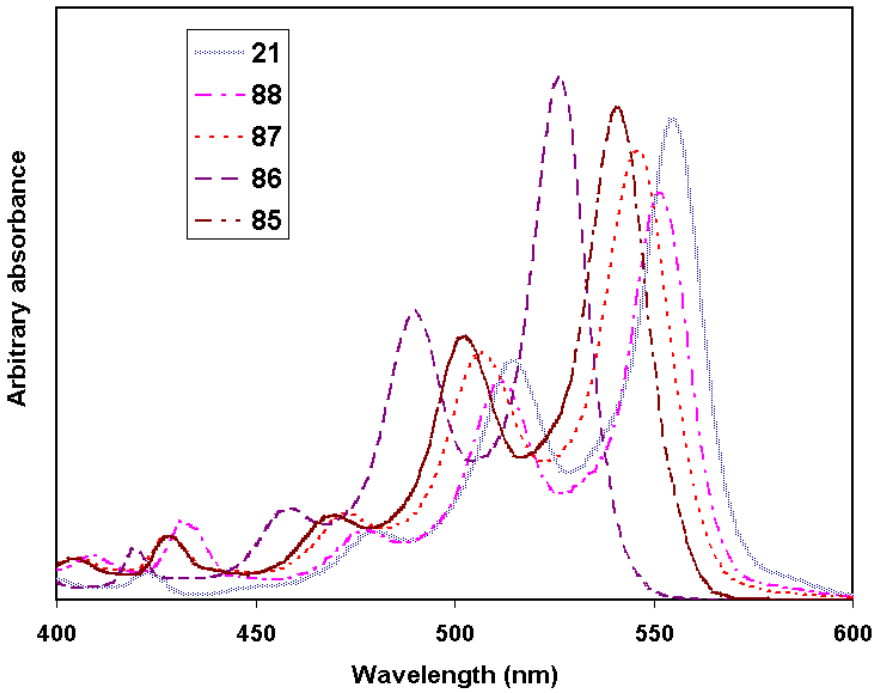

From electrochemical studies, the oxidation potential for all of the derivatives **85 - 88** was found to be about 1.0 V vs SCE, significantly greater than 0.90 V vs SCE reported for **21**. Detailed reports of the electrochemical measurements on all the functionalized anthradithiophenes in my dissertation are covered in chapter 6. Differential scanning calorimetry (DSC) experiments on fluorine-substituted anthradithiophenes (**85** and **89**) show thermal stability at higher temperature. Especially, **89** possesses very high thermal stability, which is supported by the reproducibility of the heating and cooling curves found in the DSC experiment (see Fig. 4.8) even after heating at 280°C.

Figure 4.8 DSC experiment on 89.

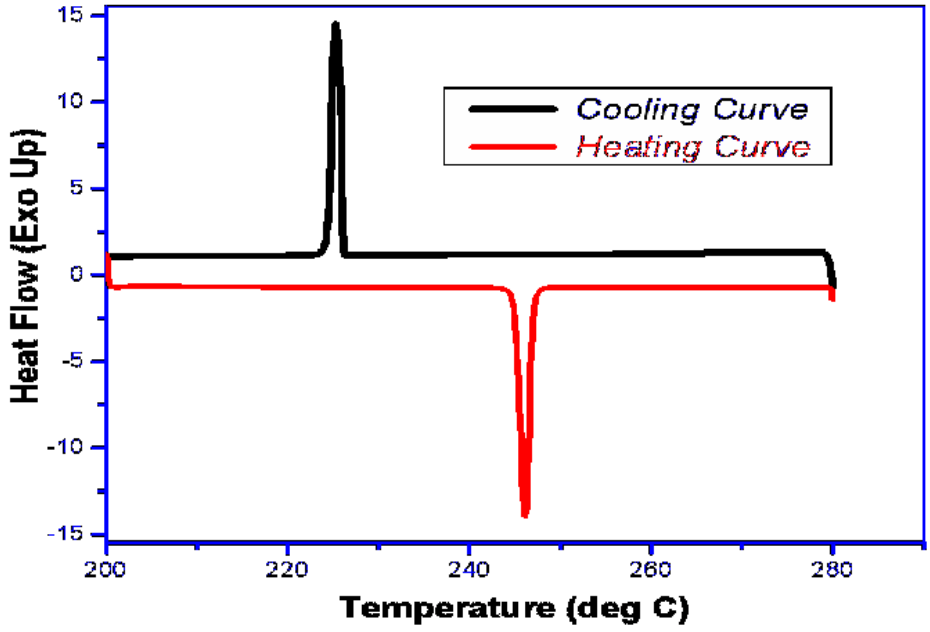

Figure 4.9 Photostability study of thin films made of 85.

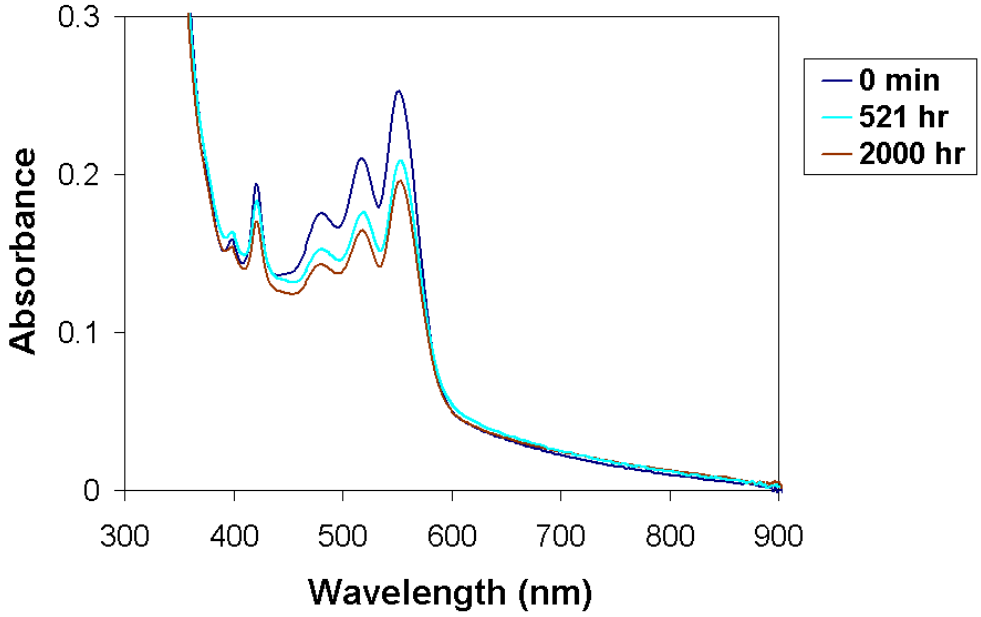

I also studied the photostability of thin films made of halogen-substituted anthradithiophenes under laboratory conditions using UV-vis spectroscopy. When exposed to light, **21** photobleached completely in 1h (see Chapter 3, Fig. 3.13). On the other hand, **85** showed exceptional photostability even after 2000 h (see Fig. 4.9).

4. 3 Organic Single Crystal Transistor Study.

The single crystal XRD analysis of the high quality crystals of halogen-substituted anthradithiophenes demonstrated the amount of π-stacking in these compounds. Most interestingly, monstrous crystals were obtained for **89** from solution. By changing the recrystallizing organic solvent from toluene to dichloroethane, the shape of the crystals were completely changed from long needle of 2 cm to cubes of 0.5 cm in dimensions (see Fig. 4.10). Organic single crystal

Figure 4.10 Crystals of 89 from (a) Toluene. (b) Dichloroethane.

transistor studies on **89** was done by our collaborator Dr. Vitaly Podzorov at Rutgers. Graphite paste was used to deposit source and drain electrodes on a relatively smooth surface of the free-standing crystal (see Fig. 4.11). Using parylene (**95**, Fig. 4.12) as insulator and silver as gate electrode, the device exhibited a gate-voltage independent single crystal hole mobility of 0.1 cm^2/Vs. It is observed that the single crystal hole mobility and threshold voltage are affected by the surface roughness.

Figure 4.11 Organic single crystal transistor characteristics of 89 (Data taken by Dr. Vitaly Podzorov's research group, Rutgers).

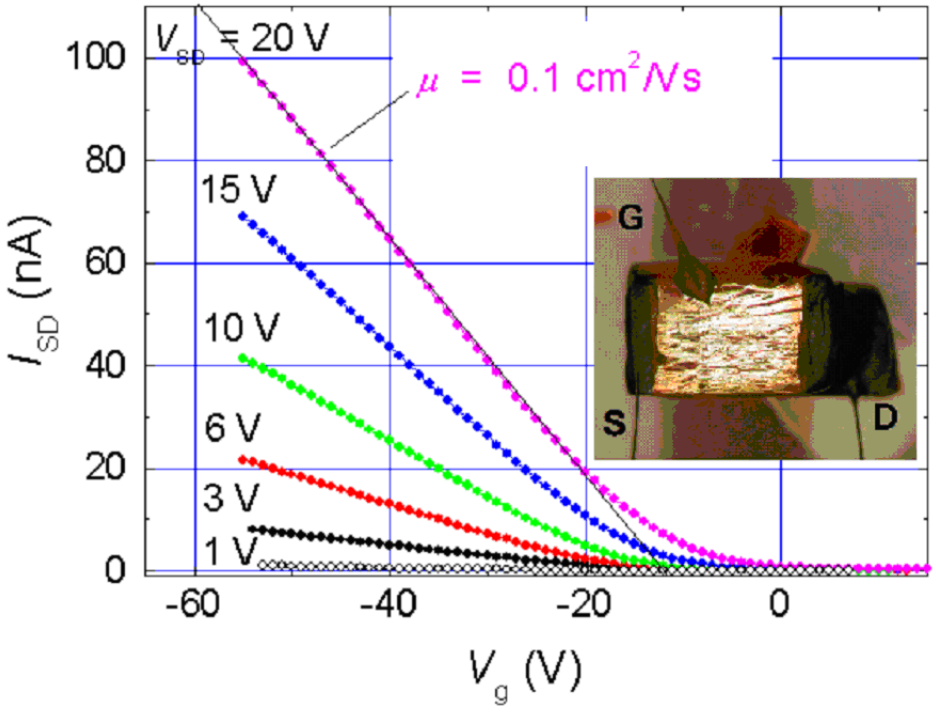

Figure 4.12 Structure of parylene (95).

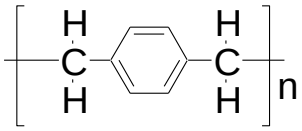

95

4.4 Organic Thin Film Transistor Study.

Due to strong two-dimensional pi-stacking, **85** and **89** were chosen for OTFT studies, which were performed in several different research groups. Our collaborator, Dr. Dave Gundlach and co-workers at NIST built bottom contact FETs on a heavily-doped silicon wafer with 200 nm thermally grown SiO_2 as gate electrode and insulator, respectively.

The source and drain electrodes consist of 5 nm Ti / 40 nm Au deposited by e-beam evaporation. The contacts were treated with pentafluorobenzene thiol (10 mM solution in ethanol) for better organic-electrode interface. Spin coated thin films of **85** were formed from 2 wt% toluene solution of the fluoro-substituted anthradithiophenes. From the devices studied with various channel lengths, it was found that the extracted field effect charge carrier mobility increases with decreasing channel length. This change in hole mobility is strongly affected by the local microstructure of the organic material in the channel region (see Fig 4.13). Device mobilities vary from ~0.2 cm^2/Vs to ~ 0.001 cm^2/Vs for channel length 5 µm to 100 µm, respectively (Fig. 4.14).

Figure 4.13 Optical Micrographs of 85 based OTFT devices with channel length (a) 5 µm, (b) 10µm, (c) 20 µm, (d) 50 µm (Pictures were taken by Dr. Dave Gundlach's research group, NIST)

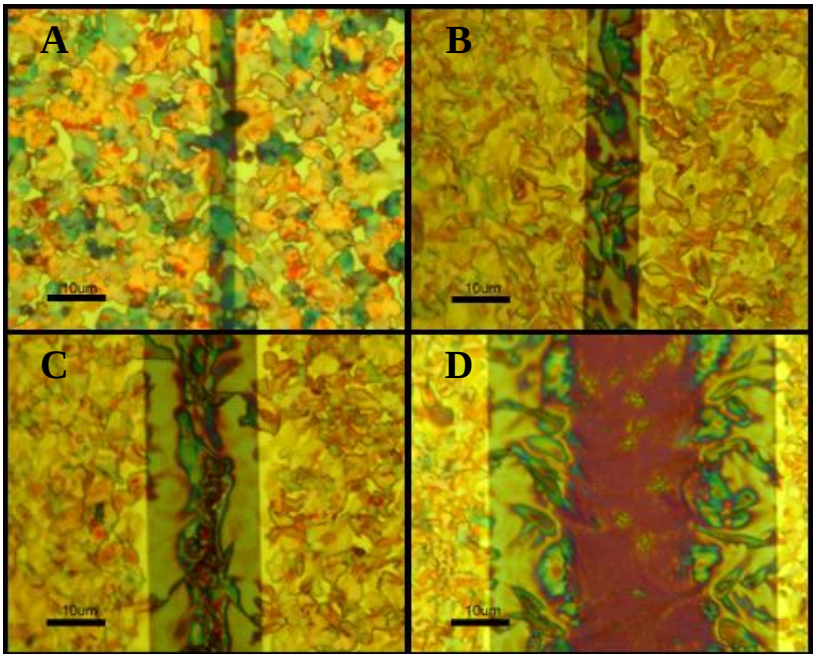

Figure 4.14 (a) bottom left : The transfer characteristics of a 85-based transistor with Channel length L = 5 µm and Channel width = 1000 µm (b) top left : The output characteristics of the same device. (c) Top right : Structure of 85 and pentafluorobenzene thiol (d) Bottom right :General structure of the OTFT device (Transistor data from Dr. Dave Gundlach's research group, NIST).

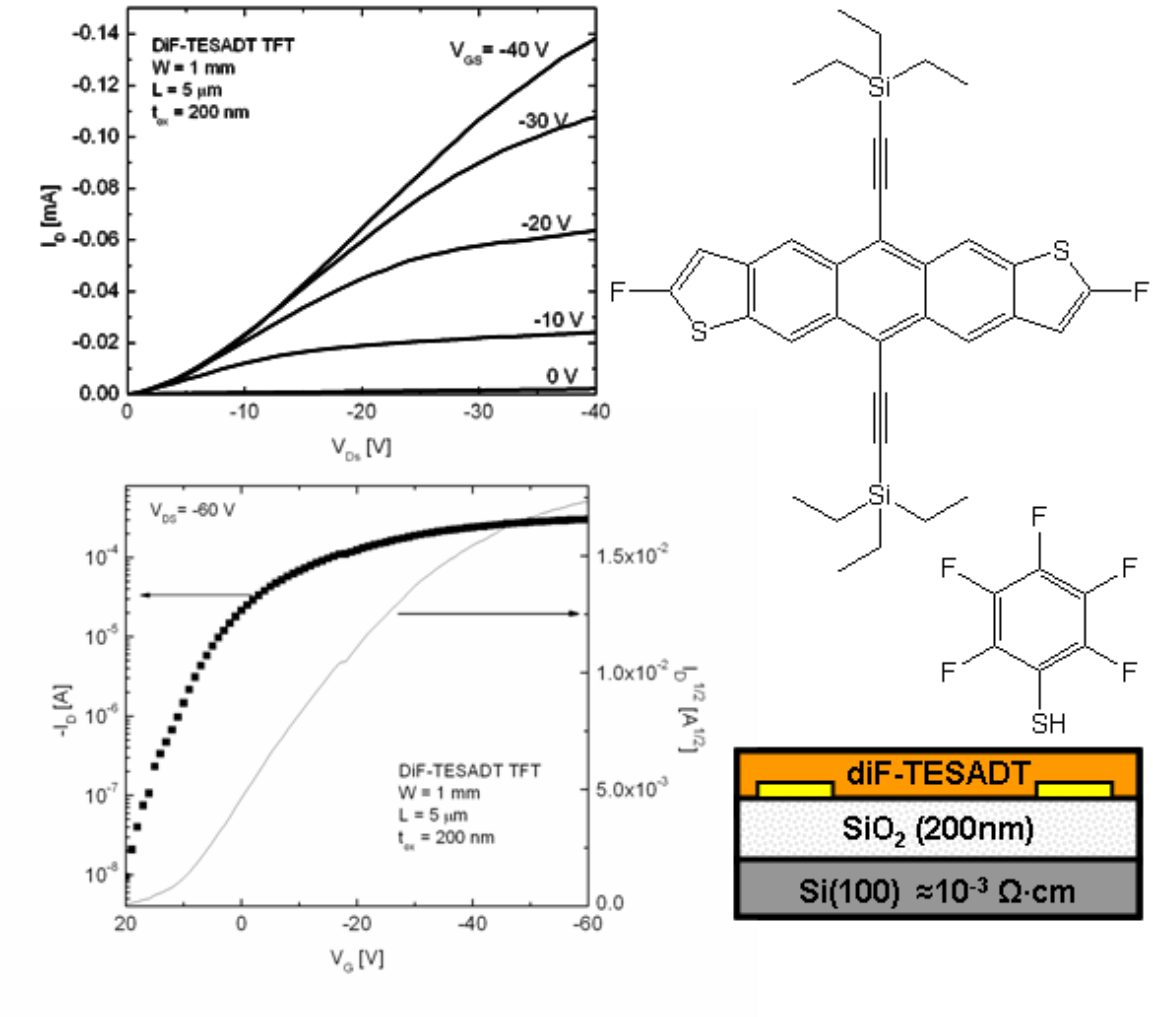

Although fluorination of **21** did not affect the crystal packing of **85**, an improvement in thin film forming ability is observed for **85**. In contrast to the unsubstituted functionalized anthradithiophene (**21**), where doctor-blading or solvent vapor annealing were required to form crystalline thin films, **85** formed high quality crystalline thin films upon spin-coating from solution. OTFT studies on **85** by a group of researchers from NIST and Penn state demonstrated the influence of source and drain contacts in obtaining improved microstructure in the conducting channel, hence, high performance of the devices. The use of hexamethyldisilazane (HMDS) to decrease the surface energy of the silicon dioxide (as is done frequently for TIPS pentacene) was found to cause significant dewetting of **85** solutions resulting in low mobility.

Of the various thiol-based monolayer treatments (octadecanethiol, benzenethiol, pentafluorobenzene thiol (PFBT)) explored to decrease the surface energy[106] of the gold interface, the use of PFBT produced the best results in terms of microstructure of the thin film in the channel region and the charge carrier mobility.

Figure 4.15 Output (left) and transfer (right) characteristics of a spin-coated 85 based OTFT device (Data taken by Dr. Tom Jackson's research group, Penn State).

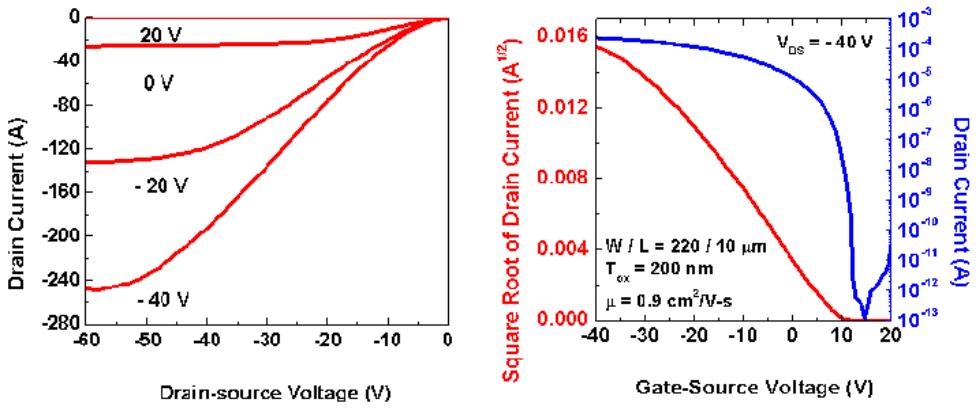

Another OTFT study on **85** by our collaborator Prof. Tom Jackson's research group at Penn State, with similar device structures that used by Dr. Dave Gundlach et al. were able to produce devices with thin film hole mobility as high as 0.9 cm^2 / Vs from spin-cast films (Fig. 4.15). On/off current ratio and threshold voltage were measured as 10^6 and 9.67 V, respectively. On the other hand, drop-cast films of **85** produced FET devices with even higher performance - the transfer characteristics of a drop-cast **85** based OTFT device is shown in Fig. 4.16.

Figure 4.16 Output characteristics of a drop-cast 85 based OTFT device (Transistor data taken from Dr. Tom Jackson's research group, Penn State).

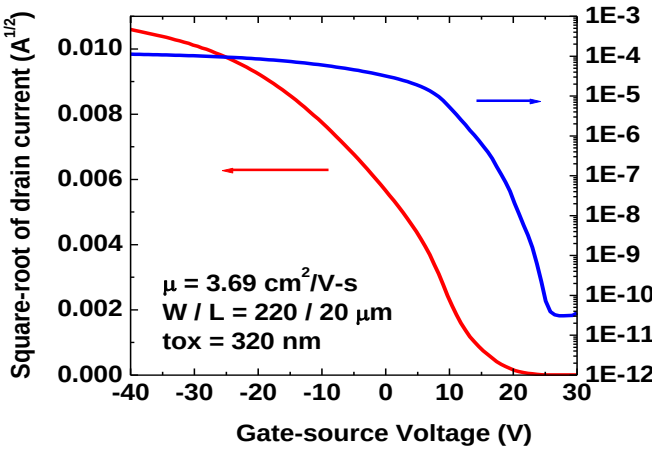

X-ray crystallographic studies revealed that the monofluoro-substituted functionalized anthradithiophene (**85a**) diffracted poorly and the random occupancy of fluorine atoms can be clearly seen from its thermal ellipsoid plot (see Fig. 4.17). OTFT experiments demonstrated that on this material exhibits thin film hole mobility in the order of 10^{-4} cm^2/Vs.

Figure 4.17 Thermal ellipsoid plot of 85a.

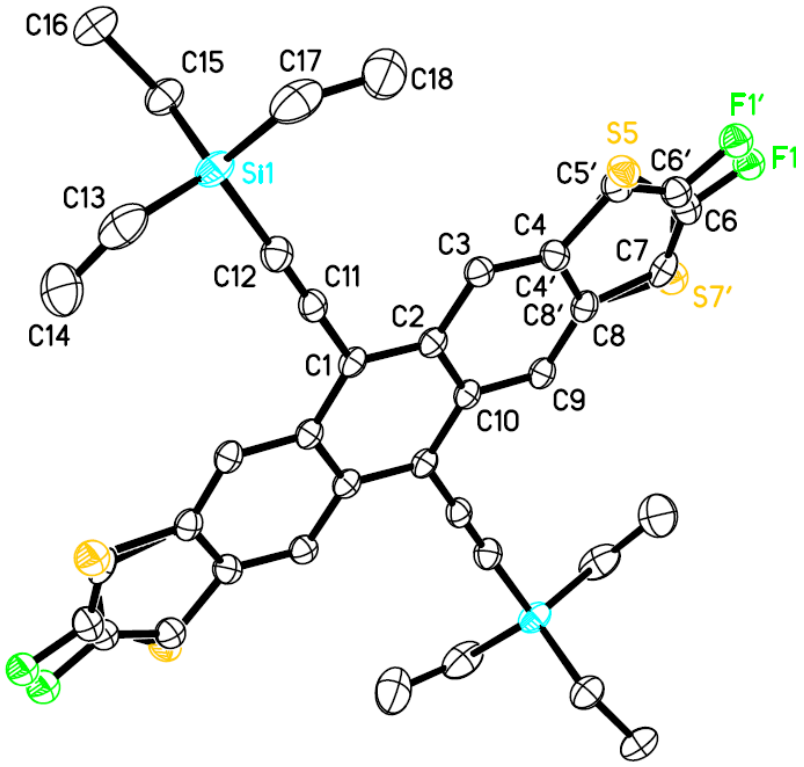

Dr. Dave Gundlach and co-workers also studied **87** and **89** with the same OTFT device structure that used for **85**. Even though **89** showed single crystal hole mobility of 0.1 cm^2/Vs from the solution grown organic crystals, **89** based OTFTs yielded devices with hole mobilities of 10^{-7} cm^2/Vs. On the other hand, **87** based OTFTs produced devices with the extracted hole mobility of 0.004 cm^2/Vs. These low thin film hole mobilities exihibited by **87** and **89** are attributed to its poor thin film forming ability as shown in Fig. 4.18.

Figure 4.18 Optical Micrographs of thin films made of 87 and 89 (Pictures were taken by Dr. Dave Gundlach research's group, NIST).

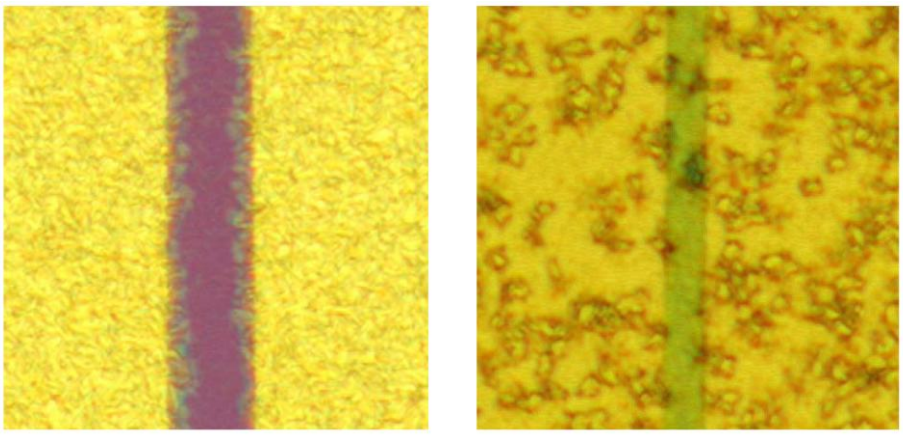

87 **89**

Halogen substitution on functionalized anthradithiophenes has produced very promising solution-processable organic semiconductors with high thermal, oxidative and photostability. Of all the halogen-substituted anthradithiophene derivatives I have discussed in this chapter, strongly two-dimensionally π-stacking **85** and **89** have yielded devices with excellent electronic properties. **89**, where nonbonded F…F interaction is predominant, crystallize with relatively smooth surface, exhibited single crystal hole mobility of 0.1 cm^2/Vs. **85**, on the other hand, where nonbonded S…F interaction is predominant, produced high quality crystalline thin films upon spin coating, and exhibited extracted thin film hole mobility of 0.9 cm^2/Vs. The **85** based OTFT study demonstrated that the device performance is dependent on the channel length and the contact-organic interface. Finally, the drop-cast film of **85** have shown thin film hole mobility of 3.69 cm^2/Vs from an unreported device data. The overall outcome of this

project is that halogen substitution on anthradithiophene chromophore produced highly stable organic semiconductors. Especially, fluorinated functionalized anthradithiophenes (**85** and **89**) are highly promising candidates for OTFT and organic single crystal transistors, respectively.

4.5 Experimental Details

General.

Solvents (acetone, methylene chloride, hexanes) were purchased from Fisher. Dry THF was either purchased from EMS Science or distilled over sodium / benzophenone under N_2 atmosphere. Trialkylsilyl acetylenes and N-Fluoro benzene sulfonamide were purchased from GFS Chemicals and Matrix Scientific respectively. Silica gel 230-400 mesh was bought from Sorbent Technologies. NMR spectra were measured on Varian instruments (Gemini 200 MHz / Unity 400 MHz) spectrometer. Chemical shifts were reported in ppm relative to $CDCl_3$ as internal standard. The UV-vis spectra were measured on a UV-2501PC Shimadzu instrument. Mass spectroscopy was analyzed in EI mode at 70 eV on a JEOL (JMS-700T) Mass Spectrometer. Cyclic voltammetry was carried out on a BAS CV-50W potentiostat, with ferrocene as an internal standard.

Thiophene-2,3-diacetal (57).

This compound was synthesized using previously reported literature.[44]

5-Flouro thiophene-2,3-dialdehyde (77).

In a flame dried flask, n-BuLi (29.6 mL, 74 mmol) was added slowly to thiophene-2,3-diacetal (13 g, 56.9 mmol) in THF (75 mL) at -78 $^{\circ}$C under N_2 atm. After one hour of stirring, N-fluorobenzene sulfonamide (NFSi) (21.86 g, 69.1 mmol) was added, the reaction mixture was warmed to room temperature, and stirred overnight. The reaction

mixture was quenched by adding cold water very carefully, extracted with diethyl ether, and washed with water. The organic layer was dried with anhydrous $MgSO_4$ and concentrated. Without purification, this material was hydrolyzed by 3M HCl (100 mL) for 1 hr. The product was extracted in ether and purified by column chromatography using hexanes / dichloromethane (120 mL / 180 mL). Yield = 2.9 g (32%). ^{1}H NMR (200 MHz, $CDCl_3$): δ 7.04 (s, 1H), 10.28 (s, 1H), 10.43 (s, 1H) ppm. ^{13}C NMR (50 MHz, $CDCl_3$): δ 110.58, 110.70, 128.05, 129.49, 134.01, 181.94, 181.96, 183.56 ppm. MS (EI 70 eV) *m/z* 158 (M^+), 129 (M^+ - CHO).

5-Chloro thiophene-2,3-dialdehyde (78).

In a flame dried flask, n-BuLi (74 mmol) was added slowly to thiophene-2,3-diacetal (56.9 mmol) in THF (75 mL) at -78 $^\circ$C under N_2 atm. After one hour of stirring, N-chloro succinimide (69.1 mmol) was added, the reaction mixture was warmed to room temperature and stirred overnight. The reaction mixture was quenched by adding cold water very carefully, extracted with diethyl ether, and washed with water. The organic layer was dried with anhydrous $MgSO_4$ and concentrated. Without purification, this was hydrolyzed by 3M HCl (100 mL) for 1 hr. This product was extracted in ether, and was purified by column chromatography by using hexanes / dichloromethane (120 mL / 180 mL). Yield = 51%. ^{1}H NMR (200 MHz, $CDCl_3$): δ 7.45 (s, 1H), 10.26 (s, 1H), 10.39 (s, 1H) ppm. ^{13}C NMR (50 MHz, $CDCl_3$): δ 128.85, 141.08, 143.34, 145.97, 181.70, 183.69 ppm. MS (EI 70 eV) *m/z* 174 (M^+), 145 (M^+ - CHO).

5-Bromo thiophene-2,3-dialdehyde (79).

In a flame dried flask, n-BuLi (74 mmol) was added slowly to thiophene-2,3-diacetal (56.9 mmol) in THF (75 mL) at -78 $^\circ$C under N_2 atm. After one hour of stirring,

N-bromo succinimide (69.1 mmol) was added and reaction mixture was warmed to room temperature, stirred for overnight. The reaction mixture was quenched by adding cold water very carefully, extracted with diethyl ether, and washed with water. Organic layer was dried in anhydrous $MgSO_4$ and concentrated. Without purification, this was hydrolyzed by 3M HCl (100 mL) for 1 hr. This product was extracted in ether, and was purified by column chromatography by using hexanes / dichloromethane (120 mL / 180 mL). Yield = 60%. ^{1}H NMR (200 MHz, $CDCl_3$): δ 7.59 (s, 1H), 10.26 (s, 1H), 10.37 (s, 1H) ppm. ^{13}C NMR (50 MHz, $CDCl_3$): δ 124.09, 132.64, 143.94, 148.74, 181.60, 183.53 ppm. MS (EI 70 eV) *m/z* 220 (M^+), 191 (M^+ - CHO).

5-Iodo thiophene-2,3-dialdehyde (80).

In a flame dried flask, n-BuLi (9.6 mL, 24 mmol) was added slowly to thiophene-2,3-diacetal (4.2 g, 18.4 mmol) in THF (50 mL) at -78 °C under N_2 atm. After 1 hr stirring, iodine (7.5 g, 29.4 mmol) was added and reaction mixture was warmed to room temperature, and stirred overnight. The reaction mixture was quenched by adding cold water very carefully, extracted with ethyl acetate, washed with 10 % sodium thiosulfate (100 mL), and water. Organic layer was dried in anhydrous $MgSO_4$ and concentrated. Without purification, this was hydrolyzed by 3M HCl (100 mL) for 1 hr. This product was extracted in ether, and was purified by column chromatography by using hexanes / dichloromethane (120 mL / 180 mL). Yield = 3.58 g (90%). ^{1}H NMR (200 MHz, $CDCl_3$): δ 7.79 (s, 1H), 10.24 (s, 1H), 10.34 (s, 1H) ppm. ^{13}C NMR (50 MHz, $CDCl_3$): δ 86.54, 139.61, 144.54, 152.87, 181.37, 183.34 ppm. MS (EI 70 eV) *m/z* 354 (M^+), 325 (M^+ - CHO).

General procedure for the preparation of 2,8-dihalo anthradithiophene-5,12-diones.

To the mixture 1.4-cyclohexanedione (5.5 mmol) and 2.0 equivalent of 5-substituted thiophene dialdehyde (11.0 mmol) in tetrahydrofuran / ethanol (5 mL / 15 mL) 15 % of KOH (a few drops) was added, and the mixture stirred at RT for 3 h. The quinone was filtered through buchner funnel and washed with methanol and dried in air.

2,8-Difluoro anthradithiophene-5,12-dione (81). Yield = 78%. MS (MALDI, TCNQ matrix) *m/z* 356 (100%, M^+).

2,8-Dichloro anthradithiophene-5,12-dione (82). Yield = 65%. MS (MALDI, TCNQ matrix) *m/z* 389 (16%, M^+).

2,8-Dibromo anthradithiophene-5,12-dione (83). Yield = 50%. MS (MALDI, TCNQ matrix) *m/z* 478 (100%, M^+).

2,8-Diiodo anthradithiophene-5,12-dione (84). Yield = 91%. MS (MALDI, TCNQ matrix) *m/z* 572 (100%, M^+).

General procedure of halogen substituted trialkylsilylethynyl anthradithiophene.

n-BuLi (1.86 mL, 4.66 mmol) was added to the trialkylsilylacetylene (5.32 mmol) in hexanes (50 mL) under N_2 atm at RT in a flame dried 500 mL RB flask, and the mixture stirred for 30 min. To that, halogen substituted anthradithiophenequinone (1.33 mmol) was added along with additional hexanes (200 mL) and the mixture heated at 66 °C overnight. The next day, stannous chloride (0.9 g, 3.99 mmol), 0.5 mL of water and 1.5 mL of 10% H_2SO_4 were added and the heating was continued for 5 more hrs. The reaction mixture was cooled and dried over anhydrous $MgSO_4$. It was purified by silica plug, washed by using hexanes and concentrated to get pure product.

2,8-Difluoro-5,12-bis(triethylsilylethynyl)anthradithiophene (85). Yield = 51%. ^{1}H NMR (400 MHz, $CDCl_3$): δ 0.91 (q, J = 2.0Hz, 12H), 1.24 (t, J = 2.0Hz, 18H), 6.82 (s, 2H), 8.86 (s, 2H), 8.93 (s, 2H) ppm. ^{13}C NMR (100 MHz, $CDCl_3$): δ 4.92, 8.01, 102.76, 102.99, 103.16, 103.29, 107.10, 117.22, 120.56, 120.65, 120.76, 120.85, 120.94, 121.03, 129.62, 129.76, 130.14, 130.35, 134.08, 136.69, 136.74, 136.83, 136.87, 163.09, 169.03. MS (EI 70 eV) *m/z* 602 (100%, M^+ - 1), 603 (45%, M^+), 517 (17%). Anal. calcd. % C: 67.73, % H: 6.01, Found % C: 67.38, % H: 5.78.

2-fluoro-5,12-bis(triethylsilylethynyl)anthradithiophene (85a). This derivative was isolated as a byproduct from the synthesis of **90**. ^{1}H NMR (400 MHz, $CDCl_3$): δ 0.92 (m, 12H), 1.25 (m, 18H), 6.82 (d, J = 0.7Hz, 1H), 7.47 (d, J = 1.4Hz, 1H), 7.58 (d, J = 1.4Hz, 1H), 8.88 (s, 1H), 8.95 (s, 1H), 9.11 (s, 1H), 9.16 (q, J = 0.27Hz, 1H) ppm. ^{13}C NMR (100 MHz, $CDCl_3$): δ 4.92, 8.03, 102.87, 103.42, 106.95, 107.22, 116.51, 117.15, 117.76, 118.42, 120.22, 120.62, 120.87, 120.96, 121.46, 123.93, 129.73, 130.03, 130.38, 133.95, 136.69, 139.88, 140.29, 164.49, 167.46 ppm. MS (EI 70 eV) *m/z* 584 (7%, M^+ - 1), 585 (4%, M^+).

2,8-Dichloro-5,12-bis(triethylsilylethynyl)anthradithiophene (86). Yield = 60%. ^{1}H NMR (400 MHz, $CDCl_3$): δ 0.92 (q, J = 2.0Hz, 12H), 1.24 (m, 18H), 7.30 (td, J = 0.2Hz, J = 0.8Hz, 2H), 8.89 (dd, J = 0.15Hz, J = 1.25Hz, 2H), 8.93 (td, J = 0.2Hz, J = 0.73Hz, 2H) ppm. ^{13}C NMR (100 MHz, $CDCl_3$): δ 4.88, 8.03, 102.97, 103.09, 103.20, 107.16, 107.45, 107.75, 116.69, 117.80, 118.92, 119.55, 119.61, 120.61, 120.68, 122.66, 129.75, 129.82, 130.12, 130.18, 135.29, 135.33, 139.05, 139.12 ppm. MS (EI 70 eV) *m/z* 634 (66%, M^+ - 2), 636 (61%, M^+). Anal. calcd. % C: 64.22, % H: 5.70, Found % C: 63.85, % H: 5.65.

2,8-Dibromo-5,12-bis(triethylsilylethynyl)anthradithiophene (87). Yield = 43%. ^{1}H NMR (400 MHz, $CDCl_3$): δ 0.92 (q, J = 2.0Hz, 12H), 1.24 (m, 18H), 7.46 (d, J = 1.1Hz, 2H), 8.92 (dd, J = 0.2Hz, J = 2.1Hz, 2H), 8.94 (td, J = 0.2Hz, J = 1.2Hz, 2H) ppm. ^{13}C NMR (100 MHz, $CDCl_3$): δ 4.88, 8.01, 102.97, 103.11, 103.25, 107.20, 107.50, 107.82, 116.75, 117.90, 119.24, 119.30, 119.77, 119.83, 120.40, 120.46, 126.57, 129.69, 129.78, 130.10, 130.18, 139.91, 140.85 ppm. MS (EI 70 eV) *m/z* 724 (17%, M^+). Anal. calcd. % C: 56.34, % H: 5.0, Found % C: 56.56, % H: 5.20.

2,8-Diiodo-5,12-bis(triethylsilylethynyl)anthradithiophene (88). Yield = 65%. ^{1}H NMR (200 MHz, $CDCl_3$): δ 0.92 (q, J = 3.3Hz, 12H), 1.25 (t, J = 3.7Hz, 18H), 7.68 (s, 2H), 8.94 (s, 2H), 8.97 (s, 2H) ppm. ^{13}C NMR (50 MHz, $CDCl_3$): δ 4.88, 7.95, 84.20, 84.30, 103.31, 107.65, 118.12, 118.78, 120.04, 129.80, 129.98, 130.12, 130.30, 134.08, 141.16, 141.24, 143.78, 143.94. MS (EI 70 eV) *m/z* 818 (30%, M^+ - 1), 692 (12%, M^+ - I). Anal. calcd. % C: 49.87, % H: 4.43, Found % C: 50.00, % H: 4.27.

2,8-Difluoro-5,12-bis(triisopropylsilylethynyl)anthradithiophene (89). Yield = 52%. ^{1}H NMR (200 MHz, $CDCl_3$): δ 1.32 (s, 42H), 6.81 (d, J = 1.2Hz, 2H), 8.92 (s, 2H), 8.98 (s, 2H) ppm. ^{13}C NMR (50 MHz, $CDCl_3$): δ 11.74, 19.03, 102.77, 102.99, 103.89, 103.94, 103.99, 106.12, 106.19, 120.63, 120.73, 120.89, 120.98, 121.07, 121.16, 129.85, 130.03, 130.38, 130.58, 134.16, 136.77, 136.95 163.19, 169.13 ppm. MS (EI 70 eV) *m/z* 686 (6%, M^+ - 1), 687 (5%, M^+). Anal. calcd. % C: 69.92, % H: 7.04, Found % C: 70.19, % H: 7.19.

2-fluoro-5,12-bis(triisopropylsilylethynyl)anthradithiophene (89a). MS (EI 70 eV) *m/z* 668 (6%, M^+ - 1), 669 (4%, M^+).

2,8-Diiodo-5,12-bis(triisopropylsilylethynyl)anthradithiophene (91). Yield = 70%. ^{1}H NMR (200 MHz, $CDCl_3$): δ 1.32 (s, 42H), 7.67 (s, 2H), 9.03 (t, J = 1.0Hz, 4H) ppm. MS (EI 70 eV) *m/z* 902 (30%, M^+ - 1), 903 (15%, M^+). Anal. calcd. % C: 53.2, % H: 5.35, Found % C: 54.10, % H: 5.61.

Tri-n-propylsilyl acetylene (93).

Ethynyl magnesium bromide (0.5 M, 10 mmol) in THF was added to tri-n-propylchlorosilane **92** (10 mmol, purchased from GFS chemicals) in a 250 mL round bottom flask. The reaction mixture was stirred at room temperature overnight. It was then quenched with cold ammonium chloride solution, was extracted with ether. The organic layer was washed with water, dried over anhydrous $MgSO_4$ and concentrated. It was then purified on a short pad of silica gel using hexanes. The desired product was obtained after removal of solvent. Yield = 89 %. ^{1}H NMR (200 MHz, $CDCl_3$): δ 0.64 (m, 6H), 0.99 (t, J = 7.4 Hz, 9H), 1.42 (m, 6H), 2.36 (s, 1H). ^{13}C NMR (50 MHz, $CDCl_3$): δ 16.01, 17.61, 18.37, 88.46, 94.25.

2,8-Difluoro-5,12-bis(tri-n-propylsilylethynyl)anthradithiophene (94).

This was synthesized using the same procedure that used for other halogen-substituted functionalized anthradithiophenes. Yield = 61 %. ^{1}H NMR (200 MHz, $CDCl_3$): δ 0.91 (m, 12H), 1.15 (t, J = 6.8 Hz, 18H), 1.67 (m, 12H), 6.81 (d, J = 2.6 Hz, 2H), 8.84 (s, 2H), 8.93 (s, 2H). MS (EI 70 eV) *m/z* 686 (100 %, M^+ - 1), 687 (55 %, M^+)

Chapter 5: Attempted functionalization on anthradithiophene chromophore

5.1 Methoxy substituted functionalized anthradithiophenes

With the success of the *peri*-functionalization approach on oligoacenes, the next logical strategy would be to increase the conjugation length of anthradithiophene chromophores for improved crystal packing and enhanced electronic properties. Earlier studies demonstrated that pentacene (**18**) showed thin film hole mobility as high as 1.5 cm^2/Vs on chemically treated silicon dioxide substrates.[107] That value is more than an order of magnitude higher than that observed for tetracene (**75**, 0.1 cm^2/Vs).[108] This high charge carrier mobility was attributed to the uniform thin film morphology and molecular ordering on devices exhibited by the more conjugated material **18**.

Scheme 5.1 Synthesis of 2,8-dimethoxy-5,12-bis(triethylsilylethynyl) anthradithiophene (100).

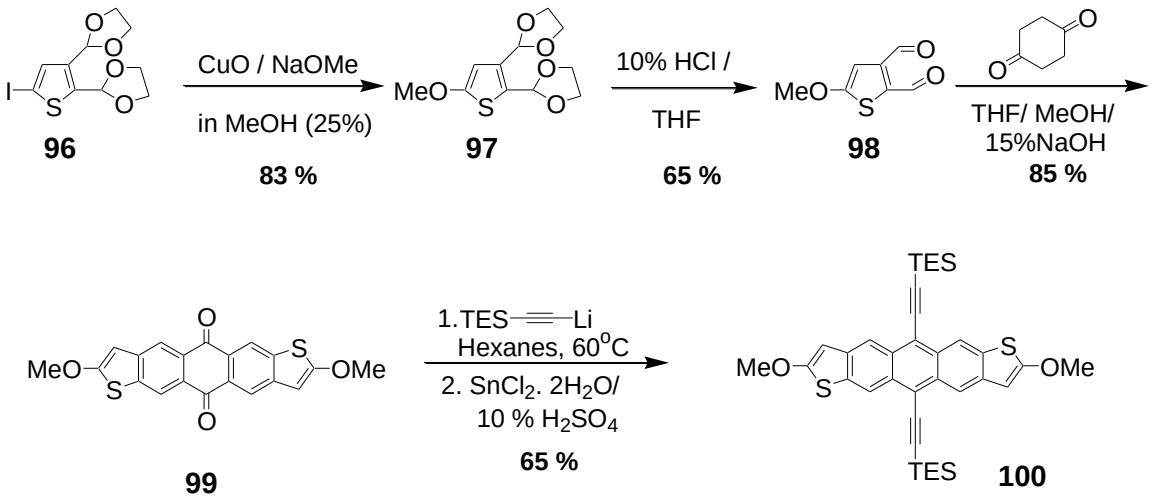

Figure 5.1 π-stacking interactions in 100.

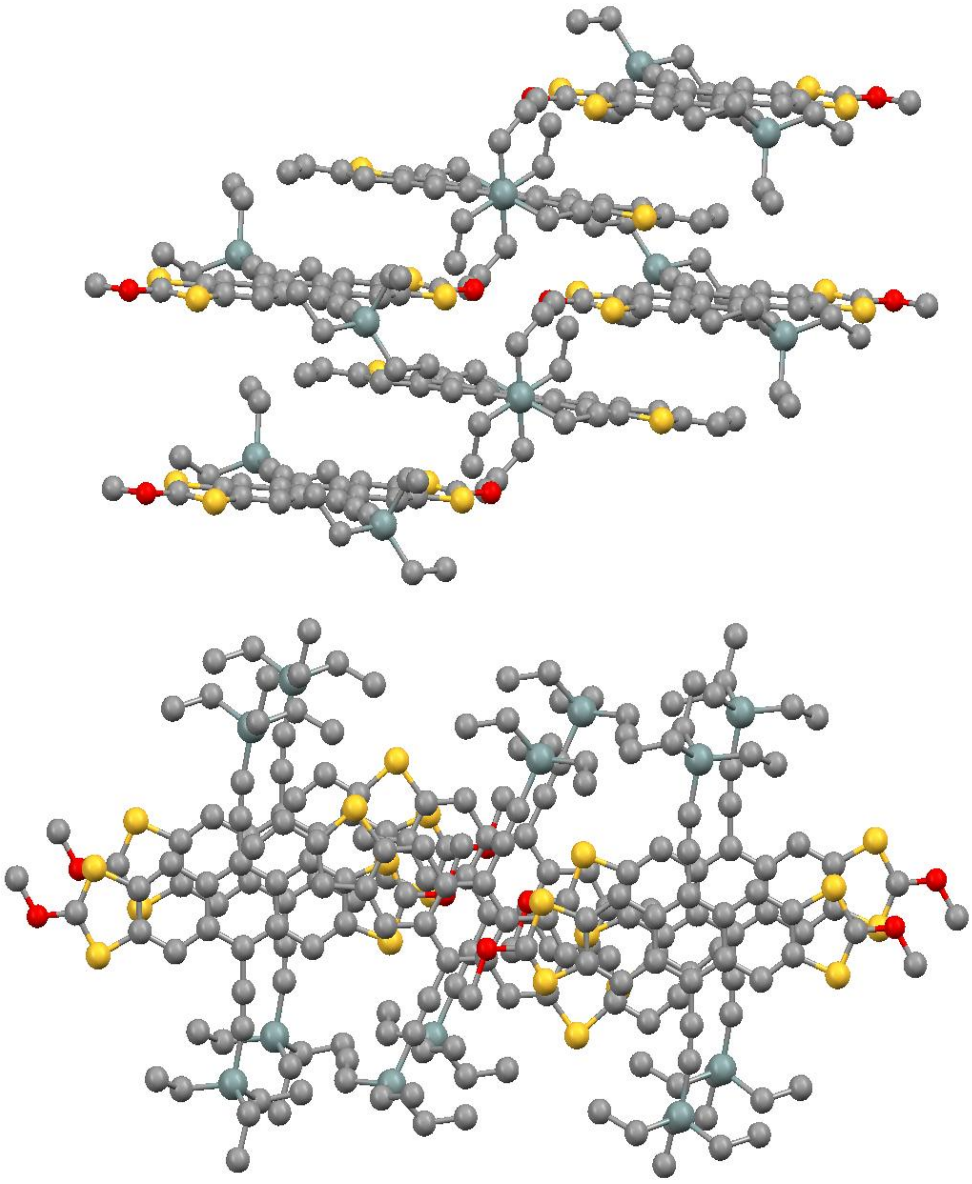

In order to improve the charge injection into the active layer from the metal electrode, my first approach was to reduce the oxidation potential of the organic semiconductor by means of introducing electron donating groups at the end positions of the acene chromophore. For this, methoxy-substituted functionalized anthradithiophene (**100**) was

synthesized in four-step process starting from the copper (II) oxide catalyzed methoxylation of **96**[109] (Scheme 5.1). The resultant organic semiconductor **100** was purified by recrystallization in hexanes. The crystals were analyzed by single crystal X-ray diffraction, which reveals that **100** diffracted poorly and exhibits weak two-dimensional π-stacking interactions with the closest interatomic carbon-carbon distance of 3.48 Å (see Fig. 5.1). Hence, neither functioning transistors nor photovoltaics could be constructed from this material.

5.2 3,4,5-Trimethoxyphenyl substituted functionalized anthradithiophene

My next rational approach for extending conjugation of the anthradithiophene chromophore was the introduction of phenyl rings. To induce more conjugation (as well as lower oxidation potential to improve charge injection), I used electron-rich 3,4,5-trimethoxy phenyl groups at the α-positions of the terminal thiophene rings (Scheme 5.2). The necessary 5-substituted thiophene-2, 3-diacetal **107** was prepared by Suzuki coupling of 5-iodothiophene-2, 3-diacetal **85** with the boronic acid **106**,[110] and the general synthesis for all of our acenes was followed to yield **110**.

Scheme 5.2 Synthesis of 3,4,5-trimethoxyphenyl-substituted functionalized anthradithiophene (107).

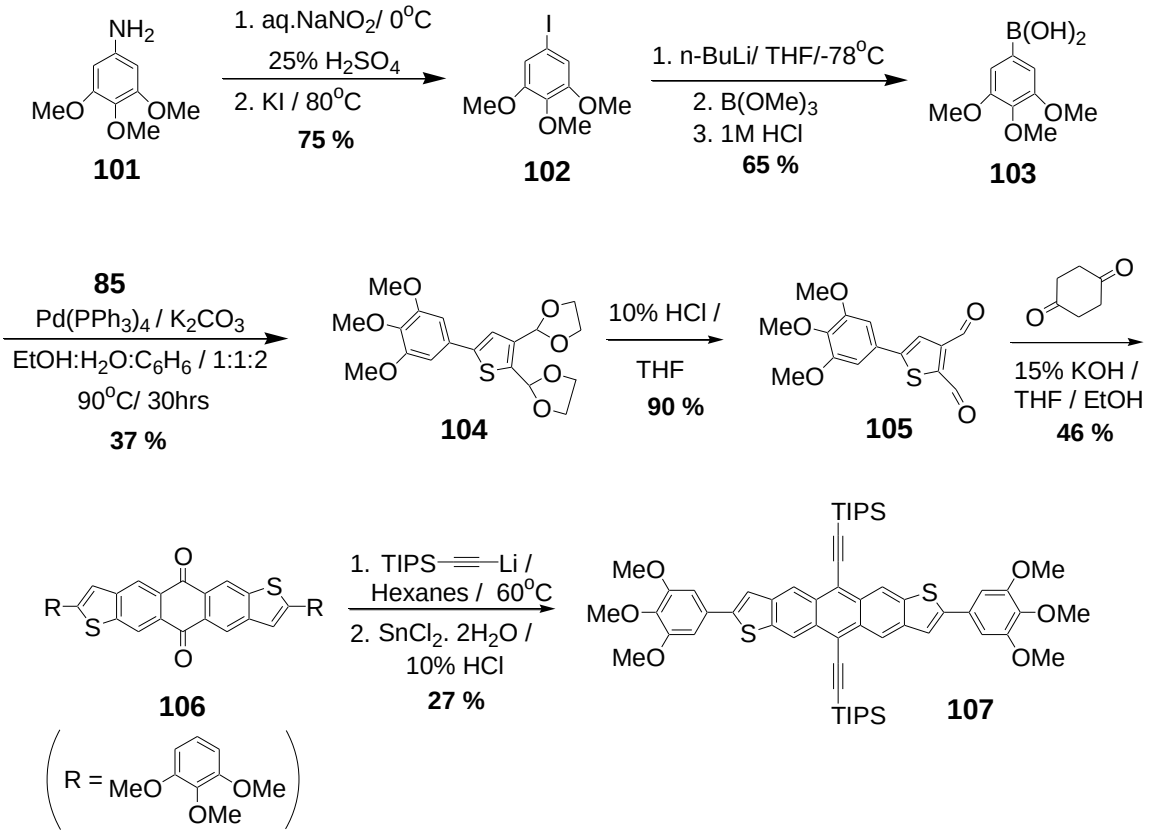

X - ray crystallographic analysis of crystals grown from toluene revealed that the molecule adopts two dimensional π-stacking with closest interatomic carbon-carbon distance of 3.56 Å. The thermal ellipsoid plot and π-stacking interactions in **107** are shown in Fig. 5.2 and Fig. 5.3, respectively.

Figure 5.2 Thermal ellipsoid plot of 107.

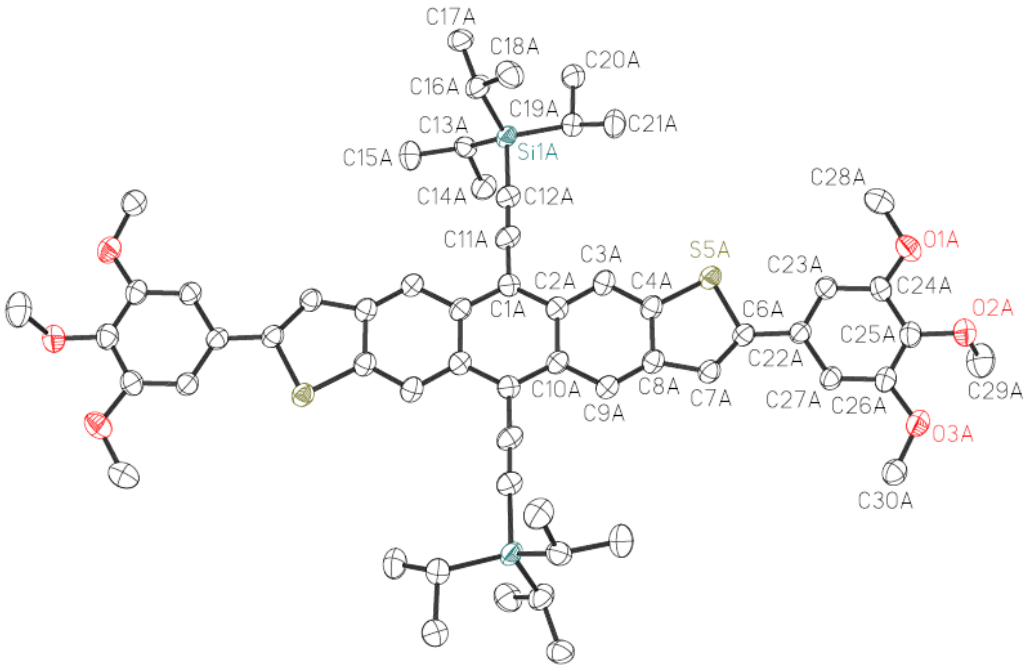

Figure 5.3 π-stacking interactions in 107.

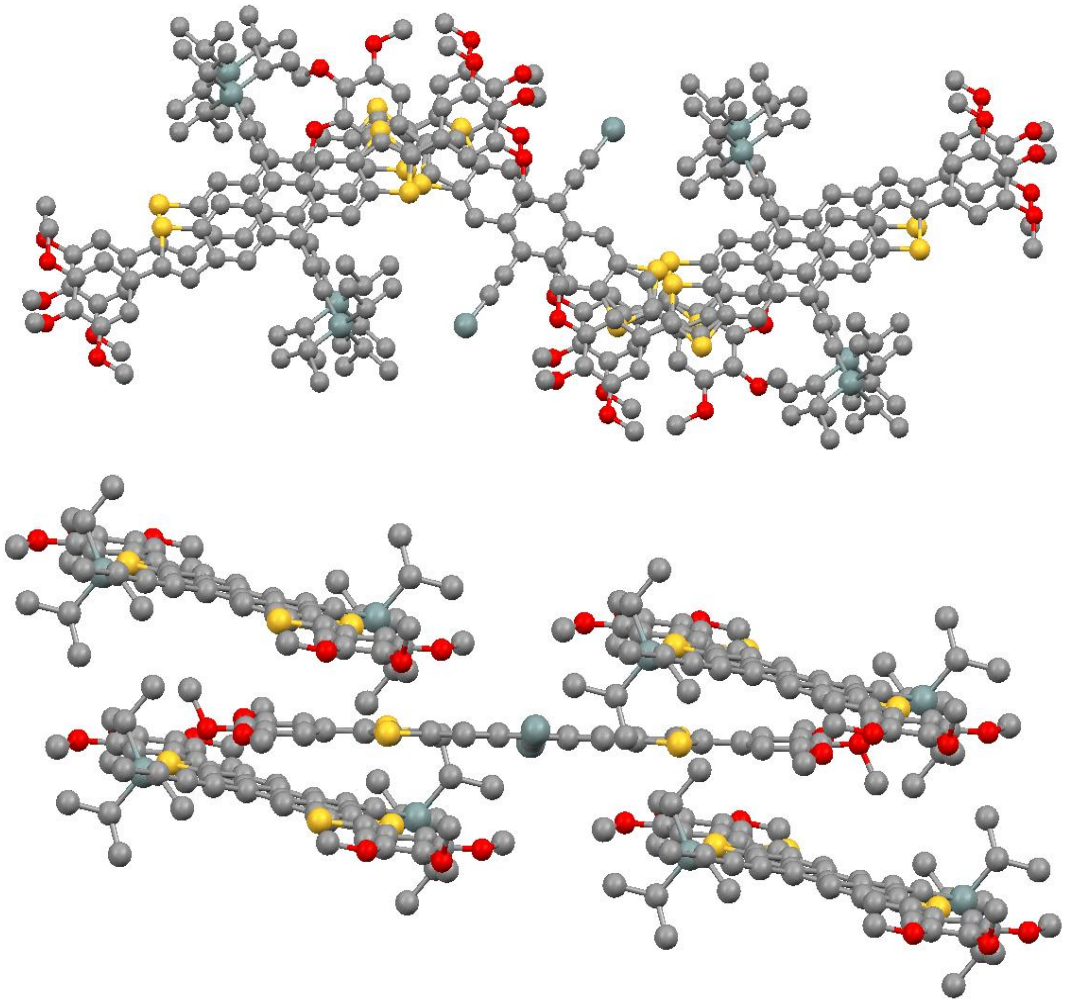

5.3 Cyano substituted functionalized anthradithiophenes

One of the advantages of the end substitution on anthradithiophene chromophore is to synthesize n-type organic semiconductors by attaching electron withdrawing groups. Here, I have tried to increase the conjugation length of the acene chromophore through electron withdrawing cyano groups. **108** and **109** were easily synthesized by a Pd (0)

catalyzed cyanation of **88** and **91** (Scheme 5.3)**,** and crystals were grown from dichloromethane.

Scheme 5.3 Synthesis of cyano-substituted functionalized anthradithiophenes (108 and 109).

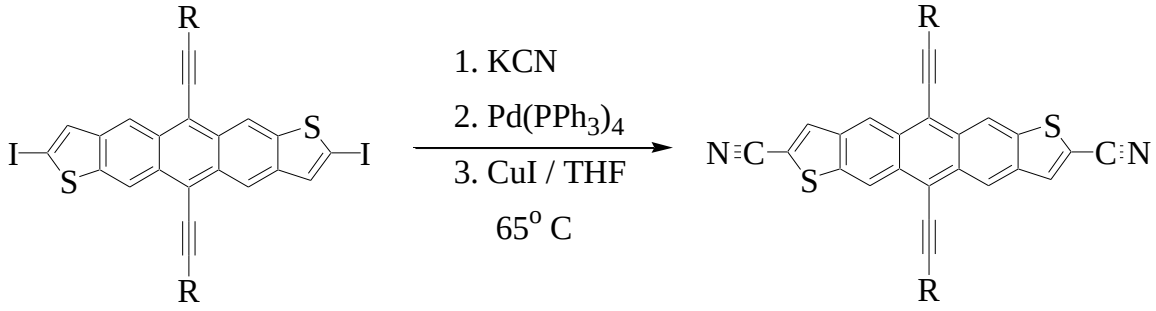

R = TES, **108, 76 %**
R = TIPS, **109, 78 %**

Single crystal X-ray diffraction studies reveal that **109** possesses one-dimensional slipped π-stacking with a closest carbon-carbon interatomic distance of 3.49 Å. The thermal ellipsoid plot and π-stacking interactions are shown in Fig. 5.4 and Fig. 5.5, respectively. Unfortunately, attempts to recrystallize **108** from various organic solvents such as hexanes, dichloromethane, dichloroethane, toluene, xylene, dichlorobenzene left **108** in amorphous powders, hence, no XRD data could be derived from **108**.

Figure 5.4 Thermal ellipsoid plot of 109.

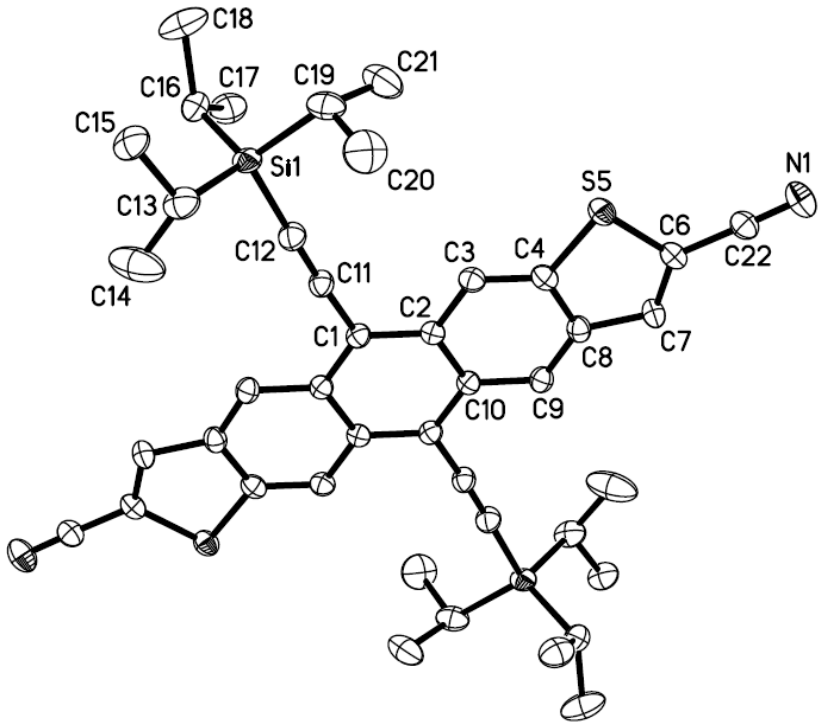

Figure 5.5 π-stacking interactions in 109.

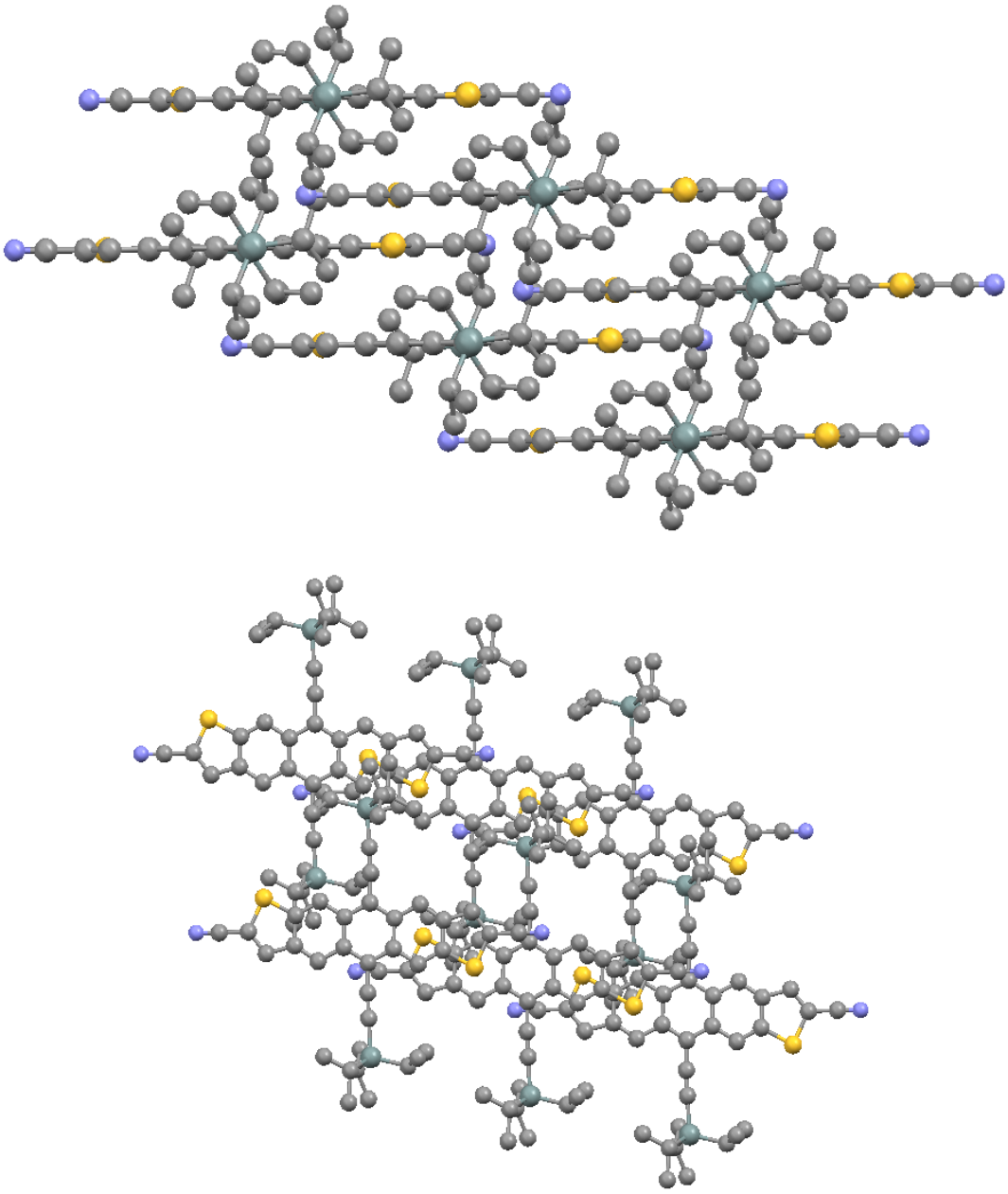

5.4 Trimethylsilylethynyl functionalized anthradithiophenes

My next strategy was to end-functionalize the anthradithiophenes with trialkylsilylethynyl groups. 2,8-bis(trimethylsilylethynyl)-substituted functionalized anthradithiophene (**110**) was easily synthesized by a palladium-catalyzed coupling between an alkyne and **91**. The product was finally purified by recrystallization from hexanes.

Scheme 5.4 Synthesis of trimethylsilylethynyl-substituted functionalized anthradithiophenes (110).

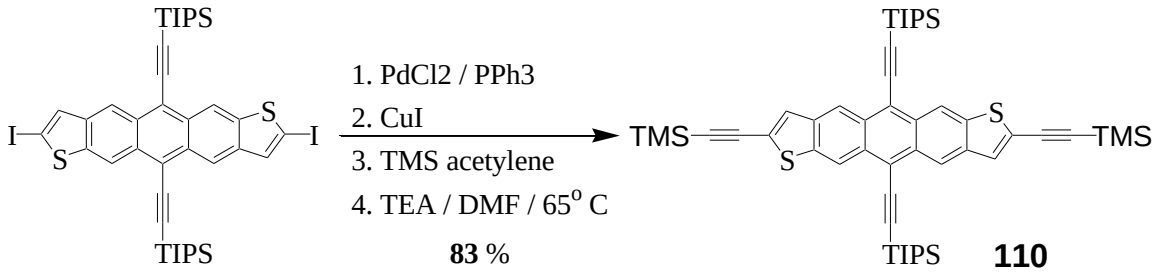

Figure 5.6 Thermal ellipsoid plot of 110.

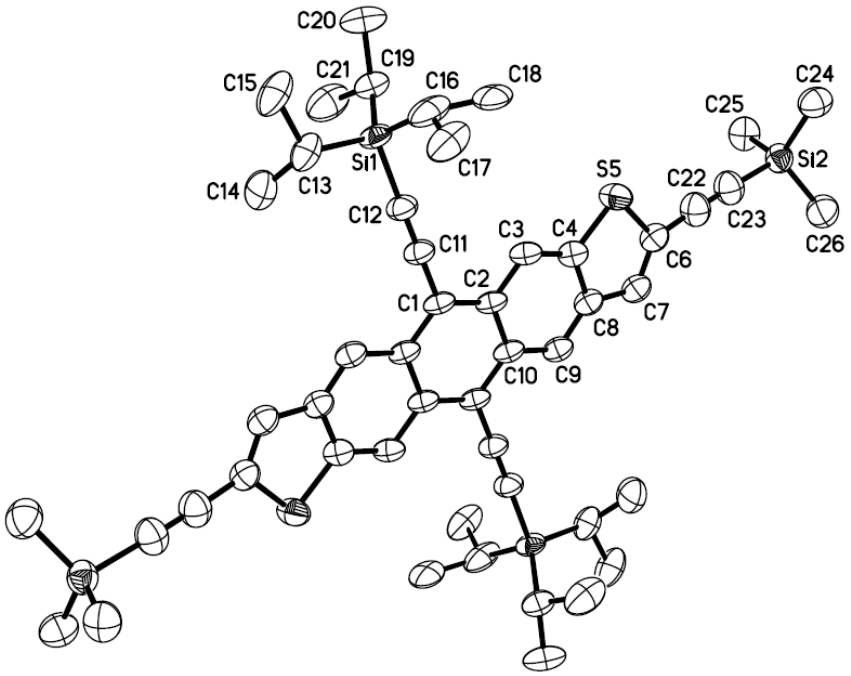

Figure 5.7 π-stacking interactions in 110.

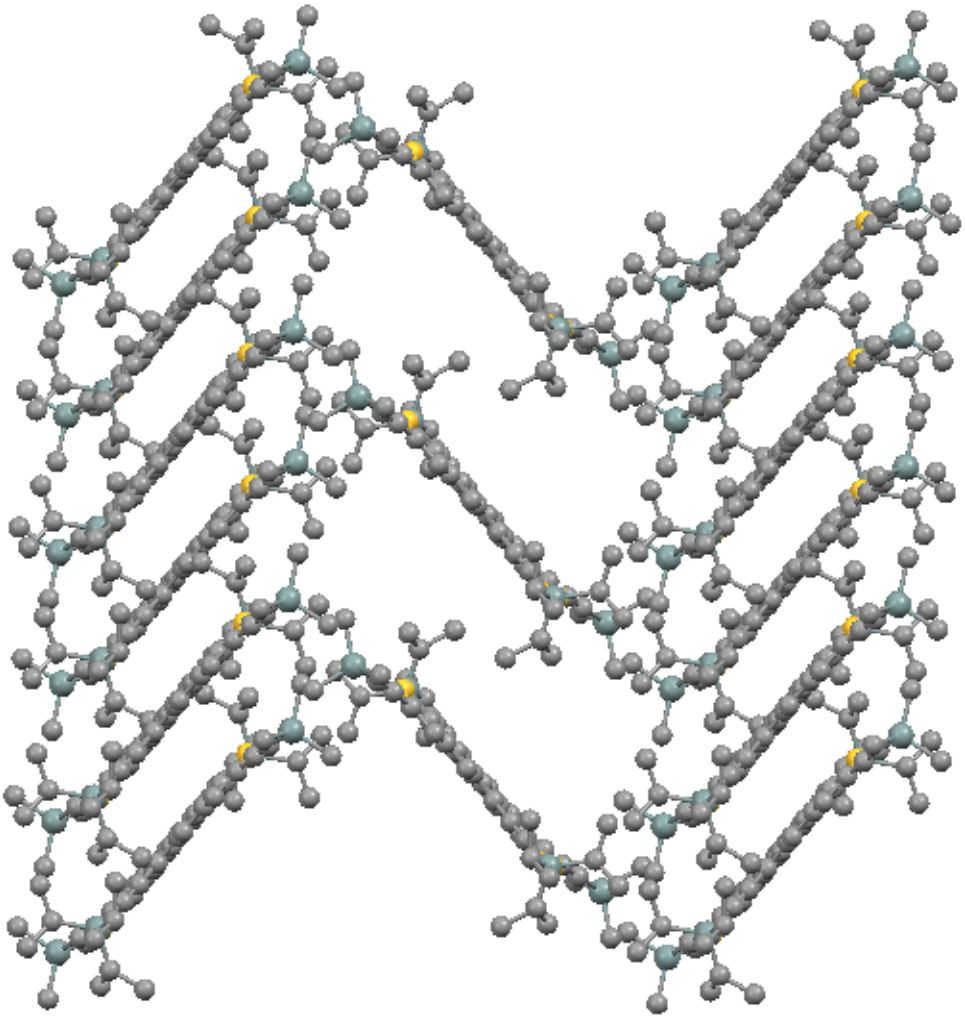

Single crystal X-ray diffraction studies revealed that **110** diffracted poorly and possesses 1-D π-stacks with *herringbone*-type interactions (edge-to-face interactions) between two adjacent stacks, with the closest interatomic carbon-carbon distance of 3.45 Å. The thermal ellipsoid plot and crystal packing of **110** are shown in Fig. 5.6 and Fig. 5.7, respectively. Solvent molecules (dichloroethane) were found between the pi-stacking of

neighboring molecules. Upon selective desilylation of trimethylsilyl group using potassium carbonate in methanol (with little THF for solubility), **110** (dark red) turned into black solution indicating decomposition.

5.5 Experimental Details

General.

Solvents (acetone, methylene chloride, hexanes) were purchased from Fisher. Dry THF was either purchased in anhydrous form from EMS Science or distilled over sodium / benzophenone under N_2 atmosphere. Trialkylsilyl acetylenes were purchased from GFS Chemicals. Silica gel 230-400 mesh was bought from Sorbent Technologies. NMR spectra were measured on a Varian (Gemini 200 MHz / Unity 400 MHz) spectrometer. Chemical shifts were reported in ppm relative to $CDCl_3$ as internal standard. The UV spectra were measured on a UV-2501PC Shimadzu instrument. Mass spectroscopy was analyzed in EI mode at 70 eV on a JEOL (JMS-700T) Mass Spectrometer. Cyclic Voltammetry was carried out on a BAS CV-50W potentiostat, with ferrocene as an internal standard.

5-iodo thiophene-2,3-diacetal (96).

See the experimental section, chapter 4.

5- Methoxy thiophene 2,3-dialdehyde (98).

Copper (II) oxide (0.51g, 6.4 mmol) and **96** (4.5g, 12.7 mmol) were added to a solution of 25 wt % sodium methoxide (9 ml, 51 mmol) in methanol in a flame dried single necked 250 mL round bottom flask, and the reaction mixture was refluxed for 24 h. It was then filtered and poured into cold water (250 mL), and extracted with ether. The organic layer was separated, dried over anhydrous $MgSO_4$ and the solvent was

evaporated to yield 83 % of 5-methoxy thiophene-2,3-diacetal (**97**). MS (EI 70 eV) *m/z* 258 (100 %, M^+). Without purification, this material was hydrolyzed with 3M HCl (100 mL) for 1 hr. This product was extracted in ether, and was purified by column chromatography using hexanes / dichloromethane (120 mL / 180 mL). Yield = 65%. ^{1}H NMR (200 MHz, $CDCl_3$): δ 4.02 (s, 3H), 6.63 (s, 1H), 10.33 (s, 1H), 10.35 (s, 1H) ppm. ^{13}C NMR (50 MHz, $CDCl_3$): δ 60.99, 106.10, 135.02, 144.07, 174.16, 181.43, 184.38 ppm. MS (EI 70 eV) *m/z* 170 (M^+), 142 (M^+ - CHO).

2,8-Dimethoxy anthradithiophene-5,12-dione (99).

To the mixture of 1.4-cyclohexanedione (5.5 mmol) and 5-methoxy thiophene -2,3-dialdehyde (11.0 mmol) in tetrahydrofuran / ethanol (5 mL / 15 mL), 15 % of KOH (few drops) was added, stirred at RT for 3 hrs. The quinone was filtered through buchner funnel and washed with ethanol and dried in air. Yield = 85%. MS (MALDI, TCNQ matrix) *m/z* 380 (100%, M^+).

2,8-Dimethoxy-5,12-bis(triethylsilylethynyl)anthradithiophene (100).

n-BuLi (1.54 mL, 3.85 mmol) was added to triethylsilylacetylene (0.8 mL, 4.4 mmol) in tetrahydrafuran (50 mL) under N_2 atm at RT in a flame dried 500 mL RB flask, stirred for 30 min. To that, methoxy substituted anthradithiophenequinone (0.42 g, 1.1 mmol) was added and stirred for overnight. The next day, stannous chloride (3.3 mmol), 0.5 mL of water and 1.5 mL of 10% HCl were added, and the reaction mixture allowed to stir for 5 h. The reaction mixture was dried over anhydrous $MgSO_4$ and concentrated. It was purified by silica plug, washed by using hexanes and concentrated to get pure product. Yield = 65%. ^{1}H NMR (400 MHz, $CDCl_3$): δ 0.90 (m, 12H), 1.24 (m, 18H), 4.09 (s, 6H), 6.39 (s, 2H), 8.68 (s, 2H), 8.84 (s, 2H) ppm. ^{13}C NMR (100 MHz, $CDCl_3$): δ 4.94, 8.04,

59.92, 96.70, 103.52, 103.79, 104.05, 105.78, 105.88, 116.30, 116.45, 117.84, 118.04, 119.45, 119.66, 128.92, 129.41, 130.09, 130.59, 134.45, 134.74, 139.54, 139.77, 166.97, 167.07 ppm. MS (EI 70 eV) *m/z* 628 (12%, M^+), 627 (16%, M^+ - 1), 626 (32%, M^+ - 2). Anal. calcd. % C: 68.96, % H: 6.75, Found % C: 68.58, % H: 6.67.

3, 4, 5-Trimethoxyphenyl iodide (102).

In a two necked 500 mL round bottom flask, 3, 4, 5-trimethoxy aniline **101** (5 g, 27.3 mmol) in 25% H_2SO_4 was added slowly to $NaNO_2$ (5.66 g, 82 mmol) in water (40 mL) at 0-4 °C. After stirring for 30 minutes, potassium iodide pellets (13.6 g, 82 mmol) were added, followed by vigorous evolution of N_2. It was then heated at 80 °C for 90 minutes until the evolution of the gas ceased. The reaction mixture was cooled and extracted with ether, washed with 10% sodium thiosulphate (100 mL), water and saturated brine solution. The organic layer was dried over anhydrous $MgSO_4$ and concentrated. It was purified by silica plug using hexanes / methylene chloride (200 mL / 300 mL). Yield = 6 g (75%). ^{1}H NMR (200 MHz, $CDCl_3$): δ 3.84 (s, 9H), 6.89 (s, 2H) ppm.

3, 4, 5-Trimethoxyphenyl boronic acid (103).

In a single necked 250 mL RB Flask, n- BuLi (3.5 mL, 8.7 mmol) was added to **102** (1.5 g, 5.1 mmol) in dry THF at -78 °C under N_2 atm. After stirring for 30 min. at -78 °C, the reaction mixture was was warmed to 0 °C and then cooled back to -78 °C immediately. To the mixture, trimethyl borate (1.4 g, 13.3 mmol) was then added and stirred at RT for 14 hrs. It was then quenched by addition of 1M HCl (18 mL) and was extracted with ether, washed with water and brine solution. It was then dried and concentrated. Yield = 0.7 g (65%). Without purification, it was taken to the next step.

5-(3, 4, 5-trimethoxyphenyl) thiophene-2,3-diacetal (104).

In a single necked 250 mL RB Flask, a mixture of **103** (0.7 g, 3.3 mmol) and 5-iodo thiophene-2,3-diacetal **96** (0.98 g, 2.8 mmol), was taken in EtOH:H_2O:C_6H_6 (1:1:2) (50 mL) and sparged with N_2 for 30 min. To that, potassium carbonate (1.4 g, 10.08 mmol) and tetrakis(triphenylphosphine) palladium(0) (0.5 g, 0.4 mmol) were added, the mixture sparged for a further 15 min. then heated at 90 °C for 30 hours. The solvents were evaporated, cooled to room temperature and extracted with ether, washed with water and the organic layer was dried over anhydrous $MgSO_4$ and concentrated. It was then purified by silica plug using hexanes / ethyl acetate mixture (200 mL / 300 mL). Yield = 0.4 g (37%). MS (EI 70 eV) *m/z* 394 (100%, M+).

5-(3, 4, 5-trimethoxyphenyl) thiophene-2,3-dialdehyde (105).

The diacetal **104** was hydrolysed with 1 M HCl in 2 h and the reaction mixture was extracted with ether. The organic layer was separated, dried over anhydrous $MgSO_4$ and concentrated. Without any purification, the dialdehyde **105** was taken to next step. Yield = 90%. MS (EI 70 eV) *m/z* 306 (100%, M+), 263 (70%, M+ – 43).

2,8-Di(3, 4, 5-trimethoxyphenyl)anthradithiophene-5,12-dione (106).

To the mixture of 1,4-cyclohexanedione (5.5 mmol) and 5-(3, 4, 5-trimethoxyphenyl) thiophene -2,3-dialdehyde (11.0 mmol) in tetrahydrofuran / ethanol (5 mL / 15 mL), 15 % of KOH (few drops) was added, stirred at RT for 3 hrs. The quinone was filtered through a buchner funnel and the solid washed with ethanol and dried in air. Yield = 46%. MS (MALDI, TCNQ matrix) 652 (100%, M+).

2,8-Di(3,4,5-trimethoxyphenyl)-5,12-bis(triisopropylsilylethynyl)anthradithiophene (107).

n-BuLi (0.72 mL, 1.8 mmol) was added to triisopropylsilylacetylene (0.36 g, 2.0 mmol) in hexane (50 mL) under N_2 atm at RT in a flame dried 500 mL round bottom flask, and stirred for 30 min. To that, 5-(3, 4, 5-trimethoxy phenyl) anthradithiophene quinone (0.5 g, 0.5 mmol) and hexanes (200 mL) were added and the solution heated at 66 °C overnight. The next day, stannous chloride (1.5 mmol), 0.5 mL of water and 1.5 mL of 1% sulphuric acid were added and the mixture heated for 5 hrs. The reaction mixture was cooled and dried over anhydrous $MgSO_4$. It was purified by filtration through a silica plug (hexanes) and concentrated to get pure product. Yield = 0.2 g (27 %). ^{1}H NMR (200 MHz, $CDCl_3$): δ 1.31 – 1.37 (s, 42H), 3.94 (s, 6H), 4.02 (s, 12H), 7.07 (s, 4H), 7.56 (s, 2H), 9.02 – 9.16 (d, J = 6.2 Hz, 4H). MS (EI 70 eV) *m/z* 984 (35%, M+ + 1), 983 (40%, M+), 982 (45%, M+ - 1). Anal. calcd. % C: 70.83, % H: 7.17, Found % C: 70.38, % H: 6.88.

General procedure for the preparation of cyano-substituted trialkylsilylethynyl anthradithiophenes:

In a 250 mL round bottom flask, the iodo-substituted functionalized anthradithiophenes (**88** or **91,** 0.44 mmol) was added to the mixture of Pd $(PPh_3)_4$ (76.2 mg, 0.066 mmol), potassium cyanide (120 mg, 1.85 mmol), and copper (I) iodide (16.75 mg, 0.088 mmol) in degasified THF, and the reaction mixture was heated at 65 °C for overnight. The room temperature cold reaction mixture was then extracted with ether, and washed with water. The organic layer was separated, dried over anhydrous $MgSO_4$, and concentrated. The

desired cyano-substituted anthradithiophenes were purified on a short pad of silica gel using hexanes / dichlormethane (2 : 5).

2,8-Dicyano-5,12-bis(triethylsilylethynyl)anthradithiophene (108). Yield = 76%. ^{1}H NMR (200 MHz, $CDCl_3$): δ 0.96 (s, 12H), 1.26 (s, 18H) 8.02 (s, 2H), 9.09 (s, 2H), 9.18 (s, 2H) ppm. MS (EI 70 eV) *m/z* 618 (25%, M+ + 1), 617 (50%, M+), 616 (100%, M+ - 1).

2,8-Dicyano-5,12-bis(triisopropylsilylethynyl)anthradithiophene (109). Yield = 78%. This was recrystallized in dichloromethane. ^{1}H NMR (200 MHz, $CDCl_3$): δ 1.34 (s, 42H), 8.04 (s, 2H), 9.18 (s, 2H), 9.30 (s, 2H) ppm. ^{13}C NMR (50 MHz, $CDCl_3$): δ 11.71, 19.05, 97.29, 103.15, 108.09, 108.72, 109.34, 113.30, 113.50, 114.20, 117.33, 119.35, 120.74, 120.81, 121.40, 125.17, 130.30, 130.82, 131.16, 131.68, 135.64, 137.91, 138.20, 139.14, 139.58 ppm. MS (EI 70 eV) *m/z* 702 (30%, M+ + 1), 701 (65%, M+), 700 (100%, M+ - 1).

2,8-Di(trimethylsilylethynyl)-5,12-bis(triisopropylsilylethynyl)anthradithiophene (110).

In a flame dried 100 mL single necked round bottom flask, the mixture of **91** (1g, 1.1 mmol), trimethylsilyl acetylene (0.27g, 2.77 mmol), palladium (II) chloride (19.5 mg, 0.11 mmol), triphenyl phosphine (57.6 mg, 0.22 mmol), and copper (I) iodide (21 mg, 0.11 mmol) in a degasified solvent mixture of triethylamine (30 mL) and DMF (10 mL) was heated at 70 °C for overnight. The reaction mixture was extracted in ether, washed with water, the organic layer was dried over anhydrous $MgSO_4$ and concentrated. It was then purified on a short pad of silica gel, followed by recrystallization in hexanes. Yield = 83%. ^{1}H NMR (400 MHz, $CDCl_3$): δ 0.33 (s, 18H), 1.33 (s, 42H), 7.58 (t, J = 0.2Hz, 2H),

9.05 (q, J = 2.3Hz, 2H), 9.06 (s, 2H) ppm. ^{13}C NMR (100 MHz, $CDCl_3$): δ -0.04, 11.80, 19.13, 97.97, 103.96, 104.03, 106.11, 106.54, 106.99, 116.48, 118.01, 119.57, 119.59, 122.09, 122.13, 126.05, 126.19, 129.48, 130.23, 130.48, 130.73, 139.74, 139.77, 139.91, 140.02 ppm. MS (EI 70 eV) *m/z* 843 (5%, M+), 746 (10%, M+ - trimethylsilylethynyl).

Chapter 6: Conclusion

6.1 Summary of New Functionalized Pentacenes and Anthradithiophenes.

Extensive investigation of organic semiconductors over the past two decades has helped to produce high performance electronic devices. However, more research is needed to allow the commercialization of organic electronic devices. Using our group's *peri*-functionalization approach, I have synthesized a variety of stable and soluble functionalized pentacenes and anthradithiophenes (along with a few unstable derivatives). In the second chapter, I discussed my attempts to induce liquid crystallinity through functionalization of pentacene in order to form high quality, uniform thin films. I found that alkyl chain length is directly related to crystal packing as well as to the stability of the organic semiconductors. As the number of carbons in the alkyl substitutent increases, the aryl - aryl interactions shift to aryl - alkyl interactions, leading to poor electronic interactions in the solid state. Oxidative stability of these functionalized pentacenes was greatly enhanced by the introduction of silyl substitutents at the *peri*-positions of pentacene. The multiple thermal phase transitions observed for **53** by DSC experiment suggested the possibility of thermotropic liquid crystalline phases. However, due to lack of π-stacking between the neighboring molecules, **53** is a poor organic semiconductor. As found in the alkynyl pentacenes, optimal alkyl chain lengths on silyl substitutents are required for strong π-stacking interactions in *peri*-functionalized trialkylsilylethynyl pentacenes.

Substitution of the reactive thiophene positions of **21** produced materials with increased stability. In the third chapter, the effect of small increases in alkyl chain length on crystal packing and thin film morphology of functionalized anthradithiophenes had

been addressed. **66** showed the highest thin film hole mobility (0.3 cm^2/Vs) among the alkylated anthradithiophene derivatives, which was attributed to its crystal packing and its uniform thin film forming ability. On the other hand, other alkylated anthradithiophenes (**67** and **68**) showed promising results in stacked organic photovoltaic devices. **68**-based organic solar cells exhibited 0.33 % power conversion efficiency, where C_{60} and **68** were deposited through vacuum evaporation and from solution, respectively. Interestingly, **67**-based bulk heterojunction solar cells, where both **67** and PCBM were deposition from solution, produced 1.003% power conversion efficiency.

Chapter 4 discussed halogen substitution on functionalized anthradithiophenes, which produced devices with excellent electronic properties in organic field effect transistors. The fluorine-substituted anthradithiophene derivatives possessed strong two-dimensional pi-stacking, and the single crystal XRD studies disclose that the other halogen-substituted anthradithiophenes adopt weak 1-D π-stacked solid state arrangements. In addition to the exceptional photostability, oxidative stability and thermal stability shown by **85** and **89**, the type of spatial fluorine and sulfur-fluorine interactions determine the nature of thin films and solution grown crystals made from these anthradithiophenes. **89**, in which the nonbonded F…F interactions are predominant, forms the moderately smooth surface solution grown big (~ 2 cm long or 1 cm^3) crystals, which exhibited single crystal hole mobility of 0.1 cm^2/Vs from the organic single crystal transistors. In contrast, **85**, in which the nonbonded S…F interactions are predominant, forms uniform thin films on devices and exhibited thin film hole mobility of 1 cm^2/Vs consistently from organic thin film transistors.

In chapter 5, the use the methoxy and trimethoxyphenyl substitution on anthradithiophene chromophore didn't help to achieve my goal of reducing the oxidation potential of the organic semiconductor in order for better charge injection from the metal electrode. Also, it is observed that the electron withdrawing cyano group substitution on acene chromophore was not sufficiently electron deficient to synthesize n-type organic semiconductor. Attempt to increase the conjugation length of the acene chromophore through dimerisation using ethynyl spacer was not successful since decomposition of **110** upon the selective desilylation of **110**.

6.2 Future Targets

The presence of acidic hydrogens at the terminal thiophene rings of anthradithiophene chromophore allows us to engineer the acene crystal packing further. In continuation with this extended conjugation approach, the following type of materials (**111** and **112**) might be expected to improve the crystal packing because of larger pi-orbital overlap between neighboring molecules (Fig. 5.8). Due to time constraints, those compounds were not synthesized and studied for organic electronic devices. In addition to different functionalization that can be done on phenyl and thienyl groups of **111** and **112**, respectively, much more non-bonded sulphur…halogen interactions could be explored by attaching halogens (especially fluorine atom from the outcome of this dissertation) on thienyl groups of **112**. Another interesting and challenging material would be increasing the fluorine substituents on trialkylsilylethynyl anthradithiophenes. Synthesizing more fluorine substituted anthradithiophenes such as **113** are expected to enhance the nonbonded S…F and F…F interactions compared to **85** and **89**, thereby, increasing the

amount of pi-overlapping of neighboring molecules, could eventually yield novel high performing organic semiconductors for electronic applications.

Figure 5.8. Future Targets.

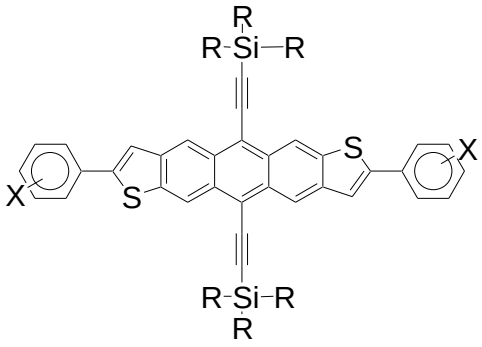

111

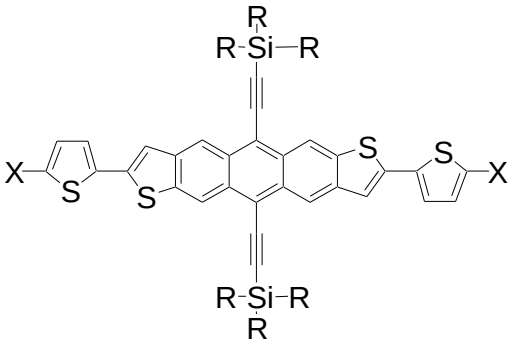

112

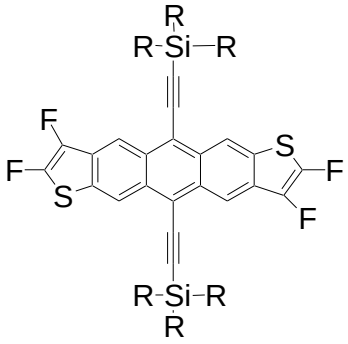

113

R = alkyl chains
X = substituents

Our approach to peri-functionalize acene oligomers has produced materials with increased oxidative stability, solubility in organic solvents, and remarkably improved pi-stacking solid state arrangements. A slight change in solubilizing silyl groups as well as end-substitution on acene chromophore has enormous influence on the crystal packing, thin film morphology and charge transport properties. Taking advantage of chemical tunability and rationalizing the structure and property relationships of the functionalized oligoacenes, we can design and synthesize improved organic electronic materials. In

addition, it allows us to provide proper direction for the scientific community in the field of organic electronics to develop novel solution processable organic semiconductors.

Table 5.1 UV-vis and electrochemical measurements on functionalized anthradithiophenes.

No.	Materials	λmax[a] (nm)	E_{ox}[b] (mV)	Optical Gap (eV)	E_{HOMO} (eV)	E_{LUMO} (eV)
1.	TES anthradithiophene, **21**	555	904	2.17	5.22	3.05
2.	Methyl TES anthradithiophene, **66**	549	839	2.19	5.16	2.97
3.	Ethyl TES anthradithiophene, **67**	550	833	2.19	5.15	2.96
4.	Propyl TES anthradithiophene, **68**	550	829	2.18	5.15	2.97
5.	Butyl TES anthradithiophene, **69**	551	823	2.18	5.14	2.96
6.	Fluoro TES anthradithiophene, **85**	527	1017	2.29	5.34	3.05
7.	Chloro TES anthradithiophene, **86**	541	1021	2.23	5.34	3.11
8.	Bromo TES anthradithiophene, **87**	545	1015	2.20	5.34	3.14
9.	Iodo TES anthradithiophene, **88**	551	996	2.19	5.32	3.13
10.	Methoxy TES anthradithiophene, **100**	537	800	2.22	5.12	2.90
11.	Trimethoxyphenyl TIPS anthradithiophene, **107**	571	870	2.11	5.19	3.08
12.	Cyano TES anthradithiophene, **108**	583	1216	2.06	5.55	3.49
13.	Trimethylsilylethynyl TIPS anthradithiophene, **110**	570	971	2.13	5.29	3.16

[a]Recorded in dichloromethane. [b]Performed in 0.1 M solution of Bu_4NPF_6 in dichloromethane, Pt electrode, scan rate 150 mV/s, Ferrocene as internal standard.

References

1. Zhang, Y.; Petta, J. R.; Ambily, S.; Shen, Y.; Ralph, D. C.; Malliaras, G. G. *Adv. Mater.* **2003**, *15*, 1632.

2. Katz, H. E. *J. Mater. Chem*. **1997**, *7*, 369.

3. Xiang, M.; Li, X.; Ober, C. K.; Char, K.; Genzer, J.; Sivaniah, E.; Kramer, E. J.; Fisher, D. A. *Macromolecules*, **2000**, *33*, 6106.

4. Bao, Z.; Dodabalapur, A.; Lovinger, A. J. *Appl. Phys. Lett.* **1996**, *69*, 4108.

5. Loo, Y. -L.; Someya, T.; Baldwin, K. W.; Bao, Z.; Ho, P.; Dodabalapur, A.; Katz, H. E.; Rogers, J. A. *Proc. Natl. Acad. Sci*. **2002**, *99*, 10252.

6. Blanchet, G. B.; Loo, Y. -L.; Rogers, J. A.; Gao, F.; Fincher, C. R. *App. Phys. Lett*. **2003**, *82*, 463.

7. Shirakawa, H.; Louis, E. J.; MacDiarmid, A. G.; Chiang, C. K.; Heeger, A. J. *J. C. S. Chem. Comm.* **1977**, 578.

8. Dimitrakopoulos, C. D.; Malenfant, P. R. L. *Adv. Mater.* **2002**, *14*, 99.

9. Horowitz, G. *J. Mater. Res*. **2004**, *19*, 1946.

10. Tang, C. W.; Slyke, V. S. A. *Appl. Phys. Lett*. **1987**, *51*, 913.

11. Peumans, P.; Forrest, S. R. *Appl. Phys. Lett*. **2001**, *79*, 126.

12. a) Li, S. S.; Thurber, W. R. *Solid-St. Electron*. **1977**, *20*, 609. b) Dorkel, J. M.; Leturcq, Ph. *Solid-St. Electron*. **1981**, *24*, 821.

12. Kepler, R. G. *Phys. Rev*. **1960**, *119*, 1226.

14. Leblanc, O.H. *J. Chem. Phys*. **1960**, *33*, 626.

15. de Boer, R. W. I.; Jochemsen, M.; Klapwijk, T. M.; Morpurgo, A. F.; Niemax, J.; Tripathi, A. K.; Pflaum, J. *J. Appl. Phys*. **2004**, *104*, 4891.

16. Horowitz, G. *Adv. Mater*. **1998**, *10*, 365.

17. Dodabalapur, A.; Torsi, L.; Katz, H. E. *Science.* **1995**, *268*, 270.

18. a) see ref 14. b) J. E. Lilienfield, US Patent 1 745 175, **1930**.

19. a) Kahng, D.; Atalla, M. M. DRC, Pittsburg, **1960**. b) US Patent No. 3, 102, 230, **1963**. c) https://www.electrochem.org/dl/ma/201/pdfs/0366.pdf

20. Barbe, D. F.; Westgate, C. R. *J. Phys. Chem. Solids*. **1970**, *31*, 2679.

21. Koezuka, H.; Tsumura, T.; Ando, Y. *Synth. Met*. **1987**, *18*, 699.

22. Tsumura, T.; Koezuka, H.; Ando, Y. *Synth. Met*. **1988**, *25*, 11.

23. Lanquindanum, J. G.; Katz, H. E.; Lovinger, A. J.; Dodabalapur, A. *Adv. Mater*. **1997**, *9*, 36.

24. Mas-Torrent, M.; Hadley, P.; Bromley, S. T.; Crivillers, N.; Veciana, J.; Rovira, C. *Appl. Phys. Lett*. **2005**, *86*, 012110.

25. See ref. 17.

26. Burroughes, J. H.; Friend, R. H.; Allen, P. C. *J. Phys. D: Appl. Phys*. **1989**, *22*, 956.

27. a) Bao, Z.; Lovinger, A. J.; Dodabalapur, A. *Adv. Mater*. **1997**, *9*, 42. b) Bao, Z.; Lovinger, A. J.; Dadabalapur, A. *Appl. Phys. Lett*. **1996**, *69*, 3066.

28. Pisula, W.; Menon, A.; Stepputat, M.; Lieberwirth, I.; Kolb, U.; Tracz, A.; Sirringhaus, H.; Pakula, T.; Mullen, K. *Adv. Mater*. **2005**, *17*, 684.

29. a) Hoshimono, K.; Fujimori, S.; Fujita, S.; Fujita, S. *Jpn. J. Appl. Phys*. **1993**, *32*, L1070. b) Haddon, R. C.; Perel, A. S.; Morris, R. C.; Palstra, T. T. M.; Hebard, A. F.; Fleming, R. M. *Appl. Phys. Lett*. **1995**, *67*, 121. c). Tapponnier, A.; Biaggio, I.; Gunter, P. *Appl. Phys. Lett*. **2005**, *86*, 112114.

30. Sakamoto, Y.; Suzuki, T.; Kobayashi, M.; Goa, Y.; Fukai, Y.; Inoue, Y.; Sato, F.;

Tokito, S. *J. Am. Chem. Soc*. **2004**, *126*, 8138.

31. Malenfant, P. R. L.; Dimitrakopoulos, C. D.; Gelorme, J. D.; Kosbar, L. L.; Graham, T.O. *Appl. Phys. Lett*. **2002**, *80*, 2517.

32. a) Bao. S.; Lovinger, A. J.; Brown, J. *J. Am. Chem. Soc*. **1998**, *120*, 207. b) de Oteyza, D. G.; Barrena, E.; Osso, J. O.; Dosch, H.; Meyer, S.; Pflaum, J. *Appl. Phys. Lett.* **2005**, *87*, 183504.

33. Chesterfield, R. J.; Newman, C. R.; Pappenfus, T. M.; Ewbank, P. C.; Haukaas, M. H.; Mann, K. R.; Miller, L. L.; Frisbie, C. D. *Adv. Mater*. **2003**, *15*, 1278.

34. Facchetti, A.; Yoon, M. H.; Stern, C. L.; Katz, H. E.; Marks, T. J. *Angew, Chem. Int. Ed.* **2003**, *42*, 3900.

35. Assadi, A.; Svensson, C.; Willander, M.; Inganas, O. *Appl. Phys. Lett*. **1988**, *53*, 195.

36. Sirringhaus, H.; Brown, P. J.; Friend, R. H.; Nielsen, M. M.; Bechgaard, K.; Langeveld-Voss, B. M. W.; Spiering, A. J. H.; Janssen, R. A. J.; Meijer, E. W.; Herwig, P. T.; de Leeuw, D. M. *Nature* **1999**, *401*, 685.

37. Wang, G.; Swensen, J.; Moses, D.; Heeger, A. J. *J. Appl. Phys*. **2003**, *93*, 6137.

38. a) Garnier, F.; Yassa, A.; Hajlaoui, R.; Horowitz, G.; Deloffre, F.; Servet, B.; Ries, S.; Alnot, P. *J. Am. Chem. Soc*. **1993**, *115*, 8716. b) Dimitrakopoulos, C. D.; Furman, B. K.; Graham, T.; Hedge, S.; Purushothaman, S. *Synth. Met*. **1998**, *92*, 47.

39. Halik, M.; Klauk, H.; Zschieschang, U.; Schmid, G.; Ponomarenko, S.; Kirchmeyer, S.; Weber, W. *Adv. Mater*. **2003**, *15*, 917.

40. Minakata, T.; Nagoya, I.; Ozaki, M. *J. Appl. Phys*. **1991**, *69*, 7354. Laquindanam, J. G.; Katz, H. E.; Lovinger, A. J.; Dodabalapur, A. *Chem. Mater*. **1996**, *8*, 2542.

41. Klauk, H.; Halik, M.; Zschieschang, U.; Schmid, G.; Radllik, W.; Weber, W. *J. Appl.*

Phys. **2002**, *92*, 5259.

42. Anthony, J. E.; Brooks, J. S.; Eaton, D. L.; Parkin, S. R. *J. Am. Chem. Soc* **2001**, *123*, 9482.

43. Park, S. K.; Jackson, T. N.; Anthony, J. E.; Mourey, D. A. *Appl. Phys. Lett.* **2007**, *91*, 063514.

44. Laquindanum, J. G.; Katz, H. E.; Lovinger, A. J. *J. Am. Chem. Soc.* **1998**, *120*, 664.

45. Payne, M. M.; Parkin, S. R.; Anthony, J. E.; Kuo, C. C.; Jackson, T. N. *J. Am. Chem. Soc.* **2005**, *127*, 4986.

46. United States Department of Energy Report'07 http://www.energy.gov/energysources/index.htm

47. a) Becquerel, A. E. *Comt. Rend. Acad. Sci*. **1839**, *9*, 561. b) Oh, H. S.; Lee, J. U.; Lee, W. J.; Jang, K. U.; Ahn, J. H.; Lee, D. K.; Lee, H. S.; Kim, T. W. *J. Korean. Phys. Soc*. **2006**, *48*, 1488

48. Chapin, D. M.; Fuller, C. S.; Pearson, G. L. *J. Appl. Phys*. **1954**, *25*, 676.

49. Shockley, W.; Queisser, H. J. J. Appl. Phys. **1961**, *32*, 510.

50. Zhao, J.; Wang, A.; Green, M. A.; Ferrazza, F. *Appl. Phys. Lett*. **1998**, *73*, 1991.

51. Zhao, J.; Wang, A.; Green, M.; Ferrazza. *Appl. Phys. Lett*. **1998**, *73*, 1991.

52. www.spectrolab.com

53. http://www.future-fab.com/documents.asp?d_ID=4211&grID=208#

54. a) Ramsdale, C. M.; Barker, J. A.; Arias, A. C.; MacKenzie, J. D.; Friend, R. H.; Greenham, N. C. *J. Appl. Phys*. **2002**, *92*, 4266. b) Barker, J. A.; Ramsdale, C. M.; Greenham, N. C. *Phys. Rev. B* **2003**, *67*, 075205.

55. Kallmann, H.; Pope, M. *J. Chem. Phys*. **1959**, *30*, 585.

56. Miranda, P. B.; Moses, D.; Heeger, A. J. *Phys. Rev B* **2001**, *64*, 081201.

57.Yu, G.; Zhang, C.; Heeger, A. J. *Appl. Phys. Lett*. **1994**, *64*, 1540.

58. Tang, C. W. *Appl. Phys. Lett*. **1986**, *48*, 183.

59. a) Yoo, S.; Domercq, B.; Kippelen, B. *J. Appl. Phys.* **2005**, *97*, 103706. b) Song, Q. L.; Li, F. Y.; Yang, H.; Wu, H. R.; Wang, X. Z.; Zhou, W.; Zhao, J. M.; Ding, X. M.; Huang, C. H.: Hou, X. Y. *Chem. Phys. Lett.* **2005**, *416*, 42. c) Pandey, A. K.; Nunzi, J-M. *Appl. Phys. Lett.* **2006**, *89*, 213506. d) Pandey, A. K.; Siegnon, S. D.; Nunzi, J M. *Appl. Phys. Lett*. **2006**, *89*, 113506. e) Yang, J.; Garcia, A.; Nguyen, T-Q. *Appl. Phys. Lett*. **2007**, *90*, 103514.

60. Jenekhe, S. A.; Yi, S. *Appl. Phys. Lett*. **2000**, *77*, 2635.

61. a) Yakimov, A.; Forrest, S. R. *Appl. Phys. Lett*. **2002**, *80*, 1667. b) Peumans, P.; Bulovic, V.; Forrest, S. R. *Appl. Phys. Lett*. **2000**, *76*, 2650.

62. Peumans, P.; Bulovic, V.; Forrest, S. R. *Appl. Phys. Lett*. **2001**, *79*, 126.

63. Xue, J.; Uchida, S.; Rand, B. P.; Forrest, S. R. *Appl. Phys. Lett*. **2004**, *84*, 3013.

64. a) Gebeyehu, D.; Maennig, B.; Drechsel, J.; Leo, K.; Pfeiffer, M. *Sol. Energy Mater. Sol. cells.* **2003**, *79*, 81. b) Cremer, J.; Bauerle, P.; Wienk, M. M.; Janssen, R. A. J. *Chem. Mater.* **2006**, *18*, 5832. c) Kietzke, T.; Shin, R. Y. C.; Egbe, D. A. M.; Chen, Z. K.; Sellinger, A. *Macromolecules*, **2007**, *40*, 4424. d) Rusu, M.; Vogel, M.; Lux-Steiner, M. Ch.; Fostiropoulos, K. *Appl. Phys. Lett*. **2007**, *90*, 153511.

65. Yu, G.; Gao, J.; Hummelen, J. C.; Wudl, F.; Heeger, A. J. *Science* **1995**, *270*, 1789.

66. Shaheen, S. E.; Brabec, C. J.; Sariciftci, N. S.; Padinger, F.; Fromherz, T.; Hummelen, J. C. *Appl. Phys. Lett*. **2001**, *78*, 841.

67. Rispens, M. T.; Meetsma, A.; Rittberger, R.; Brabec, C. J.; Sariciftci, N. S.;

Hummelen, J. C. Chem. Commun. 2003, 17, 2116.

68. Barber Jr, R. P.; Gomez, R. D.; Herman, W. N.; Romero, D. B. *Org. Elec*. **2006**, *7*, 508.

69. Backer, S. A.; Sivula, K.; Kavulak, D. F.; Frechet, J. M. J. *Chem. Mater*. **2007**, *19*, 2927.

70. Reyes, R. M.; Kim, K.; Carroll, D. L. *Appl. Phys. Lett*. **2005**, *87*, 083506.

71. Peet, J.; Kim, J. Y.; Coates, N. E.; Ma, W. L.; Moses, D.; Heeger, A. J.; Bazan, G. C. *Nat. Mater*. **2007**, *6*, 497.

72. Katsuhara, M.; Aoyagi, I.; Nakajima, H.; Mori, T.; Kambayashi, T.; Ofuji, M.; Takanishi, Y.; Ishikawa, K.; Takezoe, H.; Hosono, H. *Synth. Met.* **2005**, *149*, 219.

73. Heeney, M.; Bailey, C.; Giles, M.; Sukunov, M.; Sparrowe, D.; Tierney, S.; Zhang, W.; McCulloch, I. *Macromolecules*, **2004**, *37*, 5250.

74. Siringhaus, H.; Wilson, R. J.; Friend, R. H.; Inbasekaran, M.; Wu, W.; Woo, E. P.; Grell, M.; Bradley, D. D. C. *Appl. Phys. Lett.* **2000**, *77*, 406.

75. O'Neill, M.; Kelly, S. M. *Adv. Mater*. **2003**, *15*, 1135.

76. McCulloch, I.; Heeney, M.; Bailey, C.; Genevicius, K.; MacDonald, I.; Shkunov, M.; Sparrowe, D.; Tierney, S.; Wagner, R.; Zhang, W.; Chabinyc, M. L.; Kline, R. J.; Mcgehee, M. D.; Toney, M. F. *Nat. Mater*. **2006**, *5*, 328.

77. Adam, D.; Schuhmacher, P.; Simmerer, J.; Haussling, L.; Siemensmeyer, K.; Etzbach, K. H.; Ringsdorf, H.; Haarer, D. *Nature*. **1994**, *371*, 141.

78. Garnier, F.; Hajlaoui, R.; El Kassmi, A.; Horowitz, G.; Laigre, L.; Porzio, W.; Armanini, M.; Provasoli, F. *Chem. Mater*. **1998**, *10*, 3334.

79. Van Breemen, A. J. J.; Herwig, P. T.; Chlon, C. H. T.; Sweelson, J.; Schoo, H. F. M.;

Setayesh, S.; Hardeman, W. M.; Martin, C. A.; De Leeuw, D. M.; Valeton, J. J. P.; Bastiaansen, C. W. M. Broer, D. J.; Popa-Merticaru, A. R.; Meskers, S. C. J. *J. Am. Chem. Soc*. **2006**, *128*, 2336.

80. Fujiwara, T.; Locklin, J.; Bao, Z. *Appl Phys. Lett.* **2007**, *90*, 232108.
81. Picture taken by Jackson research group at Penn State.
82. Chen, J.; Martin, D.; Anthony, J. E. *J. Mater. Res*. **2007**, *22*, 1701.
83. a. Bruckner, V.; Tomasz, J. *Acta. Chim. Hung*. **1961**, *28*, 405. b. Vets, N.; Smet, M.; Dehaen, W. *Tet. Lett*. **2004**, *45*, 7287.
84. Deen, M. J.; Kazemeini, M. H.; Haddara, Y. M.; Yu, J.; Vamvounis, G.; Holdcroft, S.; Woods, W, *IEEE Trans. Electron Devices*. **2004**, *51*, 1892.
85. Wu, Y.; Li, Y.; Ong, B.; Liu, P.; Gardner, S.; Chiang, B., *Adv. Mater*. **2005**, *17*, 185.
86. Mizukami, M.; Hirohata, N.; Iseki, T.; Ohtawara, K.; Tada, T.; Yagyu, S.; Abe, T.; Suzuki, T.; Fujisaki, Y.; Inoue, Y.; Tokito, S.; Kurita, T., *IEEE Electron Device Letters*. **2006**, *27*, 249.
87. Halik, M.; Klauk, H.; Zschieschang, U.; Schmid, G.; Ponomarenko, S.; Kirchmeyer, S.; Weber, W. *Adv. Mater*. **2003**, *15*, 917.
88. a) Sirringhaus, H.; Tessler, N.; Friend, R. H., *Science*. **1998**, *280*, 1741.
    b) Sirringhaus, H.; Tessler, N.; Friend, R. H., *Synth. Met.* **1999**, *102*, 857.
89. Laquindanum, J. G.; Katz, H. E.; Lovinger, A. J.; Dodabalapur, A. *Adv. Mater*. **1997**, *9*, 36.
90. Yoo, S.; Domercq, B.; Kippelen, B. *Appl. Phys. Lett*. **2004**, *85*, 5427.
91. Lloyd, M. T.; Mayer, A. C.; Tayi, A. S.; Bowen, A. M.; Kasen, T. G.; Herman, D. J.; Mourey, D. A.; Anthony, J. E.; Malliaras, G. G. *Org. Electron*. **2006**, *7*, 243.

92. Hummer, K.; Ambrosch-Draxl, C. *Phys. Rev. B.* **2005**, *71*.081202.

93. Band-edge offset values are approximations based on the solid state energy levels of C_{60} and the TIPS-pentacene energy levels found via cyclic voltammetry.

94. Sun, X.; Zhou, Y.; Wu, W.; Liu, Y.; Tian, W.; Yu, G.; Qiu, W.; Chen, S.; Zhu, D. J. Phys. Chem. B. 2006, 220, 7702.

95. Dickey, C. K.; Anthony, J. E.; Loo, Y, -L. *Adv. Mater*. **2006**, *18*, 1721.

96. Meijer, E. J.; De Leeuw, D. M.; Setayesh, S.; Van Veenendaal, E.; Huisman, B. H.; Blom, P. W. M.; Hummelen, J. C.; Scherf, U.; Klapwijk, T. M. *Nat.Mater.* **2003**, *2*, 678.

97. Minari, T.; Seto, M.; Nemoto, T.; Isoda, S.; Tsukagoshi, K.; Aoyagi, Y. *Appl. Phys. Lett*. **2007**, *91*, 123501.

98. Koch, N.; Salzmann, I.; Johnson, R. L.; Pflaum, J.; Friedlein, R.; Rabe, J. P. *Org. Electron*. **2006**, *7*, 537.

99. Ackermann, J.; Videlot, C.; Dumas, P.; El Kassmi, A.; Guglielmetti, R.; Safarov, V. *Org. Electron*. **2004**, *5*, 213.

100. Lee, M, W.; Song, C. K. *J. Korean Phys. Soc.* **2005**, *47*, 111.

101. Grobosch, M.; Knupfer, M. *Adv. Mater*. **2007**, *19*, 754.

102. Lim, S. C.; Kim, S. H.; Lee, J. H.; Kim, M. K.; Kim, D. J.; Zyung, T. *Synth. Met*. **2005**, *148*, 75.

103. Sarma, J. A. R. P.; Desiraju, G. R. *Acc. Chem. Res*. **1986**, *19*, 222.

104. Moon, H.; Zeis, R.; Borkent, E. -J.; Besnard, C.; Lovinger, A. J.; Siegrist, T.; Kloc, C.; Bao, Z. *J. Am. Chem. Soc*. **2004**, *126*, 15322.

105. Sakamoto, Y.; Suzuki, T.; Kobayashi, M.; Gao, Y.; Inoue, Y.; Tokito, S. *Mol. Cryst.*

Liq. Cryst. **2006**, *444*. 225.

106. Kymissis, I.; Dimitrakopoulos, C. D.; Purushothaman, S. *IEEE Trans. Electron Devices*. **2001**, *48*, 1060.

107. Lin, Y.-Y.; Gundlach, D. J.; Nelson, S. F.; Jackson, T. N. *IEEE. Electr. Dev. Lett*. **1997**, *18*, 606.

108. Gundlach, D. J.; Nichols, J. A.; Zhou, L.; Jackson, T. N. *Appl. Phys. Lett*. **2002**, *80*, 2925.

109. Jean, S. *J. Am. Chem. Soc*. **1953**, *75*, 3697.

110. Lincker, F.; Bourgun, P.; masson, P.; Didier, P.; Guidone, L.; Bigot, J. Y.; Nicoud, J. F.; Donnio, B.; Guillon, D. *Org.lett.* **2005**, 7(8),1505.

Vita

Author's Name: Sankar Subramanian

Sankar Subramanian was born on 18th May 1978 in Thirunelveli, Tamilnadu, India.

EDUCATION

PhD Expected in 2008. Organic Chemistry, University of Kentucky, Lexington, KY, USA. Research Advisor: Prof. John Anthony

MSc 1998-2000. Organic Chemistry, Madurai Kamaraj University, Madurai, Tamilnadu, India

BSc 1995-1998. Chemistry, St. John's College, Palayamkottai, Thirunelveli, Tamilnadu, India

INDUSTRIAL EXPERIENCE

2000 –2003 **Scientific Associate,** *Syngene International Limited,* Bangalore, India.

AWARDS

Gill Fellowship University of Kentucky, USA 2006
First Rank Certificate Madurai Kamaraj University, India, 2000
Junior Research Fellowship Council of Scientific Industrial Research, India, 2000

PUBLICATIONS

1. Dickey, K. C.; Smith, T. J.; Stevenson, K. J.; **Subramanian, S**.; Anthony, J. E.; Loo, Y-L. Establishing efficient electrical contact to the weak crystals of triethylsilylethynyl anthradithiophene. *Chemistry of Materials* (2007), 19(22), 5210-5215.

2. Dickey, K. C.; **Subramanian, S**.; Anthony, J. E.; Han, L-H.; Chen, S.; Loo, Y-L. Large-area patterning of a solution-processable organic semiconductor to reduce parasitic leakage and off currents in thin-film transistors. *Applied Physics Letters* (2007), 90(24), 244103/1-244103/3.

3. Lloyd, M. T.; Mayer, A. C.; **Subramanian, S**.; Mourey, D. A.; Herman, D. J.; Bapat, A. V.; Anthony, J. E.; Malliaras, G. G. Efficient solution-processed photovoltaic cells based on an anthradithiophene/fullerene Blend. *Journal of the American Chemical Society* (2007), 129(29), 9144-9149.

4. Gundlach, D. J.; Royer, J. E.; Hamadani, B. H.; Teague, L. C.; Moad, A. J.; Jurchescu, O. D.; Kirillov, O.; Richter, C. A.; Kushmerick, J. G.; Richter, L. J.; Park, S. K; Jackson, T. N.; **Subramanian, S**.; Anthony, J. E. Contact induced crystallinity for high performance soluble acene-based transistors and circuits. *Nature Materials*, (2008), 7 (3), 216-221.

5. **Subramanian, S**.; Park, S.; Parkin, S. R.; Podzorov, V.; Jackson, T. N.; Anthony, J. E. Chromophore fluorination enhances crystallization and stability of soluble anthradithiophene semiconductors. (accepted in *Journal of the American Chemical Society*, 2008. Web release date: 02/09/2008).

6. Chen, J.; **Subramanian, S**.; Parkin, S. R.; Siegler, M.; Gallup, K.; Haughn, C.; Martin, D. C.; Anthony, J. E. The influence of side chains on the structure and properties of functionalized pentacenes. (accepted in *Journal of Materials Chemistry*, 2008. Web release date: 02/12/2008).

PRESENTATIONS

1. ***S. Subramanian***, J. E. Anthony, Synthesis and device characterization of functionalized anthradithiophenes, 232nd American Chemical Society (ACS) National Meeting, September 10-14, San Francisco, CA, USA, 2006.

2. ***S. Subramanian***, J. E. Anthony, Small molecule organic semiconductors for flexible electronics, Program Review, Advanced Carbon Nano-technology Program (ACNP), 30th January, Gainsville, FL, USA, 2007.

3. ***S. Subramanian***, S. R. Parkin, J. E. Anthony, Effect of functionalization on acenes and their electronic properties, 233rd ACS National Meeting, Chicago, IL, United States, March 25-29, 2007.